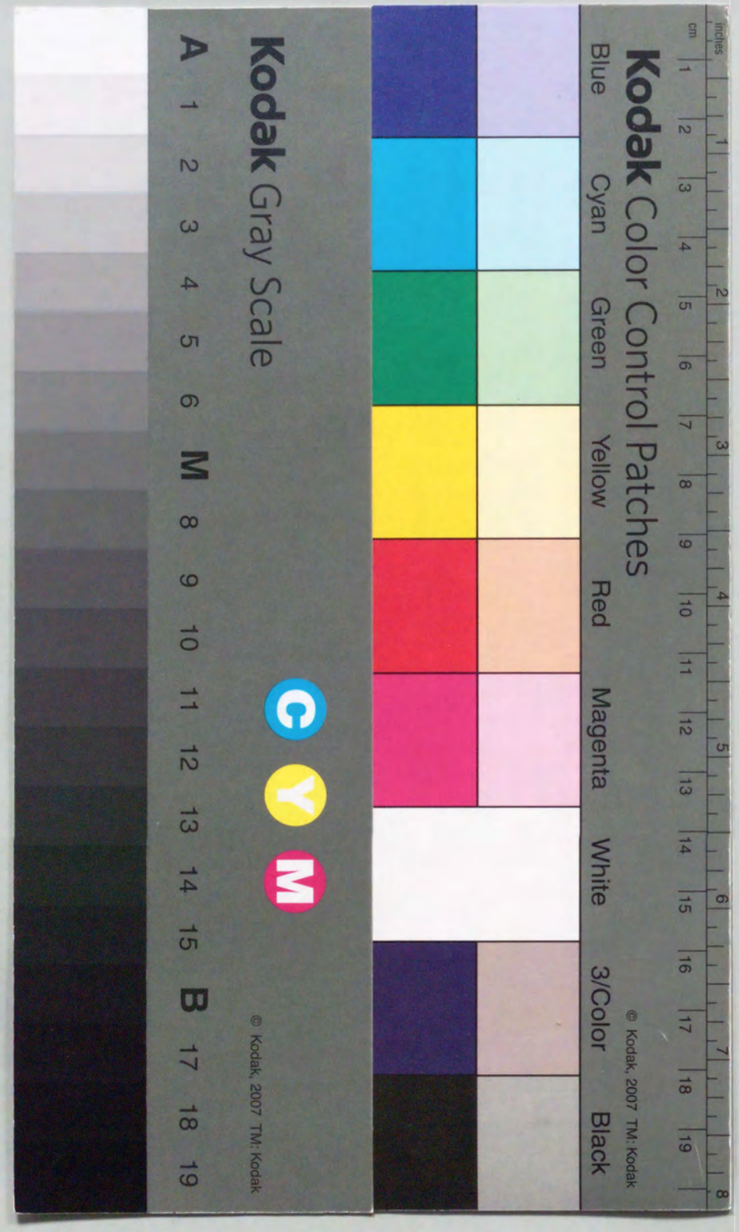

NMR Study of Magnetic Excitation and Pseudogap in High-*Tc* Cuprates

Yo Tokunaga

OSAKA UNIVERSITY

GRADUATE SCHOOL OF ENGINEERING SCIENCE
DEPARTMENT OF PHYSICAL SCIENCE
DIVISION OF MATERIALS PHYSICS

1999

NMR Study of Magnetic Excitation and Pseudogap in High-T_c Cuprates

Yo Tokunaga

OSAKA UNIVERSITY

GRADUATE SCHOOL OF ENGINEERING SCIENCE
DEPARTMENT OF PHYSICAL SCIENCE
DIVISION OF MATERIALS PHYSICS

1999

Abstract

Over the past few years, it has become increasingly clear to the high-T_c community that the key to clarifying the mechanism of high-T_c superconductivity in cuprates is related to their unusual properties in the normal state. In this thesis, we report the normal state magnetic properties in high-T_c cuprates studied by means of the nuclear magnetic resonance (NMR) technique. The key subjects in this thesis are as follows: "the roles of magnetic excitations for the high-T_c superconductivity", "the origin of the pseudogap behavior in underdoped cuprates" and "the mechanism of the superconductivity in multilayer cuprates", which are discussed together with each chapter.

In the chapter 2, we report ^{63}Cu-NQR study in Ni substituted $YBa_2Cu_3O_7$. From the universal scaling formula of the ^{63}Cu nuclear spin-lattice relaxation rate, $1/T_1$, against $t = T/T_c$, we have the novel relation between T_c and the characteristic energy of the Cu antiferromagnetic (AF) spin fluctuation, Γ_Q; $T_c \propto \Gamma_Q$. Furthermore, by combining with the same universal scaling formula of the Gaussian component of the ^{63}Cu nuclear spin-echo decay rate, $1/T_{2G}$, we derive the relation, $T_c \propto \Gamma_Q \xi^2$, which has been proposed by the theoretical model based on the spin-fluctuation-induced mechanism for the d-wave superconductivity. It is concluded that the suppression of T_c with Ni substitution in $YBa_2Cu_3O_7$ is caused by the decrease in Γ_Q rather than by either magnetic or potential impurity scattering. Our results provide a direct experimental evidence for the attractive force to be magnetic in origin irrespective of the theoretical model, moreover supports strongly the spin fluctuation mediated mechanism for high-T_c superconductivity.

In the chapter 3, we present the NMR results in the single crystal $Bi_2Sr_2CaCu_2O_{8+\delta}$ for a doping range from underdoping to overdoping. In the normal state, $1/T_1T$ has a broad maximum around T^*, showing the spin-gap behavior. We find that the ^{63}Cu Knight shift, $K(T)$, also exhibits the steep decrease below $T_K^* \sim T^*$, indicating that the pseudogap opens not only in the AF spin excitation spectrum at low energy around $\boldsymbol{Q} = (\pi, \pi)$ but also in the quasiparticle DOS. The temperature independent behavior of $1/T_{2G}$ below $\sim T^*$ suggests that the origin of the pseudogap behavior in this temperature region is due to the transfer of the spectral weight from low to high energy. In all the samples, we find that $1/T_{2G}$ starts to decrease at a certain temperature, T_c^*, which is higher than the bulk superconducting temperature (T_c) and lower than T^*. These diminution of $1/T_{2G}$ as well as K and $1/T_1T$ below T_c^* suggest S. C. fluctuation without global phase coherency. Based on our NMR results, we present a phase diagram in the Bi2212 system which is sketched by three crossover temperature, T_{mK}, T^* and T_c^* below which K, $1/T_1T$ and $1/T_{2G}$ start to decrease, respectively.

In the chapter 4 and 5, we report the NMR studies on four layers cuprates, i.e. $HgBa_2Ca_3Cu_4O_{10+y}$ (Hg1234) and $(Cu_{1-x}C_x)Ba_2Ca_3Cu_4O_{12+y}$ (Cu1234), where Cu in outer CuO_2 planes is surrounded by five oxygens (5-fold) and that in inner CuO_2 planes by four oxygens (4-fold). In Hg1234, the 4-fold (5-fold) Cu sites exhibit T_1T/T_{2G} =const. (T_1T/T_{2G}^2 =const.) behavior which has been observed for underdoped (optimally doped) cuprates. We find that the pseudogap opens up for both the optimally doped 5-fold and underdoped 4-fold Cu sites at the same temperature, $T^* \sim 190$ K and $T_K^* \sim 220$K defined by the Knight shift and $1/T_1T$. In Cu1234, we find that a conventional d-wave superconducting state is established in 4-fold at $T_c = 117K$, but not in 5-fold between $T_c > T > 60$ K. This provide the evidence that the superconductivity $T_c = 117K$ is maintained by the 4-fold layers which are near the optimum carrier condition. The d-wave superconducting state appears to be established below $60K$ in 5-fold, as if the overdoped 5-fold has own T_c . In both layers of Hg-1234, the pseudogap behavior below T_K^* is well reproduced by a model which assumes d-wave symmetry on the pseudogap. Based on this model, we suggest that the value of the normal-state pseudogap increases linearly as the temperature is lowered from T_K^* to T_c. Furthermore, this model can be applied to the

temperature dependence of K below T_c for 5-fold in Cu1234 by assuming the linear increase of a size of superconducting gap between T_c and 60K with the $d_{x^2-y^2}$ symmetry.

Contents

Chapter 1

Introduction

1.1 General Introduction of High-T_c Cuprates

Since the discovery of high-T_c cuprate[1], a key question has been "what is the origin of the superconductivity in these system?". In order to answer this question, numerous works have been carried out both experimentally and theoretically. At present, it has become increasingly clear that the mechanism of superconductivity in cuprates is directly related to their unusual properties in the normal state.

In this section, we describe the overview of the physical properties in high-T_c superconductors and introduce some topics in their normal state.

1.1.1 Phase Diagram of High-T_c cuprates

A common feature among copper based high-T_c superconductors is the existence of a plane which consists of corner shared CuO_2 squares. The carrier doping into this plane is essential for the occurrence of high-T_c superconductivity. Fig.1.1 shows the phase diagram on the plane of the doping rate, P_{CuO_2}, and the temperature, T, indicated by various experiments so far carried out for high-T_c cuprates.

High-T_c cuprates start from insulating antiferromagnet caused by a strong correlation effect. The non-doped parent compounds are Charge-transfer insulators which exhibit an antiferromagnetic (AF) ordering around 500K. The effective moment is about $0.6\mu_B$, which is lie in the CuO_2 plane.[2] By substituting divalent ions into the site of trivalent ions or by increasing the oxygen content, holes are doped into CuO_2 plane and the Néel temperature, T_N decrease dramatically. In the case of $La_{2-x}(Sr,Ba)_xCuO_4$, as small as 2% substitution of Sr^{2+} or Ba^{2+} destroy the three dimensional magnetic order, while an spin glass like order, i.e. a two dimensional antiferromagnetically sort range ordered state, appears in low temperature[3, 4]. The superconducting phase appears with further doping after the magnetic order disappears. The superconducting transition temperature, T_c , increases with hole doping (underdoped region) and having a maximum value at the characteristic doping rate (optimally-doped region). The highest T_c known to date under ambient pressure is $133K$ for $HgBa_2$ $Ca_2Cu_3O_{8+y}$,[5] which is enhanced to $\sim 150K$ by applying pressure[6]. At much higher doped region, T_c decrease with

doping (overdoped region) and finally the system enters normal metallic state. In this region, the electronic properties can be understood in terms of the normal fermi liquid.

It should be noted that the superconducting phase appear in a doping range between the AF insulator and normal Fermi liquid phases, which is covered with a range exhibiting an AF correlation. This suggests that the development of AF correlation may play an important role in the pairing mechanism of high-T_c superconductivity.

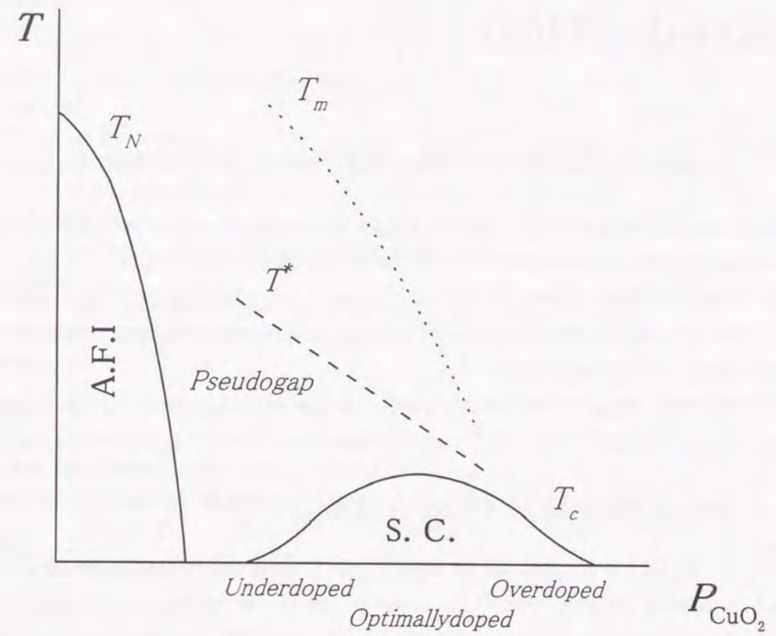

Figure 1.1: Phase diagram for a high-T_c superconductor on the plane of the doping rate. T_m and T^* mark the characteristic temperature discussed in the text.

1.1.2 Normal state properties

It has been revealed that the normal state properties of high-T_c cuprates are anomalous when compared to the Landau Fermi Liquid found in the normal state of conventional superconductors. For example,

- The inplane resistivity shows the T-linear law, in contrast to the T^2 law in the conventional Fermi liquid.[7]
- The Hall coefficient is strongly temperature dependent, while it is temperature independent in the conventional Fermi liquid.[8]
- The isotropy of resistivity $\rho c/\rho ab$ becomes large in the low temperature region. Moreover, the c-axis resistivity behaves as a semiconductor in underdoped cuprates.[9]

- The Korringa law, T_1TK^2 = constant which usually holds in a normal metallic state, does not hold in optimally and underdoped cuprates.

It is generally agreed that the strong magnetic interaction between planer quasiparticles is responsible for these anomalous normal state behaviors and thus for the superconducting transition at high temper with $d_{x^2-y^2}$ pairing.

It was revealed by the first generation of NMR experiments that the quasiparticles in even optimally doped system such as $La_{1.85}Sr_{0.15}CuO_4$ and $YBa_2Cu_3O_7$ displayed almost antiferromagnetic behavior in the normal state. The strikingly different temperature dependence of the ^{63}Cu and ^{17}O spin lattice relaxation rates indicates that $\chi(\boldsymbol{q},\omega)$ is sharply peaks at wave vectors in the vicinity of the commensurate ordering wave vector $\boldsymbol{Q}$ =(π,π).[10, 11] The Curie-Weiss like behavior of $1/^{63}T_1$ due to the development of the AF correlation in plane is commonly seen in most of high-T_c , which has been described first in term of the phenomenological AF spin fluctuation model[12], and the self-consistent renormalization (SCR) theory.[13] A remarkable finding was that the AF spin fluctuation disappeared for heavily-doped $Tl_2Ba_2CuO_{6+y}$(Tl2201) compound exhibiting no longer superconductivity, instead obeying the T_1T=constant law in a wide T-range.[14] These results have suggested that the AF spin correlation remains in the normal state of the superconducting compound, and plays a role for the occurence of the superconductivity.

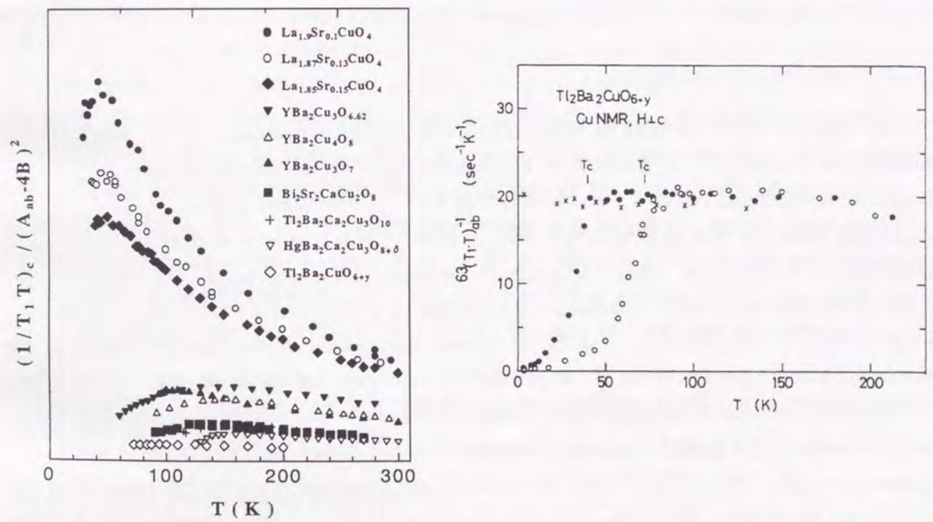

Figure 1.2: T-dependence of $1/T_1T$ /(A - 4B)^2 in several high-T_c materials which is proportional to the low-frequency component of AF spin-fluctuation, $\chi_Q/\Gamma_Q\xi^2$ (left fig.) and temperature dependence of $^{63}(1/T_1T)$ in $Tl_2Ba_2CuO_{6+y}$ with T_c =72 K (○), 40 K(●) and 0 K(×)(right fig.).

Fig.1.2, shows T-dependence of $1/T_1T$ /(A - 4B)^2 in several high-T_c materials which is proportional to the low-frequency component of AF spin-fluctuation, $\chi_Q/\Gamma_Q\xi^2$ (see the section [1.2.6]

). $1/T_1T$ /(A - 4B)^2 ($\propto \chi_Q/\Gamma_Q\xi^2$), which is largely enhanced by the AF spin correlation and follow Curie-Weiss law $c/(T+\theta)$ in underdoped regime, is markedly depressed by doping holes and consequently, becomes temperature independent in a wide temperature region in overdoped regime. This indicates that, when holes are introduced into O site, the oxygen spin decouples the antiferromagnetic spin correlation between Cu spins because of the antiferromagnetic coupling between Cu and O, which reduces χ_Q. In underdoped cuprates excluding LSCO, $1/T_1T$ /(A - 4B)^2 shows a broad peak above T_c , that is, the pseudogap (spin-gap) behavior. On the other hand, in overdoped cuprates such as Tl2201, the T_1T=const law are observed in a wide temperature range above T_c , moreover, it was experimentally confirmed that this T_1T=const law is extended to the low temperature region, when the superconductivity is destroyed by the magnetic field.[14] This suggests that the T_1T=const law in the field induced normal state in the superconducting samples is linked to the T_1T=const law in the non-superconducting sample.

From theoretical point of view, Moriya *et al* have shown that $1/T_1T$ follows a Curie-Weiss law at high temperature and approached T_1T=const law at low temperature within SCR theory for two-dimensional AF metal.[13] In this argument, the AF spin-fluctuations at the zone boundary $\boldsymbol{q}=\boldsymbol{Q}$ (π,π) have played a central role in explaining consistently the magnetic and transport properties such as the NMR relaxation behavior and the linear temperature dependence of the resistivity. Kohno and Yamada have roughly derived the relation between the resistivity, ρ and $1/T_1T$, $\rho \propto T^2/T_1T$. [15] From the result, they have given the T-linear resistivity in the underdoped region and the T^2 resistivity in the overdoped region.

1.1.3 Pseudogap problem

In the figure 1.1, T^* termed as Pseudogap or Spin-gap temperature, is the characteristic temperature defined by the maxima of the nuclear spin-lattice relaxation rate, $1/T_1T$. T^* appears in underdoped region to merge smoothly to T_c in overdoped region.

Spin-gap behavior was first reported from studies of the magnetic excitation spectrum in the bilayer system such as $YBa_2Cu_4O_8$ and underdoped $YBa_2Cu_3O_{6.6}$.[16, 17, 18, 19] It was reported that the spin-lattice relaxation rate divided by temperature, $1/T_1T$ has a broad maximum around T^* far above T_c . This anomalous suppression in the spectral weight of the low-energy spin dynamics below T^* is referred to as a *spin-gap* behavior and was confirmed by subsequent neutron experiments.[20] However it was not clear whether the spin-gap was intrinsic in underdoped high-T_c cuprates, because it has not been observed in typical single-layer cuprate, $La_{2-x}Sr_xCuO_4$ (LSCO).[21] Recently spin-gap was also observed in both single and three layers Hg system, $HgBa_2Ca_{n-1}Cu_nO_{2n+2+y}$ (n=1,3).[22, 23] From these results, it is now considered that spin-gap behavior is intrinsic to CuO_2 plane in High-T_c cuprates.

In contrast to $1/T_1T$, the Knight shift $K(T)$ decreases upon cooling from higher temperature, T_m in underdoped cuprates, even in LSCO. Since the anomaly around T^* has not been recognized apparently in the T-dependence of Knight, it has been considered for the dynamic spin susceptibility $\chi(\boldsymbol{q},\omega)$ that $\mathrm{Im}\chi(\boldsymbol{q},\omega)$ with $\boldsymbol{q}=\boldsymbol{Q}$ $(\pi/a,\pi/a)$ and $\omega \sim 0$ governing $1/T_1T$ has different temperature dependence from $\chi(0,0)$, that is, the pseudogap opens only around

$\boldsymbol{q}=(\pi/a,\pi/a)$. However, as discussed in the chapter 3 and 4, our analysis of the Knight shift data revealed that the anomaly around T^* is observed not only in $1/T_1$ but also in the Knight shift at T_K^*. This indicates that the pseudogap opens not only $\mathrm{Im}\chi(\boldsymbol{Q},0)$ but also $\chi(0,0)$.

The pseudogap in the electronic excitation spectrum is later reported from a variety of other probes. Recent studies of angle-resolved photoemission spectroscopy (ARPES) revealed that the normal-state pseudogap with the $d_{x^2-y^2}$ symmetry opens up below a temperature T^*_{ARPES}, and suggested that it develops into the d-wave SC gap once phase coherence is established below T_c.[24, 25] Namely, the result was interpreted as evidence in favor of a preformed d-wave gap.[24] T^*_{ARPES} increases up to 300 K for T_c=10 K sample with the further underdoping level.[24] Anomalous behavior around T^* is also reported in other probes. Both the Hall coefficient, R_H, and $[\rho_{ab}(T)-\rho_{ab}(0)]/T^2$, $\rho(T)$ being the in-plane resistivity, start to deviate from the high-temperature $1/T_1$-dependence around T^*.[26] The suppression of the c-axis optical conductivity, $\sigma_c(\omega)$, at low frequency[27] and the narrowing of Drude peak in the inplane conductivity, $\sigma_{ab}(\omega)$, set in $T \sim T^*$. On the other, the uniform magnetic susceptibility , χ, start to decrease gradually around much higher temperature, T_m[28]. It is also reported that the anomalous temperature dependence of the Hall coefficient, $R_H \propto 1/T$, sets around T_m.

In order to describe Pseudogap (spin-gap) behavior in underdoped cuprates, various theoretical approaches have been proposed. In a concept of a spin-charge separation based on the resonating valence bond (RVB) picture, it has been proposed that the spin-gap behavior is indispensable in bringing about the superconductivity near 2D Mott insulators.[29] On the other hand, a nearly antiferromagnetic (AF) Fermi liquid model proposed that the anomalous spin and charge behaviors in the normal state arise from the magnetic interaction among the planer quasiparticles which reflect the close approach of even an optimally doped system to the antiferromagnetism. In such a picture, Miyake *et al.* have proposed that these anomalous behaviors can be qualitatively explained on the basis of the mode-mode coupling theory of spin fluctuations in 2D metals by taking into account the technically nested Fermi surface of renormalized quasiparticles.[30] Pines *et al.* proposed that the Fermi surface evolution which accompanies the development of a precursor to a spin-density-wave (SDW) state gives rise to the $z=1$ behavior deduced from the NMR measurements and the pseudogap behavior below T^*.[31]

Other approach, a normal-state precursor scenarios including the effect of phase fluctuation, is described in the next section.

1.1.4 Phase fluctuation model

One of the approaches to understand pseudogap behavior in underdoped cuprates is "the phase-fluctuation model" suggested by V.J.Emery and S.A.Kivelson[32]. They have shown that phase fluctuation can significantly reduce the critical temperature T_c of superconductors with a small superfluid density.

The pairing scale is related to the size of the coherence length ξ_0 or equivalently the energy gap Δ_0 at zero temperature, and, in the BCS mean field theory, $\Delta_0/2$ provides a good estimate

of T_c . At the same time, the classical phase ordering temperature is determined by the "phase stiffness" V_0 which sets the energy scale for the spatial variation of the superconducting phase. If V_0 is independent of T, the phase ordering temperature $T_{phase} = AV_0$, where A is a number of order unity.[32] At zero temperature, V_0 is given in terms of the superfluid density $n_s(T=0)$ or, equivalently, the experimentally measured penetration depth $\lambda(T=0)$:

$$V_0 = \frac{\hbar n_s(0) a}{4m^*} = \frac{(\hbar c)^2 a}{16\pi(e\lambda(0))^2} \tag{1.1}$$

where a is a length scale that depends on the dimensionality of the material. An estimate for T_c is given by the smaller of T_{MF} and T_{phase}, where T_{MF} is the mean-field transition temperature predicted in BCS theory.

Emery and Kivelson argued that in conventional low-T_c superconductors, which have a large superfluid stiffness, $T_{phase} \gg T_c$, so that phase fluctuations are irrelevant and the transition is BCS-like. However, cuprate superconductors are doped Mott insulators which have a small superfluid stiffness (of order the doping x), $T_{phase} \sim T_c$ and the transition is controlled by phase ordering. This naturally explains the Uemura scaling $T_c \sim n_s(0)/m$, observed in the high-T_c cuprates[33]. In addition, the reduction of the phase stiffness $n_s(T)/4m$ is approximately linear in temperature due to the d-wave symmetry, almost all the way to T_c ,[34] in contrast to conventional s-wave superconductors, where $n_s(T)/4m$ rapidly drops to zero near T_c . Therefore the temperature range for which $n_s(T)/4m$ is a small number is much wider than in the conventional superconductor, and the effect of phase fluctuations can be observed even far from T_c .

1.1.5 Superconductivity in the multilayered cuprates

The T_c value of the high-T_c superconductor has a tendency to increase with increasing the number of CuO_2 layers per unit cell. The relation between the number of the CuO_2 sheets and T_c for Hg-, Tl-, and Bi-compounds is shown in Fig.1.3. As for the $HgBa_2Ca_{n-1}Cu_nO_{2n+2+y}$ family, the highest T_c value in the system, $T_{c,max}$, increases with the number of the CuO_2 layers per unit cell, n, and reaches a maximum of $T_{c,max} = 134$K for $n = 3$, $HgBa_2Ca_2Cu_3O_{8+y}$ (Hg1223) phase. However for n=4, $HgBa_2Ca_3Cu_4O_{10+y}$ (Hg1234) phase, the value of $T_{c,max}$ decreases to 123K. In contrast, some phenomenological models predict a monotonic increase of $T_{c,max}$ for $n = 1$ to 4,[50, 51] and actually, the $TlBa_2Ca_2Cu_3O_{11+y}$ (Tl1234) phase has a maximum $T_{c,max}$ value of 120K in the $TlBa_2Ca_{n-1}Cu_nO_{2n+3}$ family.[52] The origin of the increase of T_c in $n = 1$ to 3 and the decrease in $n = 4$ for Hg-compounds has been investigated mainly from macroscopic view points, and discussed as concerned with the carrier condition on CuO_2 layers, however not fully understood.[53]

The other interest in these compounds is the relationship between T_c and the local configuration of Cu in the CuO_2 sheets. The high-T_c compounds with three (n=3) and four (n=4) CuO_2 layers per unit cell, consist of two different types of CuO_2 layers in a unit cell: one of which is two pyramidal (5-fold) CuO_2 layers, while another is one (n=3) or two (n=4) square (4-fold) CuO_2 layers sandwiched by two 5-fold layers. Interesting questions are whether or not the local

character of 4- and 5-fold CuO_2 layers, (i.e. the carrier condition and the magnetic properties) are equivalent within a unit cell, and if not, which layers mainly contribute to the higher T_c value in these compounds. As concerns this question, two different phenomenological models are discussed in $n = 3$ and 4 compounds. In a model of Wheatley et.al,[54] it is assumed that the carriers are distributed equally between all the CuO_2 layers within a unit cell regardless of the difference in the type of the CuO_2 layers. On the other hand, in a model of Haines and Tallon,[55] a possibility of an inhomogeneous carrier distribution among the inequivalent CuO_2 layers is suggested. The investigation on the electronic structure and magnetic properties in the each CuO_2 planes from the microscopic points of view has been desired to the understanding of superconductivity mechanism in these multiple Cu-O layered systems.

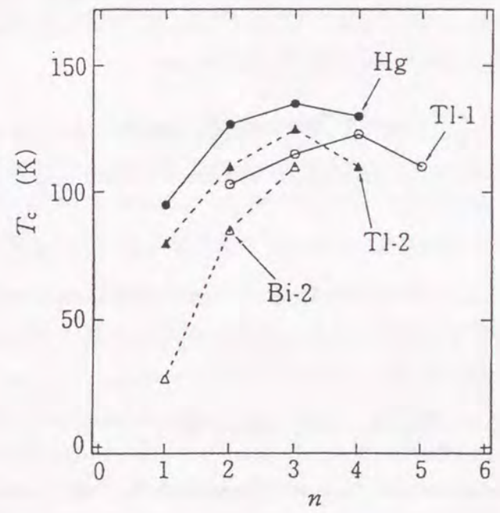

Figure 1.3: The relation of the number of the CuO_2 sheets and T_c for Hg-, Tl-, and Bi-compounds.

1.2 NMR Theory in High-T_c Cuprates

Nuclear magnetic resonance experiment (NMR) is one of the most powerful microscopic probe for the investigation of the planner spin excitations in high-T_c cuprate. Through a study of the Knight shift, K, spin-lattice relaxation rate, $1/T_1$, spin-spin relaxation rate, $1/T_{2G}$, we can gain the information of the wave-vector, $\boldsymbol{q}$, and frequency, ω dependent spin susceptibility, $\chi(\boldsymbol{q},\omega)$.

In this section, we review the NMR theory applied to high-T_c cuprates and the analysis of NMR data from the nearly antiferromagnetic fermi liquid picture.

1.2.1 Nuclear spin Hamiltonian

A nuclear spin interacts with its electronic environment through electric and magnetic hyperfine couplings. In the presence of an applied magnetic field, $\boldsymbol{H}_0$, the Hamiltonian of a nuclear spin, $\boldsymbol{I}$, having a quadrupole moment, eQ, can be written as,

$$\mathcal{H} = \mathcal{H}_{Zeeman} + \mathcal{H}_{quadrupole} + \mathcal{H}_{hyperfine} \tag{1.2}$$

The first term $\mathcal{H}_{Zeeman}$ is the Zeeman interaction between a nuclear spin moment $\mu_n = \gamma_n \hbar \boldsymbol{I}$ and $\boldsymbol{H}_0$;

$$\mathcal{H}_{Zeeman} = -\gamma_n \hbar \boldsymbol{H}_0 [\boldsymbol{I}_z \cos\theta + \boldsymbol{I}_y \sin\theta \sin\phi + \boldsymbol{I}_x \sin\theta \cos\phi], \tag{1.3}$$

The second term $\mathcal{H}_{quadrupole}$ is the electrostatic hyperfine interaction between the electric field gradient(EFG) due to the non-spherical distribution of the electron charge and the nuclear electric quadrupole moment for the nuclear spin ($\boldsymbol{I} \geq 1$);

$$\mathcal{H}_{quadrupole} = \frac{eQ\boldsymbol{V}_{zz}}{4\boldsymbol{I}(2\boldsymbol{I}-1)} \left(3\boldsymbol{I}_z^2 - \boldsymbol{I}(\boldsymbol{I}+1) + \frac{\eta}{2}(\boldsymbol{I}_+^2 + \boldsymbol{I}_-^2) \right), \tag{1.4}$$

Here, $\boldsymbol{V}_{\alpha\alpha} (\alpha = x, y, z)$ denote the principal components of the electric field gradient (EFG) tensor $\boldsymbol{V}$, with the axes labeled according to the convention $|\boldsymbol{V}_{xx}| \leq |\boldsymbol{V}_{yy}| \leq |\boldsymbol{V}_{zz}|$. The asymmetry parameter of $\boldsymbol{V}$, η, is defined as $\eta = (\boldsymbol{V}_{xx} - \boldsymbol{V}_{yy})/\boldsymbol{V}_{zz}$. For a particular site, x, y, z are chosen as the frame of reference in Eqs. 1.2,1.3,1.4 and 1.5. In High-T_c cuprates due to symmetry, one permutation of the x, y, z set coincides with orthorhombic, a, b and c crystal axes. θ and ϕ are the polar and azimuth angles of $\boldsymbol{H}_0$, respectively, in this crystal frame.

The third term in Eq.1.2 is the magnetic hyperfine interaction given as

$$\begin{aligned} \mathcal{H}_{hyperfine} &= \gamma_n \gamma_e \hbar^2 \left[\frac{8\pi}{3} \delta(\boldsymbol{r}) \boldsymbol{I} \cdot \boldsymbol{S} - \left(\frac{\boldsymbol{I} \cdot \boldsymbol{S}}{r^3} - \frac{3(\boldsymbol{I} \cdot \boldsymbol{r})(\boldsymbol{S} \cdot \boldsymbol{r})}{r^5} \right) \right. \\ &\left. + \frac{\boldsymbol{I} \cdot \boldsymbol{l}}{r^3} + \frac{8\pi}{3} \sum_i (|\Psi_i(0)^\uparrow|^2 - |\Psi_i(0)^\downarrow|^2) \boldsymbol{I} \cdot \boldsymbol{S} + \ldots\ldots \right], \end{aligned} \tag{1.5}$$

Here $\boldsymbol{S}$ and $\boldsymbol{l}$ are the total electron spin ($\boldsymbol{S} = \sum \boldsymbol{s}$) and the orbital angular momentum of electron. γ_n and γ_e are the nuclear and electron gyromagnetic rations. $|\Psi_i(0)|^2$ is the probability density of closed s-electrons. Each terms in Eq.1.5 is the Fermi contact interaction due to s-electrons, the spin dipolar interaction due to only unpaired non s-electrons, orbital interaction

due to the orbital current of non s-electron and the indirect interaction due to core polarization effect where the closed inner s-electrons are polarized by the unpaired non s-electrons through exchange polarization effects.

In general, Eq.1.5 is divided into two parts of a spin and a orbital parts as

$$\mathcal{H}_{hyperfine} = \boldsymbol{I} \cdot \boldsymbol{A} \cdot \boldsymbol{S} + \gamma_n \gamma_e \hbar^2 \frac{\boldsymbol{I} \cdot \boldsymbol{l}}{r^3}, \tag{1.6}$$

where $\boldsymbol{A}$ is the hyperfine coupling tensor.

In the absence of an applied or an internal static magnetic field, the remaining $\mathcal{H}_{quadrupole}$ gives rise to doubly degenerate energy levels between which NQR transitions can be induced. For cooper, there exist two naturally occurring isotopes ^{63}Cu and ^{65}Cu both having spin 3/2 and thus two doubly degenerate $\pm 1/2$ and $\pm 3/2$ energy levels. For each isotope, a transition between these levels yields a single NQR signal at frequency

$$^{63,65}\nu_Q = \frac{e^{63,65} Q V_{zz}}{2h} \sqrt{1 + \frac{1}{3}\eta^2}. \tag{1.7}$$

In the presence of a large external magnetic field, H_0, $\boldsymbol{H}_{quadrupole}$ causes, for each isotope and each site, a splitting of the Cu NMR signal into a central line arising from the central transition, $(+\frac{1}{2}, -\frac{1}{2})$, and two satellite lines due to the $(\pm\frac{1}{2}, \mp\frac{3}{2})$ transitions. In addition, the $\mathcal{H}_{hyperfine}$ term causes a magnetic shift of each line.

1.2.2 Mila-Rice Hamiltonian

In the t-J model, the moments are localized on Cu orbitals slightly hybridized with neighboring ones. These hybridizations can induce transferred interactions from one Cu atom to neighboring atoms. In order to explain the large anisotropy of Knight shift in $YBa_2Cu_3O_7$ which cannot be explained by only the on-site hyperfine interaction, F.Mila and T.M.Rice proposed the transferred hyperfine field from the nearest neighboring Cu spins[35].

For Cu, they derived an interaction Hamiltonian

$$\mathcal{H}_{MR} = \sum_{\alpha=x,y,z} A^\alpha \boldsymbol{I}_0^\alpha \boldsymbol{S}_0^\alpha + \sum_i B \boldsymbol{I}_0 \boldsymbol{S}_i, \tag{1.8}$$

where $\boldsymbol{I}$ and $\boldsymbol{S}$ are Cu nuclear and electronic spins, the index i runs over the four Cu nearest neighbors of the central Cu atom denoted by 0. The first term, A represent coupling of Cu nuclear moment to the electronic spin in the same cell. They are anisotropic because the Cu atomic wave function with the greatest weight at the Fermi surface is the $3d_{x^2-y^2}$ state which is spatially anisotropic and couples to the nuclear spin via spin-orbit and dipolar coupling. B is a supertransferred hyperfine coupling connecting a Cu moment in one cell to an electron in an adjacent cell through Cu($3d_{x^2-y^2}$)-O($2p$)-Cu($4S$) covalent bonding. It is isotropic because the coupling to the nuclear spin is via the Fermi contact interaction.

From the $K - \chi$ plot in $YBa_2Cu_3O_{6.5}$ the hyperfine coupling $A_\perp + 4B = 195 kOe/\mu_B$ is obtained[36], whereas $A_\parallel + 4B = 0$. The internal field at the Cu site in the antiferromagnetic $YBa_2Cu_3O_6$ is estimated to be $79.6 kOe/0.66\mu_B$[37] which provides $|A_\perp - 4B|$ to be $121 kOe$.

Thus from these relations $A_\perp = 37KOe/\mu_B$, $A_\parallel = -158kOe/\mu_B$, $B = 39kOe/\mu_B$ are obtained for $YBa_2Cu_3O_7$.[38] Here the difference between $YBa_2Cu_3O_7$ and $YBa_2Cu_3O_{6.5}$ shown to be negligible.

1.2.3 Knight shift

The magnetic coupling between the nuclear spin and its electronic environment as expressed by the hyperfine Hamiltonian, $H_{hyperfine}$, can be viewed as a coupling of the nuclear spin with a time dependent local magnetic hyperfine field, $H_L(t)$, generated by the electron spin and the electron orbital motion. The static part of $H_L(t)$, $\langle H_L(t) \rangle$ gives rise to a NMR lines shift expressed by the magnetic shift, K_α, which is usually called the Knight shift.

When the second-order electronic quadrupole interaction is taken into account as a perturbation to the Zeeman interaction, the resonance shift of the centerline of the e^2qQ split lines is expressed as,

$$\Delta\omega = \gamma_n K_\alpha H_{res} + \frac{4\pi^2\nu_Q^2(I(I+1)-3/4)\sin^2\theta(1-9cos^2\theta)}{16(1+K_\alpha)\gamma_n H_{res}}, \tag{1.9}$$

where H_{res} is the field where the resonance is observed, θ is the angle between the principal axis of the field gradient tensor, c axis, and the external magnetic field. The first term in eq.(1.9) is due to the Knight shift and the second is the second-order quadrupole term. When the external magnetic field is parallel to the c axis, the second term is zero.

$$\Delta\omega = \gamma_n K_\parallel H_{res} \tag{1.10}$$

Thus obtained $K_\parallel$. When the external magnetic field is perpendicular to the c axis,

$$\Delta\omega = \gamma_n K_\perp H_{res} + \frac{4\pi^2\nu_Q^2(I(I+1)-3/4)}{16(1+K_\perp)\gamma_n H_{res}}, \tag{1.11}$$

and then

$$\frac{\Delta\omega}{\gamma_n H_{res}} = K_\perp + \frac{4\pi^2\nu_Q^2(I(I+1)-3/4)}{16(1+K_\perp)(\gamma_n H_{res})^2} \tag{1.12}$$

Thus liner relation is expected between $\Delta\omega(\gamma_n H_{res})$ and H_{res}^{-2}. $K_\perp$ and ν_Q are obtained from the intercept and slope of the linear line.

The Knight shift K consists of the spin part K_S and the orbital (Van Vleck)part K_{orb}, which are connected to the spin susceptibility, χ_s and the Van Vleck orbital susceptibility χ_{vv}, respectively.

$$K_\alpha = K_{s\alpha} + K_{vv\alpha} \tag{1.13}$$

where

$$K_{s\alpha} = \frac{1}{g\mu_B}\sum_j A_{j\alpha}\chi_{s\alpha} \tag{1.14}$$

and

$$K_{vv\alpha} = \frac{1}{\mu_B}O_\alpha\chi_{vv\alpha} \tag{1.15}$$

Here, A_j and O_α are the spin and the orbital hyperfine tensor.

In the case of in-plane Cu(2) site in High-T_c cuprate, χ_{vv} is temperature independent and expressed as,

$$\chi_{vv\parallel} = \frac{8\mu_B^2 W}{E(d(xy)) - E(d(x^2-y^2))}, \tag{1.16}$$

$$\chi_{vv\perp} = \frac{2\mu_B^2 W}{E(d(yz)) - E(d(x^2-y^2))}, \tag{1.17}$$

In the superconducting state, χ_s decreases with temperature decreasing due to the formation of the spin singlets. Thus the residual part of K extrapolated to $T = 0K$ is attributed to K_{vv} with a small diamagnetic part associated with the Meissner shielding effect of about -0.03%, if the spin part disappears perfectly.

The spin part of the Knight shift, K_s, is obtained as

$$K_{s\alpha} = K_\alpha - K_{vv\alpha} \tag{1.18}$$

According to the Mila-Rice Hamiltonian, the ^{63}Cu spin Knight shift, $^{63}K_s$ is expressed as,

$$^{63}K_{s\parallel} = \frac{(A_\parallel + 4B)}{^{63}\gamma_n\gamma_e\hbar^2}\chi_s(T), \tag{1.19}$$

$$^{63}K_{s\perp} = \frac{(A_\perp + 4B)}{^{63}\gamma_n\gamma_e\hbar^2}\chi_s(T), \tag{1.20}$$

From this relation, one can estimate the magnitude of the uniform spin susceptibility in High-T_c cuprates.

Since the spin susceptibility is considered to be isotropic,

$$\frac{K_{s\parallel}}{K_{s\perp}} = \frac{A_\parallel + B}{A_\perp + B}, \tag{1.21}$$

Using this relation, by assuming $A_\parallel$, $A_\perp$ to be independent of the material, one obtains the values of B in several High-T_c cuprates. B is increases with increasing hole content at the $O(p\sigma)$.

1.2.4 Nuclear Spin-Lattice Relaxation Rate, $1/T_1$

The nuclear spin-lattice relaxation rate, $1/T_1$ probes the $\boldsymbol{q}$ -averaged imaginary part of the dynamical electron spin susceptibility $\chi''(\boldsymbol{q},\omega)$,

$$\frac{1}{T_1T} = \frac{\gamma_n k_B}{2\mu_B^2}\sum_q |A(\boldsymbol{q})|^2 \frac{\chi''(\boldsymbol{q},\omega_n)}{\omega_n}, \tag{1.22}$$

and

$$A(\boldsymbol{q}) = \sum_j A_j exp(i\boldsymbol{q}\cdot\boldsymbol{r}_j) \tag{1.23}$$

where ω_n and γ_n are the resonance frequency and nuclear (electronic) gyromagnetic ratios, respectively, and A_j is the on-site ($\boldsymbol{r}_j = 0$) and the transferred ($\boldsymbol{r}_j \neq 0$) hyperfine coupling tensor for the nuclei under consideration. Because of the site and wave-vector dependence of the form factor, ^{63}Cu probes $\chi''(\boldsymbol{q},\omega_n)$ primarily around $\boldsymbol{q} = \boldsymbol{Q}(\pi/a,\pi/a)$.

According to the Mila-Rice Hamiltonian[35], $1/T_1$ of ^{63}Cu are given as,

$$\frac{1}{^{63}T_{1\parallel}T} = \frac{^{63}\gamma_n k_B}{2\mu_B^2}\sum_q F_\perp(\boldsymbol{q})^2 \frac{\chi''(\boldsymbol{q},\omega_n)}{\omega_n} \tag{1.24}$$

$$\frac{1}{^{63}T_{1\perp}T} = \frac{^{63}\gamma_n k_B}{4\mu_B^2}\sum_q [F_\perp(\boldsymbol{q})^2 + F_\parallel(\boldsymbol{q})^2] \frac{\chi''(\boldsymbol{q},\omega_n)}{\omega_n} \tag{1.25}$$

where the form factors are given as,

$$F_\perp(\boldsymbol{q}) = A_\perp + 2B[cos\boldsymbol{q}_x a + cos\boldsymbol{q}_y a] \tag{1.26}$$

$$F_\parallel(\boldsymbol{q}) = A_\parallel + 2B[cos\boldsymbol{q}_x a + cos\boldsymbol{q}_y a] \tag{1.27}$$

where a is the distance between Cu atoms.

In carrying comparison with the spin-spin relaxation rate, $1/T_{2G}$, it is useful to define the effective spin-lattice relaxation rate with a static field applied perpendicular to the c axis by

$$\frac{1}{^{63}T_{1\perp}^{eff}} = \frac{2}{^{63}T_{1\perp}} - \frac{1}{^{63}T_{1\parallel}} = (2R-1)\frac{1}{^{63}T_{1\parallel}} \tag{1.28}$$

where R is $R = (^{63}T_{1\parallel}/^{63}T_{1\perp})$. The relaxation rate is then given by

$$\frac{1}{^{63}T_{1\perp}^{eff}T} = \frac{^{63}\gamma_n k_B}{2\mu_B^2}\sum_q F_\parallel(\boldsymbol{q})^2 \frac{\chi''(\boldsymbol{q},\omega_n)}{\omega_n} \tag{1.29}$$

It has been established that the antiferromagnetic spin fluctuations play the crucial role in $1/T_1$ of the planner Cu nuclei in High-T_c cuprate, whereas for other nuclei (for example, O and Y in $YBa_2Cu_3O_7$) the contribution of the antiferromagnetic spin fluctuations is filtered away through the Mila-Rice hyperfine form factor.

1.2.5 Nuclear Spin-Spin Relaxation Rate, $1/T_{2G}$

Pennington and Slichter[39] have shown that the ^{63}Cu nuclear spin echo decay (transverse spin-lattice) relaxation occurs through their coupling to the itinerant Cu^{2+} spins [the RKKY mechanism] and so depends on the filter function

$$^{63}F_{eff}(\boldsymbol{q}) = \left[A_\parallel + 2B(cos\boldsymbol{q}_x + cos\boldsymbol{q}_y)\right], \tag{1.30}$$

and the real part of the static spin susceptibility, $\chi'(q)$. Itoh *et al.*[40] and Thelen and Pines[41] showed that the resulting expression for $^{63}T_{2G}$ is given by

$$\frac{1}{^{63}T_{2G}} = \left(\frac{0.69}{128}\right)^{1/2} (^{63}\gamma_n)^2 \left(\frac{1}{N}\sum_q^{63} F_{eff}^2(q)[\chi'(q)]^2 - \left[\frac{1}{N}\sum_q^{63} F_{eff}^2(q)\chi'(q)\right]^2\right) \tag{1.31}$$

where 0.69 is the abundance of ^{63}Cu isotope.

Experimentally, spin-echo amplitude E recorded as a function of the time τ between the first and second pulses is well fitted to the expression [39]

$$E(2\tau) = E_0 \exp\left[-(\frac{2\tau}{T_{2L}}) - \frac{1}{2}\left(\frac{2\tau}{T_{2G}}\right)^2\right] \tag{1.32}$$

where $1/T_{2L}$ is the Lorentzian spin-echo decay rate associated with the T_1 process. $1/T_{2L}$ was determined using the relation $1/T_{2L} = 3(1/T_1)_\parallel + (1/T_1)_\perp$.[42]

An important concern when performing NQR (or NMR) measurement of $1/T_{2G}$ is the size of the rf excitation amplitude (H_1) relative to the width of the resonance line $\Delta\omega$. T_{2G} arises through a magnetic interaction between a nuclear spin and nuclear spin in neighbor because of the change in precession frequency of a nucleus resulting from the inversion of neighbor spins. For the center transition only those neighbors which are both the same isotope and in either the $m = 1/2$ or $-1/2$ state contribute. When there is quadrupole line broadening the resonance frequency of these neighbor shifted sufficiently that the rf pulse does not invert them. Then, the measured T_{2G} will depend on the size of H_1. An incorrect value of T_{2G} will result. If $\gamma H_1 \gg \omega$ one can be sure the rf pulse flips all the neighbors. If $\gamma H_1 \leq \omega$ there is no such assurance, however the effect of line converge can be tested by measuring T_{2G} as a function of H_1.

The relationship between NMR and NQR measurements of T_{2G} is given by[43]

$$\left(\frac{1}{T_{2G}}\right)_{NQR} = \frac{\sqrt{2}}{1.03}\left(\frac{1}{T_{2G}}\right)_{NMR}, \tag{1.33}$$

and for T_1 measurements, $3T_{1,NQR} = T_{1,NMR}$. The factor of 1.03 arises because the NQR data are taken on a randomly oriented powder whereas the NMR data are taken on an oriented powder.

1.2.6 Nearly Antiferromagnetic Fermi Liquid Model (MMP Model)

A quantitative fit to NMR experiments can be obtained with a phenomenological expression for the dynamical spin susceptibility, $\chi_(\boldsymbol{Q},\omega)$, which reflects this close approach to antiferromagnetism. Quite generally, one finds four peaks in χ at wave vectors, $\boldsymbol{Q}_i$, in the vicinity of the commensurate AF wave vector, $\boldsymbol{Q} = (\pi/a, \pi/a)$, which are located symmetrically about $\boldsymbol{Q}$. In the vicinity of a given peak at $\boldsymbol{Q}_i$, χ displays considerable structure; it takes the form proposed by Millis, Monien and Pines (MMP).[44] For low frequency, ω, and momentum, $\boldsymbol{q}$, near the antiferromagnetic ordering wave vector $\boldsymbol{Q} = (\pi/a, \pi/a)$, the MMP susceptibility is

$$\chi(\boldsymbol{q},\omega) = \frac{\chi_Q}{1+(\boldsymbol{q}-\boldsymbol{Q})^2\xi^2 - i\omega/\Gamma_Q} \tag{1.34}$$

$$\equiv \frac{\chi_0\sqrt{\beta}(\xi/a)^2}{1+(\boldsymbol{q}-\boldsymbol{Q})^2\xi^2 - i\omega/\Gamma_Q} \tag{1.35}$$

and

$$\chi_Q = \chi_0\sqrt{\beta}(\xi/a)^2 = \alpha(\xi/a)^2 \tag{1.36}$$

where χ_0 is the static long-wavelength susceptibility on unit of states/eV, χ_Q is the corresponding static susceptibility at $\boldsymbol{Q}$, β reflects the scale of the antiferromagnetic enhancement, ξ is the antiferromagnetic correlation length ($\gg$ lattice spacing, a), and Γ_Q is the characterizes the energy of the spin fluctuation near $\boldsymbol{Q}$. For $YBa_2Cu_3O_7$ in the expression eq.(1.35) only ξ varies with temperature.

For the planar copper, eq.(1.29) in the limit of $\xi \gg a$ simplifies to

$$\frac{1}{{}^{63}T_{1\perp}^{eff}T} = (2R-1)\frac{1}{{}^{63}T_{1\parallel}T} \cong \frac{k_B(\gamma_n\hbar)^2}{2\hbar\mu_B^2}F_c(\boldsymbol{Q})\frac{\chi_Q}{\hbar\Gamma_Q\xi^2}\left[\propto\frac{\alpha}{\Gamma_Q}\right]. \tag{1.37}$$

In the same limit, the expression for eq.(1.31) also can be simplified to,

$$\left[\frac{1}{{}^{63}T_{2G}}\right]^2 \simeq \frac{0.69({}^{63}\gamma_n\hbar)^4}{32\pi\hbar^2\mu_B^4}F_c^4(Q)\frac{\chi_Q^2}{(\xi/a)^2}\left[\propto\alpha^2(\xi/a)^2\right]. \tag{1.38}$$

In the theoretical work on MMP and many subsequent papers[45] the assumption has been that α is independent of temperature, but ξ is not. Thus eq.(1.37) and eq.(1.38) show that ${}^{63}(1/T_1)$ measures the characteristic energy of the antiferromagnetic spin fluctuation and ${}^{63}1/T_{2G}$ measures the correlation length.

Because $1/T_{2G}$ and $1/T_{1\perp}^{eff}T$ are both proportional to ξ^{-2}, one then has (from eq.(1.37) and (1.38)),

$$\frac{{}^{63}T_{1\parallel}T}{T_{2G}^2} \simeq \frac{0.69({}^{63}\gamma_n\hbar)^2F_\parallel(Q)^2}{16\pi\mu_B^2\hbar k_B}(2R-1)\chi_Q\hbar\Gamma_Q \tag{1.39}$$

so that in the limit of long correlation length, one can determine directly from experiment the product of the characteristic energy and the staggered susceptibility of spin fluctuation at $\boldsymbol{Q}$, $\chi_Q\hbar\Gamma_Q$. Experimentally one finds that $\chi_Q\hbar\Gamma_Q$ is nearly temperature independent above T_c in the optimally and overdoped cuprates.

Within a model of spin-fluctuation induced pairing, Monthoux and Pines (MP) [12] found that, for the NAFL case, T_c is determined by an expression analogous to the usual BCS one

with the Debye energy replaced by the product, $\Gamma_Q\xi^2$ (i.e., the range of energy in which the pairing interaction is effective). In MP's expression,

$$T_c = \Gamma_Q\left(\frac{\xi}{a}\right)^2\frac{(1-\delta)}{0.79}\exp(-1/\lambda) \qquad (0.42 \le \lambda \le 0.48), \tag{1.40}$$

where δ and λ are the doping level and the dimensionless coupling constant, respectively.

1.2.7 Magnetic scaling behavior in the normal state

Of the various anomalous aspects of normal state behavior of the superconducting cuprates, the low frequency magnetic response is perhaps the most unusual, in that one finds nearly antiferromagnetic behavior and three distinct magnetic phases in all but the highly overdoped system.

An extensive body of theoretical[45, 46, 47] and experimental work[48, 49, 23] has provided evidence for the magnetic scaling behavior in the normal state of the High-T_c cuprates, expressed in term of a relationship between Γ_Q and ξ:

$$\Gamma_Q \sim \xi^{-z} \tag{1.41}$$

Barzykin and Pines (BP) proposed a phase diagram for the magnetic behavior in those materials as a function of planar hole doping and temperature, which is shown in Fig.1.4. They identify two crossover temperatures, T^* and T_{cr}, which vary with doping. They propose that between T^* and T_{cr} one should find a possibly nonuniversal, $z = 1$ scaling regime (the quantum critical (QC) regime), subsequently termed *pseudoscaling* by Pines, characterized by

$$\Gamma_Q(T) \sim \xi^{-1}(T) \sim a + bT, \tag{1.42}$$

Thus, in this QC regime, the ratio

$$\frac{T_1T}{T_{2G}} \propto \Gamma_Q\xi \tag{1.43}$$

is expected to be independent of temperature. At temperatures below T^*, one enters the *Pseudogap* regime. On the other hand, above a temperature, T_{cr}, χ displays $z = 2$ mean-field or RPA behavior characterized by the relation,

$$\Gamma_Q(T) \sim \xi^{-2}(T) \sim c + dT, \tag{1.44}$$

In this regime, if we make the assumption that α is temperature independent, so the ratio

$$\frac{T_1T}{T_{2G}^2} \propto \Gamma_Q\chi_Q = \alpha\Gamma_Q\xi^2 \tag{1.45}$$

should be temperature independent above T_{cr}. In $YBa_2Cu_4O_8$, Corey *et al.* found $z = 1$ ($T_1T/T_{2G} \sim const.$) behavior above $T^* \sim 150K$, and recently Curro *et al.* also demonstrated the crossover behavior from $z = 1$ to $z = 2$ ($T_1T/T_{2G}^2 \sim const.$) behavior at $T_{cr} \sim 500K$, which are shown in Fig.1.5.[48]

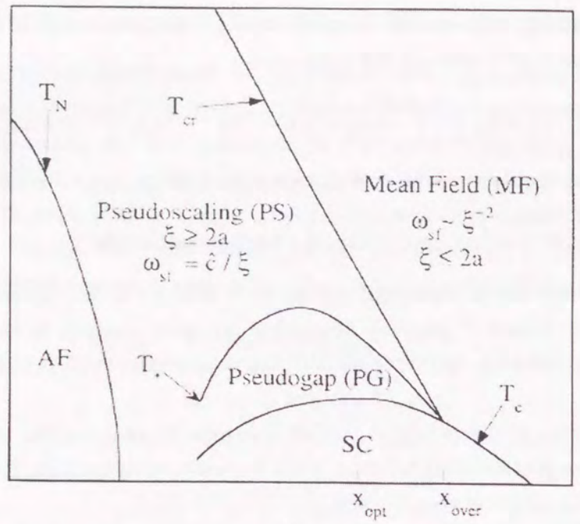

Figure 1.4: Magnetic Phase diagram for a high-T_c superconductor proposed by D.Pines *et al* from various NMR results.

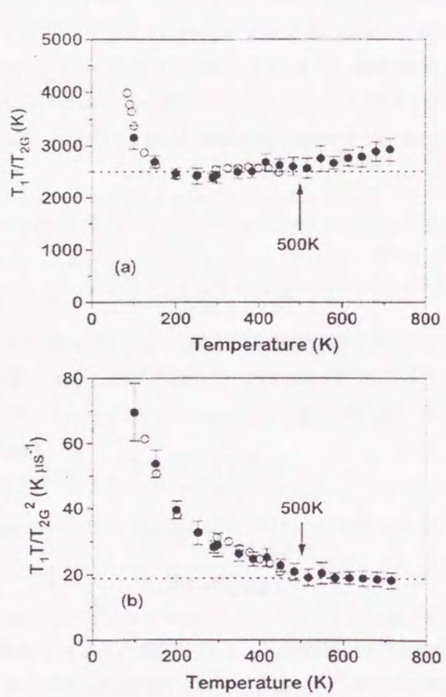

Figure 1.5: T_1T/T_{2G} and T_1T/T_{2G}^2 are plotted against T for $YBa_2Cu_4O_8$ ().

Bibliography

[1] J. G. Bedonortz and K. A. Muller, Z.Physik B**64** 189 (1986)

[2] S.M.Hayden *et al* Phys. Rev. Lett. **58** 2802 (1987)

[3] Y.Kitaoka, S.Hiramatu, T.Kondo and K.Asayama, J.Phys.Soc.Jpn. **57** 30 (1988)

[4] J.Watanabe, K.Kumagai, Y.Nakamura, T.Kimura, Y.Nakamichi, H.Nakajima, J.Phys.Soc.Jpn. **56** 3028 (1987)

[5] A.Schilling, M.Cantoni, J.D.Guo and H.R.Ott, Nature **363** 56 (1993)

[6] C.W.Chu, L.Gao, F.Chen, Z.J.Huang, R.L.Meng and Y.Y.Xue, Nature **365** 323 (1993)

[7] For example, H. Takagi, T Ido, S. Ishibashi, M. Uota, S. Uchida and Y. Tokura, Phys. Rev. B**40** (1989) 2254

[8] For example, H.Y.Hwang, B.Batalog, H.Takagi, H.L.Kao, J.Kwo, R.J.Cava, J.J.Krajewski and W.F.Peck.Jr, Phys Rev. Lett. **72** 2636 (1994)

[9] For example, K.Takenaka, K.Mizuhashi, H.Takagi and S. Uchida, Phys. Rev. B**50** 6534 (1994)

[10] P.C.Hammel, M.Takigawa, R.H.Heffner, Z.Fisk and K.C.Ott, Phys. Rev. Lett. **63** 1992 (1989)

[11] B.S.Shastry, Phys. Rev. Lett. **63** 1288 (1989)

[12] P. Monthoux and D. Pines, Phys. Rev. B**49** 4261 (1994)

[13] T. Moriya and K. Ueda, J. Phys. Soc. Jpn. **63** (1994) 1871

[14] Y. Kitaoka, K. Fujiwara, K. Ishida, K. Asayama, Y. Shimakawa, T. Manako and Y. Kubo, Physica C**179**, 107 (1991).

[15] H.Kohno and K.Yamada, Prog. Theor. Phys. **85** 13 (1991)

[16] H. Yasuoka, T. Imai and T. Shimizu, Springer Series in Solid State Science 89, Strong Correlation and Superconductivity, p.254 Springer-Verlag (1989).

[17] W.W. Warren, Jr., R.E.Walstedt, G.F. Brennert, R.J. Cava, R. Tycko, R.F. Bell, and G. Dabbagh, Phys. Rev. Lett. **62**, 1193 (1989).

[18] M. Takigawa, A.D. Reyes, P.C. Hammel, J.D. Thompson, R.H. Heffner, Z. Fisk and K.C. Ott, Phys Rev B**43**, 247 (1991).

[19] H. Alloul, A. Mahajan, H. Casalta and O. Klein, Phys. Rev. Lett. **70**, 1171 (1993).

[20] J. Rossat-Mignod et al, Physica B **186-188**, 1 (1993).

[21] S.Ohsugi *et al.*, J. Phys. Soc. Jpn. **63** 700 (1993)

[22] Y. Itoh. T. Machi, A. Fukuoka, K. Tanabe and H. Yasuoka, J. Phys. Soc. Jpn. **65**, 3751 (1996).

[23] M.-H. Julien, P. Carretta, M. Horvatic, C. Berthier, Y. Berthier, P. Segransan, A. Carrington, and D. Colson, Phys. Rev. lett. **76**, 4238 (1996).

[24] H. Ding, T. Yokoya, J. C. Campuzano, T. Takahashi, M. Randeria, M. R. Norman, T. Mochiku, K. Kadowaki and J. Giapintzakis, Nature **382**, 51 (1996); Phys. Rev. Lett. **78**, 2628 (1997).

[25] A. G. Loeser, Z. -X. Shen, D. S. Marshall, C. H. Park, P. Fournier and A. Kapitulnik, SCIENCE **273**, 325 (1996).

[26] B.Bucher, P.Steiner, J.Karpinski, E.Kaldis and P.Wachter, Phys. Rev. Lett. **70** 2012 (1993)

[27] C.C.Homes, T.Timusk, R.Liang, A.Bonn and W.N.Hardy, Phys. Rev. Lett **71** 1645 (1993)

[28] M.Oda *et al.* Physica C **281** 135 (1997)

[29] T. Tanamoto, H. Kohno, and H. Fukuyama, J. Phys. Soc. Jpn. **63**, 2739 (1994).

[30] K. Miyake and O. Narikiyo, J. Phys. Soc. Jpn. **63**, 3821 (1994).

[31] A. V. Chbukov, D. Pines and B. P. Stojkovic, J. Phys. Condens. Matter **8**, 10017 (1996).

[32] V.J.Emery and S.A.Kivelson, Nature (London) **374**, 434 (1995),Phys. Rev. Lett **74** 3253 (1995)

[33] Y.J.Uemura *et al.* Phys. Rev. Lett. **62**, 2317 (1989)

[34] T.Jacobs *et al.* Phys. rev. Lett. **75**, 4516 (1995)

[35] F. Mila and T.M. Rice, Phys. Rev. B**40**, 11382 (1989); Physica C**157**, 561 (1989).

[36] T.Shimizu, H.Yasuoka, T.Tsuda, K.Koga and Y.Ueda, Proc. of the 10th ISMAR meeting , Morzine, France, 1989

[37] H. Yasuoka, T.Shimizu, Y.Ueda and K.Kosuge, J. Phy. Soc. Jpn. **57** 2659 (1988)

[38] H.Monien, D.Pines and M. Takigawa, Phys. Rev. **43** 258 (1991)

[39] C.H. Pennington, D.J.Durand, C.P. Slichter, J.P. Rice, E.D. Bukowski and D.M. Ginsberg, Phys. Rev. B**39**, 274 (1989): C.H. Pennington and C.P. Slichter, Phys. Rev. lett. 66, 381 (1991).

[40] Y.Itoh, H.Yasuoka, Y.Fujiwara, Y.Ueda, T.Machi, I.Tomeno, K.Taki, N.Koshizuka and S.Tanaka, J. Phys. Soc. Jpn **61** 1287 (1992)

[41] D.Thelen and D.Pines, Phys. Rev.B**49** 3528 (1994)

[42] R. E. Walstedt and S-W. Cheong, Phys. Rev. B**51**, 3163 (1995).

[43] T.Imai, C.P.Slichter, K.Yoshimura, M.Katoh and K.Kosuge, Phys. Rev. Lett.**71** 1254 (1993)

[44] A.Millis, H.Monien and D.Pines, Phys. Rev. B**42** 167 (1990)

[45] V.Barzykin and D.Pines, Phys Rev. B**52** 13585 (1995)

[46] S. Chakravarty, B. I. Halperin and D. R. Nelson, Phys. Rev. B**39** 2344(1989).

[47] A. Chubukov and S. Sachdev, Phys. Rev. Lett. **71** 169 (1993)

[48] R.L. Corey, N.J. Curro, K. O'Hara, T. Imai, C.P. Slichter, K. Yoshimura, M. Katoh and K. Kosuge, Phys. Rev. B**53**, 5907 (1996); N. J. Curro, T. Imai, C. P. Slichter and B. Dabrowski, Phys. Rev. B**56**, 877 (1997).

[49] K. Magishi, Y. Kitaoka, G.-q. Zheng, K. Asayama, K. Tokiwa, A. Iyo and H. Ihara, J. Phys. Soc. jpn. **64**, 4561 (1995).

[50] C.-H. Eab and I.-M. Tang: Phys. Lett. A**134** (1989) 253

[51] J.L. Birman and J.-P. Lu: Phys. Rev. B**39** (1989) 2238

[52] H. Ihara, R. Sugise, M. Hirabayashi, N. Terada, M. Jo, A. Negishi, M. Tokumoto, Y. Kimura and T. Shimomura: Nature **334** (1988) 510.

[53] D. Tristan Jover, R.J. Wijngaarden, H. Wilhelm, R. Griessen, S.M. Loureiro, J.-J. Capponi, A.Schilling and H.R. Ott: Phys.Rev. B**54** (1996) 4265

[54] J.M. Wheatley, T.C. Hsu and P.W. Anderson: Nature **333** (1988) 121

[55] E.M. Haines and J.L. Tallon: Phys. Rev. B**45** (1992) 3172

K.Asayama, J. Phys. Soc. Jpn. **63**, 700 (1994).

Chapter 2

^{63}Cu -NMR/NQR Study in Ni Substituted $YBa_2Cu_3O_7$

2.1 Introduction

Since the discovery of high-T_c superconductor, various kinds of experiments have been carried out to elucidate the mechanism of the superconductivity. Among them the NMR measurements made important contributions to the study of the normal and superconducting properties[1, 2, 3, 4, 5, 6, 7, 8, 9]; in particular the NMR study on the impurity effect provided important clues to the determination of the symmetry of the order parameter to be of d-wave[11, 12, 13].

In High-T_c cuprates, partial substitution of nonmagnetic impurities such as Zn for Cu leads to strong suppression of the superconductivity than substitution of nominally magnetic Ni, which is in sharp contrast with the conventional superconductors. In the case of Zn substitution in $YBa_2Cu_3O_7$ (YBCO7), it has been revealed from the T_1T=constant relation and the residual spin Knight shift at low temperatures probed by Cu-NQR and NMR measurements that the superconductivity was found to be in the gapless regime with a finite density of states (DOS) at the Fermi level by the strong impurity scattering in the unitarity limit by Zn, which provided a crucial evidence for the high-T_c superconductivity to be of d-wave. .[11] The relation between the induced residual DOS, N_{res} and the rapid suppression of T_c with Zn doping can be qualitatively explained on the basis of a d-wave superconductor by assuming that nonmagnetic Zn act as strong potential scatters in the unitarity limit. Furthermore, the disruption of the AF spin fluctuation in the vicinity of Zn impurity was demonstrated to lead to a stronger reduction in T_c than in the unitarity limit associated with the change of the spin fluctuation spectrum.

In comparison with nonmagnetic Zn substitution, the magnetic Ni substitution in $YBa_2Cu_3O_7$, reduces T_c by one-fifth smaller than Zn. NMR measurement at low temperature below T_c shows that the partial substitution of Ni induces no residual DOS at E_F. Thus the effect of Ni impurity spin was possible to to be explained in terms of the Born approximation[11, 13].

In this chapter 2, we report the novel relation between T_c and the Cu antiferromagnetic (Cu-AF) spin fluctuation which has been found from ^{63}Cu NQR measurement in the normal state. This relation reveals experimentally that T_c is intimately correlated with the Cu-AF

spin fluctuation that governs $1/^{63}T_1$ and $1/^{63}T_{2G}$, which hence provides crucial evidence for the pairing mechanism to be magnetic in origin. The reduction in T_c by the Ni substitution is considered to be neither due to the magnetic nor the potential scattering effect, but due to the decrease in the characteristic energy scale, Γ_Q of the Cu-AF spin fluctuation around $Q = (\pi/a, \pi/a)$.

2.2 Sample Preparation and Characterization

A series of samples, $YBa_2(Cu_{1-x}Ni_x)_3O_7$ with $x = 0.03$, 0.05, 0.07 and 0.1 were prepared by the standard solid state reaction method. The appropriate quantities of Y_2O_3, $BaCO_3$, CuO and NiO were mixed thoroughly and reacted at 935°C for 16 hours in air after crushed into powder. These procedures were repeated by twice. Then the pellet was annealed under flowing O_2 gas at 350°C for 24 hours.

$YBCO_7$ has two inequivalent Cu sites, i.e. Cu(1) in the CuO chain and Cu(2) in the CuO_2 plane. There is a consensus that the Ni and the Zn impurities are preferentially substituted for Cu(2) from various experiments such as Y-NMR [14], X-ray [15, 16] and neutron diffraction[17].

The superconducting transition temperature, T_c was determined to be 82, 76, 70 and 65 K for $x = 0.03$, 0.05, 0.07 and 0.1, respectively from the AC susceptibility measurement. Figure 2.1 shows the Ni content dependence of T_c in Ni-doped $YBCO_7$ together with that in Zn-doped $YBCO_7$ reported in the literatures. T_c decreases linearly up to $x = 0.10$ and 0.03 in the Ni- and Zn-doped $YBCO_7$ as displayed by solid lines, respectively. The reduction rate in T_c for the Ni-substitution is by one-fifth smaller than that for the Zn-substitution. When exceeding $x = 0.15$, the value of T_c deviates from a linear decrease, indicating that the Ni impurity may not be preferentially replaced into Cu(2). Accordingly, we concern with the Ni-substituted $YBCO_7$ for $x \leq 0.1$.

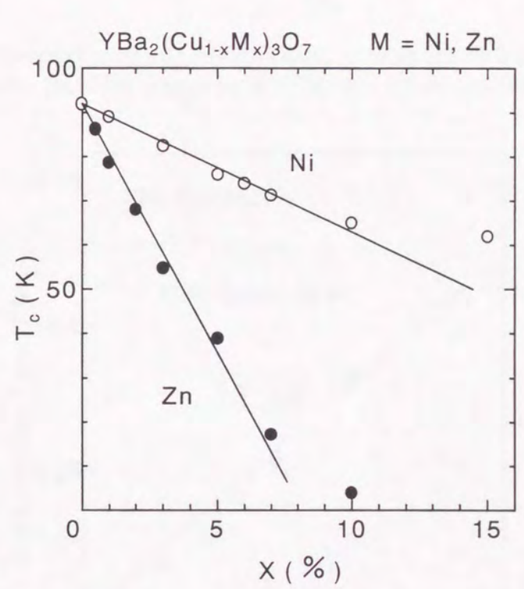

Figure 2.1: Ni content dependence of T_c in Ni-doped $YBCO_7$ together with that in Zn-doped $YBCO_7$

Figure 2.2 shows the T-dependence of magnetic susceptibility, χ, measured by a superconducting quantum interference device (SQUID) magnetmeter. χ is nearly temperature independent

above T_c in non-doped $YBa_2Cu_3O_7$, however the additional Curie term appears in Ni-doped samples. This suggests that the local magnetic moments are induced by Ni substitution in CuO_2 plane. Thus, T-dependence of χ in Ni-doped samples are analyzed by assuming that it contains a T-independent spin component, χ_0, and a T-dependent Curie component, $\chi_c(T)$, i.e.,

$$\chi = \chi_0 + \chi_c(T) \tag{2.1}$$

where χ_0 is independent of Ni content, however $\chi_c(T)$ largely depend on it. As expected, the temperature dependence of $\chi_c(T)$ are well fitted by the Curie low, C/T, as shown in the inset in Fig.2.2, and thus the Curie constants are obtained as shown in Fig.2.3. The Curie constant corresponds to $S = 1/2$ rather than $S = 1$, though usually $S = 1$ is expected for Ni^{2+} ions. The same results are reported by Mendels *et al.*.[18]

The local magnetic moments induced by Ni substitution in CuO_2 plane however largely depends on both the carrier content and systems. In underdoped $YBa_2Cu_3O_{6.6}$, it is reported that Ni-substitution induces $S = 1$ moments in plane.[18] On the other hand, Nakano *et al* recently demonstrated in $La_{2-x}Sr_xCu_{1-y}Ni_yO_4$ ($0.14 \leq x \leq 0.22$) that there exists no additional Curie term in Ni substituted samples up to a certain value, y_0. To explain this experimental results, they proposed that Ni atoms is substituted as trivalent Ni^{3+} and take the low spin state in this regime[27].

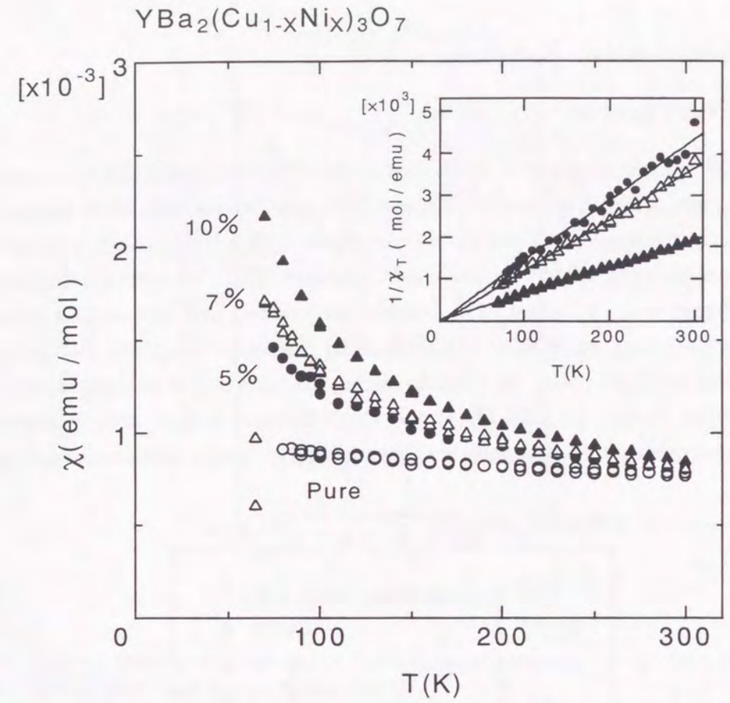

Figure 2.2: T-dependence of magnetic susceptibility, χ, measured by a superconducting quantum interference device (SQUID) magnetmeter. The inset shows the T-dependence of $\chi_c(T)$.

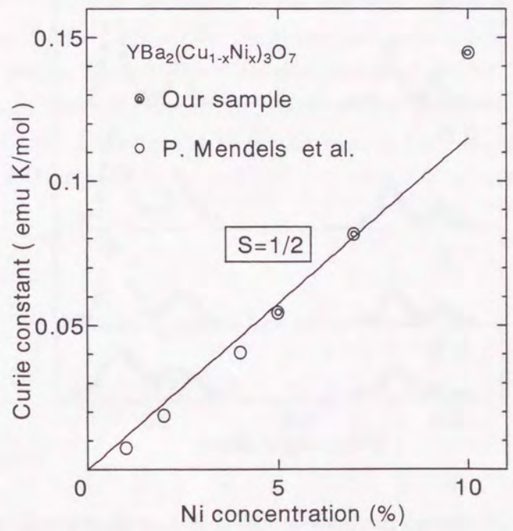

Figure 2.3: Ni content dependence of the Curie constants. The Curie constant corresponds to $S = 1/2$ rather than $S = 1$ as shown by the solid line in figure.

2.3 Experimental Results

2.3.1 Cu-NQR spectra

The Cu-NQR spectra obtained at 100 K in a series of the Ni-doped $YBCO_7$ are presented in Fig. 2.4. Two sets of NQR spectra of ^{63}Cu and ^{65}Cu are observed around 20 and 30 MHz for Cu(1) and Cu(2), respectively. There are no remarkable shift in the Cu NQR spectra for Cu(1) and Cu(2) sites, showing that the electric field gradients (EFG) at both the Cu sites do not appreciably change with Ni content. This provides the evidence that inplane hole contents does not vary with Ni-doping, since EFG is dominated by the on-site holes and thus probe for the local hole density in CuO_2 plane. On the other hand, the full-width at half-maximum (FWHM) of the ^{63}Cu NQR spectra for both Cu(1) and Cu(2) increase linearly with Ni content up to $x = 0.10$. This shows that Ni impurities are systematically doped in the samples until $x = 0.10$.

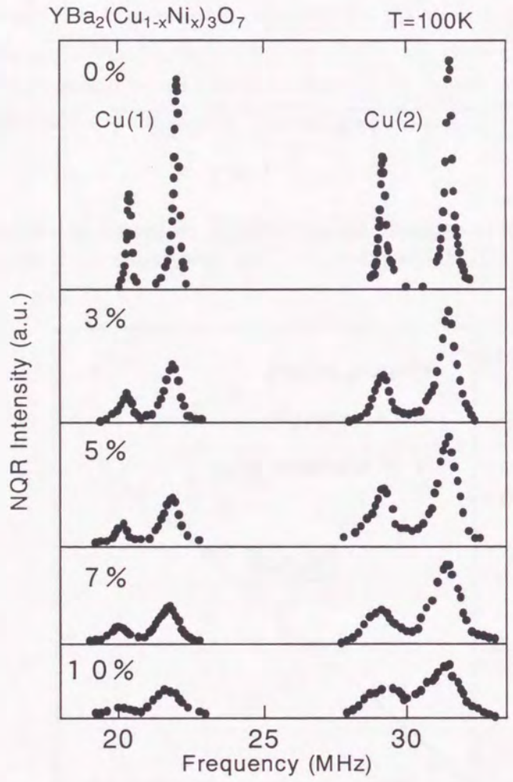

Figure 2.4: Cu-NQR spectra obtained at 100 K in a series of the Ni doped $YBCO_7$

The Ni content dependence of the integrated intensity, $I_{Ni}(x)$ for the Cu(2) NQR spectrum is displayed together with that for Zn-doped $YBCO_7$ in Fig.2.5. Solid line for Ni-doped $YBCO_7$

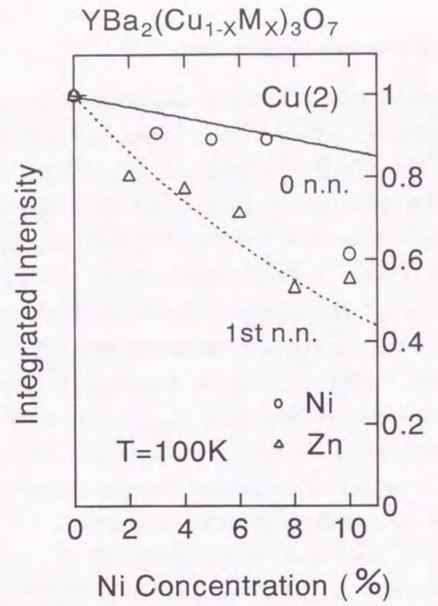

Figure 2.5: The Ni content dependence of the integrated intensity, $I_{Ni}(x)$ for the Cu(2) NQR spectrum together with that for Zn-doped $YBCO_7$

corresponds to the decreasing rate, $I(x) = 1 - (3/2)x$ expected for the simple dilution, which is in good agreement with the experiment. This result assures that all Cu nuclei including nearest neighbors to Ni impurity contribute to the observed NQR spectrum. By contrast, the reduction rate of $I_{Zn}(x) = [1 - (3/2)x]^5$ for Cu(2) deduced in Zn-doping[19] is much larger than in the Ni-doping as seen in Fig.2.5. Since the disturbance of the EFG is substantial for four nearest neighbor Cu(2) sites surrounding Zn, the Cu-NQR signals are out of observation for these Cu(2) sites. It is evident that the Ni-substitution is much moderate as compared with the Zn-substitution, although the former behaves as a magnetic impurity.

2.3.2 Nuclear spin-lattice relaxation rate, $1/T_1$

Nuclear spin-lattice relaxation rate, $1/T_1$ was measured by the saturation recovery method in zero magnetic field at the peak of the ^{63}Cu NQR spectrum for Cu(2). The relaxation function of the nuclear magnetization defined as $m(t) = [M(\infty) - M(t)]/M(\infty)$, where $M(t)$ is the nuclear magnetization at time t after the saturation pulse, could fit a simple exponential in the normal state even in the Ni substituted system, and hence T_1 was uniquely determined. This is in contrast to the case of Zn doping. In the Zn-doped samples, T_1 is largely distributed due to a local suppression of the Cu-AF spin correlation in the vicinity of the Zn impurity [11]. This contrast between Zn-and Ni-impurity effect in the nuclear relaxation behavior suggests that Zn impurity affects strongly and locally the magnetic properties in the CuO_2 planes whereas Ni impurity does not. At low temperatures well below T_c, T_1 is distributed in the $x = 0.07$ and 0.10 samples. Here, we tentatively extract a short component, T_{1s}, estimated from a slope where $m(t)$ decreases from 1 to $1/e$ and a long component, T_1, from a slope where $m(t)$ decreases from 0.1 to 0.01 in order to show an overall temperature dependence.

In Figs.2.6 and 2.7, we plot the T and (T/T_c) dependence of $1/T_1$ for $x = 0, 0.03, 0.07$ and 0.10, respectively. As seen in Fig.2.6, $1/T_{1s}$'s for $x = 0.07$ and 0.10 experience a large increase well below T_c. Both the increase and distribution of $1/T_1$ observed at low temperatures are attributed to the fluctuation of the localized Ni spin associated with the magnetic order [20]. In the normal state, $1/T_1$ above T_c is also successively increased with increasing Ni content. From the dependence of $1/T_1$ on the Ni content, magnetic field and temperature,the contribution of the localized Ni spin fluctuation to $1/T_1$ could be excluded for $T \geq T_c$ as discussed later. Therefore this increase of $1/T_1$ suggests that the Cu-AF spin fluctuation that governs $1/T_1$ is progressively changing with Ni doping.

The most remarkable findings are that all the experimental data on $1/T_1$ when plotted against $t = T/T_c(x)$ as illustrated in Fig.2.7 are entirely on a universal curve with respect to the variation of t in a T range of T_c- 400 K and even below T_c except at low temperature, regardless of the Ni content. This means that all the T dependence of $1/T_1$ in these samples undergoes a universal scaling with a single parameter, $t = T/T_c(x)$ above and just below T_c. The scaling below T_c indicates that the energy gap scales with T_c which is a natural consequence, and any other effects such as localized Ni spin fluctuation are ruled out. On the other hand, the scaling above T_c indicates that the change of the Cu-AF spin fluctuation, originating from Ni substitution, has an intimate relation to the reduction in T_c with Ni doping.

Before proceeding further, we have to comment on a possibility that the increase in $1/T_1$ in the normal state upon doping Ni would be associated with spin fluctuations of Ni local moments, which can, however, be ruled out as follows: In the case of the nuclear relaxation process being dominated by local spin fluctuations of a magnetic impurity, T_1 would be distributed depending upon the distance between impurity and host nuclei which is actually seen in the present system at low temperatures well below T_c. If T_1 was not distributed as just in the present case, it would be spatially averaged by the spin diffusion process. Since the relaxation function is of a simple exponential type regardless of the Ni content as seen in Fig.2.8 (a), the rapid spin diffusion

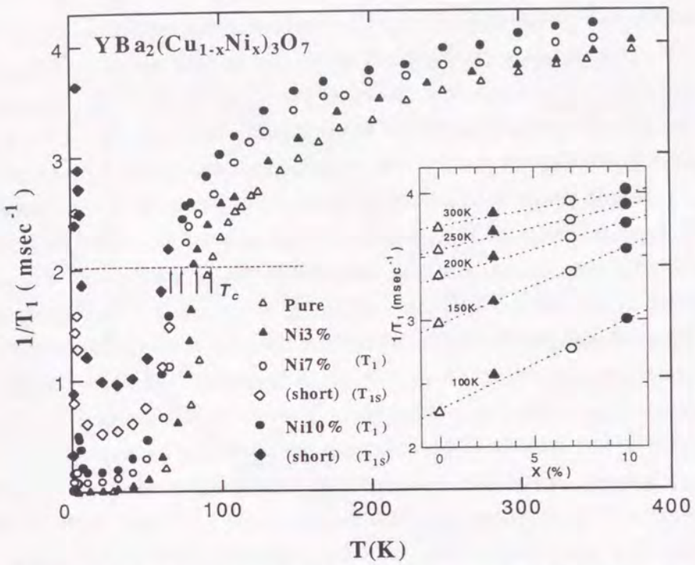

Figure 2.6: T-dependence of $1/T_1$ at Cu(2) sites in $YBa_2(Cu_{1-x}Ni_x)_3O_7$.

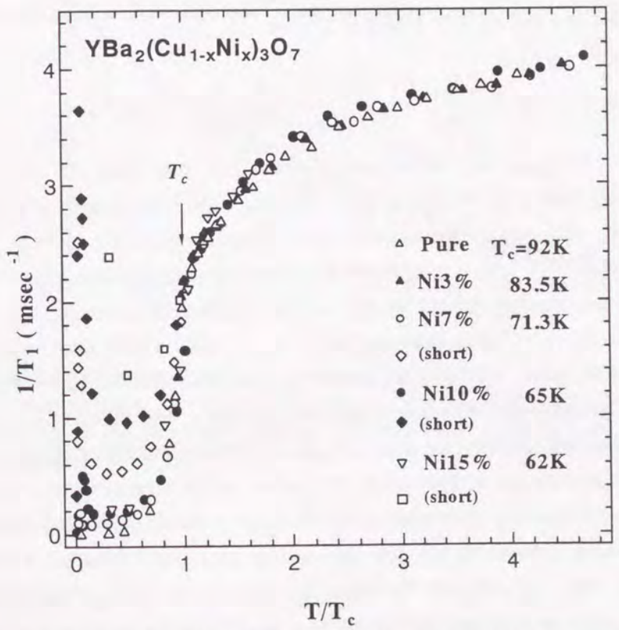

Figure 2.7: $1/T_1$ of Cu(2) in $YBa_2(Cu_{1-x}Ni_x)_3O_7$ plotted against $t = T/T_c(x)$.

process should be incorporated if localized Ni spin fluctuations were a relaxation channel for the Cu-T_1 in the normal state.

First, we present experimental evidence from the absence of the field dependence of $1/T_1$ to exclude such a relaxation channel. In Fig.2.8 is shown the field dependence of the relaxation function of $m(t)$ at $H = 1$ kOe(b) and $H = 129$ kOe(c) at the same $t = T/T_c$, respectively. The application of the minute magnetic field, $H = 1$ kOe make the NQR line split, which is expected to quench the spin diffusion process more or less, resulting in a non-simple exponential behavior in $m(t)$. Although the non-simple exponential behavior of $m(t)$ even for $x = 0$ emerges due to the split of the NQR spectrum by the Zeeman effect, $m(t)$'s at $t = T/T_c = 1.07$ for $x = 0.03$ and 0.07 also scale well with that of $x = 0$ for both zero and 1 kOe, indicating that the non-simple exponential behavior in $m(t)$ for $x = 0.03$ and 0.07 at 1 kOe is not due to the distribution of T_1 caused by local spin fluctuations. Fig.2.8(c) shows the the relaxation function, $m(t)$ of NMR measurement at satellite transition $(3/2 \leftrightarrow 1/2)$ in the magnetic field $H = 129$ kOe applied parallel to the c axis. The application of high field, $H = 129$ kOe is expected to suppress the spin diffusion largely by the increase of the inhomogeneous broadening associated with the Ni spin polarization. However, $m(t)$'s also scale even in high field, moreover could be fitted by the relaxation function of the satellite transition with the same $1/T_1$ as in NQR measurement. These results suggesting the absence of the field dependence of $1/T_1$, provide clear evidence that the localized Ni spin fluctuation does not affect the nuclear relaxation process above T_c.

Furthermore, the absence of a relaxation channel due to Ni spin fluctuations is ensured in another context as follows; $(1/T_1)_{imp}$ originating from local spin fluctuations may be given in a rapid diffusion limit by

$$\left(\frac{1}{T_1}\right)_{imp} = \Delta\left(\frac{1}{T_1}\right) = \left(\frac{1}{T_1}\right)_{obs} - \left(\frac{1}{T_1}\right)_{pure} \sim n_{imp} H_{hf}^2 \tau_e, \tag{2.2}$$

where $(1/T_1)_{obs}$ and $(1/T_1)_{pure}$ are the respective relaxation rates with and without impurity spins. Here n_{imp}, H_{hf} and $1/\tau_e$ are the impurity content, the hyperfine field at the neighbor nuclei around impurity spin and the fluctuation rate of impurity spin, respectively. $1/\tau_e$ consists of two terms as $1/\tau_e = 1/\tau_K + 1/\tau_{ex}$. $1/\tau_K$ arises from the s-d exchange interaction between local moments and conduction electron spins through the electron Korringa process; it is proportional to the temperature as $1/\tau_K \propto T$ and independent of n_{imp}. $1/\tau_{ex}$, which arises from the RKKY interaction among local spins, is proportional to n_{imp}. As shown in the inset of Fig. 2.6, the experimental result demonstrates a linear dependence against x, and hence τ_e is independent of n_{imp}, which means that the contribution from $1/\tau_{ex}$ is neglected. If localized Ni spin fluctuations were responsible for the increase of $1/T_1$ with Ni content in the normal state, the reduction of $1/\tau_K$ below T_c due to the opening of the gap at the Fermi level should increase $\Delta(1/T_1)$[21], since $(1/T_1)_{imp} \sim \tau_K$. This is apparently not the case as can be noticed from the result indicated in Fig.2.7, where all the $1/T_1$ data of Ni-doped samples are on a universal curve even just below T_c. This is a natural consequence of the fact that T_c scales with energy gap and any extra contribution to $1/T_1$ such as the localized Ni spin fluctuation is negligible. From these experimental results, the effect of the local spin fluctuations of Ni spins on the nuclear relaxation

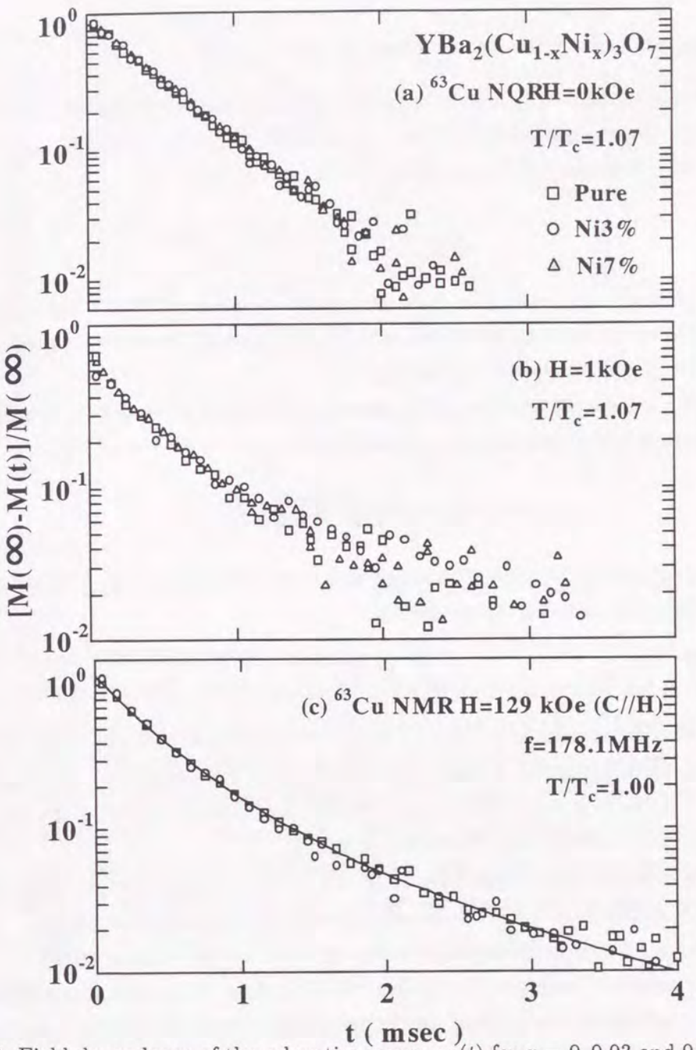

Figure 2.8: Field dependence of the relaxation curve, $m(t)$ for $x = 0, 0.03$ and 0.07 at the same t in the field, (a)$H = 0$kOe, (b) $H = 1$kOe and (c) $H = 129$kOe, respectively. Solid line in (c) is the results fitted by the relaxation function of the satellite transition with the $1/T_1$ obtained by NQR measurement.

process is unambiguously ruled out in the normal state.

2.3.3 Gaussian spin-echo decay rate, $1/T_{2G}$

The Gaussian spin-echo decay rate $1/T_{2G}$ gives a direct measure of the behavior of ξ in both the normal and superconducting state. The expression for $^{63}T_{2G}$ can be simplified considerably by using the MMP form for the susceptibility in the limit $\xi \gg a$,

$$\left[\frac{1}{^{63}T_{2G}}\right] \sim \frac{\chi_Q(T)}{\xi(T)} \sim \alpha\xi. \tag{2.3}$$

since,within the MMP approach, the value of the static susceptibility at the commensurate antiferromagnetic vector χ_Q may be written as $\chi_Q \sim \alpha\xi^2$, where α is a temperature-independent constant which depends on the doping level.[22]

Experimentally, spin-echo amplitude E recorded as a function of the time τ between the first and second pulses is well fitted to the expression [8]

$$E(2\tau) = E_0 \exp\left[-(\frac{2\tau}{T_{2L}}) - \frac{1}{2}\left(\frac{2\tau}{T_{2G}}\right)^2\right] \tag{2.4}$$

where $1/T_{2L}$ is the Lorentzian spin-echo decay rate associated with the T_1 process. $1/T_{2L}$ was determined independently using the relation[10]

$$\frac{1}{T_{2L}} = \frac{(\beta+R)}{T_1} \tag{2.5}$$

where R is the anisotropy ratio and $\beta = 2$ for NQR. We have used the value 3.6 for R, representative of the generally agreed upon value for $YBa_2Cu_3O_7$. Fig.2.9 shows the spin-echo decay curves, $E(2\tau)$ at T_c for $x = 0$ and 3% $YBa_2Cu_3O_7$ Ni. As shown by the solid line in figure, the spin-echo decay curves, $E(2\tau)$ were well fitted to eq.2.4.

An important concern when performing NQR (or NMR) measurement of $1/T_{2G}$ is the size of the rf excitation amplitude (H_1) relative to the width of the resonance line $\Delta\omega$. T_{2G} arises through a magnetic interaction between a nuclear spin and nuclear spin in neighbor because of the change in procession frequency of a nucleus resulting from the inversion of neighbor spins. When there is quadrupole line broadening the resonance frequency of these neighbor shifted sufficiently that the rf pulse does not invert them. Then, the measured T_{2G} will depend on the size of H_1. An incorrect value of T_{2G} will result. If $\gamma H_1 \gg \Delta\omega$ one can be sure the rf pulse flips all the neighbors. If $\gamma H_1 \leq \Delta\omega$ there is no such assurance, however the effect of line converge can be tested by measuring T_{2G} as a function of H_1.

Fig.2.10 shows the H_1 dependence of $1/T_{2G}$ in $YBa_2(Cu_{1-x}Ni_x)_3O_7$ at $T = 100K$. H_1 is estimated from the width of the 1st excitation pulse. $1/T_{2G}$ are nearly independent of H_1 above 90KHz, indicating that we are able to know the correct $1/T_{2G}$ values by smaller H_1 compared to the line width. Similar H_1 dependence of T_{2G} is found by R.L.Cory *et al.* in $YBa_2Cu_4O_8$, and they discuss the possibility that the field gradients which give rise to the linewidth are slowly varying with the position in crystallites relative to the range of the spin-spin coupling. [28]

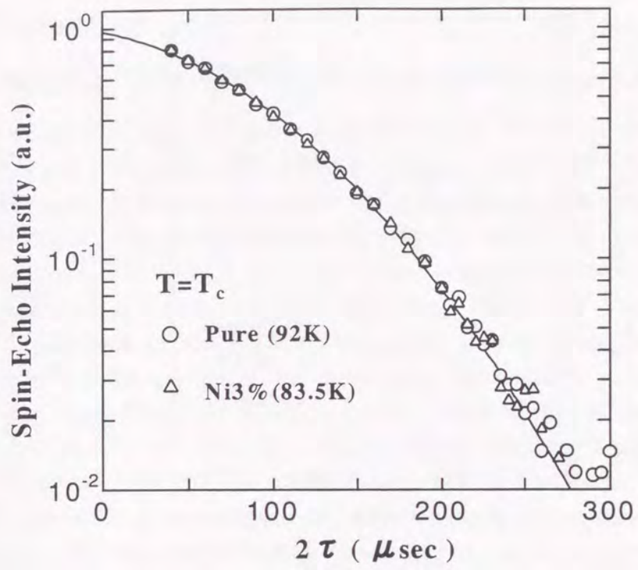

Figure 2.9: Spin-echo decay curves, $E(2\tau)$ at T_c for $x = 0$ and 3% $YBa_2Cu_3O_7$ Ni.

In Figs.2.11, we plot the T and (T/T_c) dependence of $1/T_{2G}$ for $x = 0$ and 0.03, respectively. As shown in Fig.2.11, the increasing of $1/T_{2G}$ with T-decreasing above T_c indicates the increasing of the magnetic correlation length, ξ that governs $1/T_{2G}$. When we observed at a fixed temperature, $1/T_{2G}$ is successively decreased with increasing Ni content. This decrease of $1/T_{2G}$ suggests that ξ is progressively changing with Ni doping. However, as shown in Fig.2.11, when we plotted the temperature dependence of $1/T_{2G}$ against $t = T/T_c(x)$, all the experimental data on $1/T_{2G}$ are entirely on a universal curve with respect to the variation of T_c . This means that all the T dependence of $1/T_{2G}$ in these samples undergoes a universal scaling with a single parameter, $t = T/T_c(x)$ above T_c .

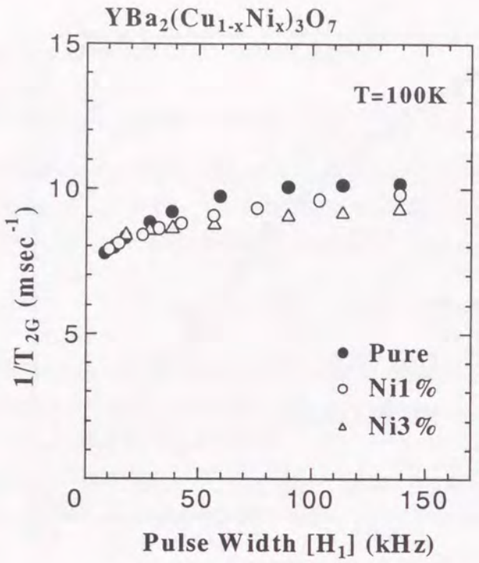

Figure 2.10: H_1 dependence of $1/T_{2G}$ in $YBa_2(Cu_{1-x}Ni_x)_3O_7$ at $T = 100K$

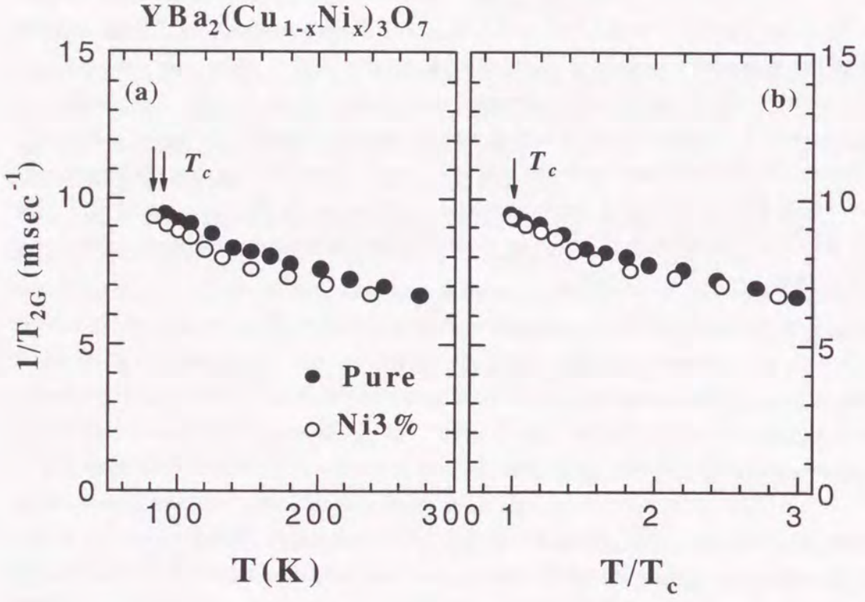

Figure 2.11: $1/T_{2G}$ in $YBa_2(Cu_{1-x}Ni_x)_3O_7$ are plotted against (a)T and (b)$T/T_c(x)$.

2.4 Discussion

2.4.1 Character of two holes in Ni $3d_{x^2-y^2}$ and $3d_{3z^2-r^2}$ orbits

It has been found in NQR experiment in Zn substituted $YBa_2Cu_3O_7$ that $1/^{63}T_1$ on planner Cu sites is largely distributed with an additional longer components. This indicates that the AF spin fluctuation is modified around Zn ions due to a local disturbance of spin correlation among Cu $3d_{x^2-y^2}$ spins. On the other hand, magnetic Ni ions lead to a moderate effect not only on the superconductivity but also on the local magnetism at host Cu sites neighboring Ni. The results that $1/T_1$ in Ni substituted $YBa_2Cu_3O_7$ do not exhibit any longer components than that in nondoped one proves that the Ni impurity does not cause any local suppression of the AF spin fluctuation around Ni ions. In addition, the integrated intensity of the spectrum indicates that Ni impurity dose not cause any disturbance in EFG at nearest neighbor Cu(2) sites around Ni in contrast to the case of Zn which has the closed d-shell. These results are explained as follow; From the susceptibility measurement, it is confirmed that the Ni impurity in $YBa_2Cu_3O_7$ act as a magnetic impurity [18] with $S = 1/2$ rather than $S = 1$. This implies that for Ni^{2+} with two holes in Ni $3d_{x^2-y^2}$ and $3d_{3z^2-r^2}$ orbits, one d electron sitting in Ni $3d_{x^2-y^2}$ orbit is smoothly hybridized with Cu $3d_{x^2-y^2}$ through the oxygen $2p_\sigma$ orbits. On the other hand, another hole in $3d_{3z^2-r^2}$ orbit behaves as nearly local moment with $S = 1/2$ as a consequence of the orthogonality between the Ni $3d_{3z^2-r^2}$ orbit and the Ni $3d_{x^2-y^2}$-$2p_\sigma$-Cu $3d_{x^2-y^2}$ hybridized bond. In this case, the magnetic interaction between conducting holes and local moments in Ni $3d_{3z^2-r^2}$ orbit is considered to be weak, and the spin correlation among Cu $3d_{x^2-y^2}$ spins is preserved even around Ni ions. This is also consistent with the result that Ni impurity dose not cause any disturbance in EFG at nearest neighbor Cu sites around Ni. In Zn substituted samples, the local disturbance of spin correlation among Cu $3d_{x^2-y^2}$ spins is considered to be one reason for a large suppression of T_c with Zn doping. However, in the case of Ni substitution, any local disturbance of AF spin fluctuation is not induced around Ni. Therefore it is not reason for the suppression of T_c in Ni substituted $YBa_2Cu_3O_7$.

2.4.2 Novel Relation between Spin-Fluctuation and Superconductivity

In spite of these evidences that the Ni substitution acts as rather weak impurity scatterer, it is remarkable that the AF spin fluctuation in the normal state is significantly and uniformly affected by the Ni impurity in such a manner that the values of $^{63}(1/T_1)$ at T_c stays constant regardless of the Ni content and that all the $1/T_1$ data plotted against $t = T/T_c(x)$ are on a single curve. We have thus found an intimate relation between T_c and the AF spin fluctuation.

In general, $1/T_1$ is given in terms of the imaginary part of the dynamical susceptibility as follows,

$$\frac{1}{T_1} \propto \sum_q F(q)^2 \frac{\chi''_\perp(q,\omega_0)}{\omega_0} T, \tag{2.6}$$

where $F(q)$ and ω_0 are the hyperfine form factor and the NMR frequency, respectively. As $F(q)$ is considered to be independent of the Ni content, the above experimental results allow us to

derive a scaling formula of $1/T_1$ against $t = T/T_c$

$$\frac{1}{T_1} \propto \left(\sum_q \frac{\chi''_\perp(q,\omega_0)}{\omega_0} \right)_{x,t} T_c(x) \cdot t = t \cdot f(t), \tag{2.7}$$

where $f(t)$ is a universal function of t as presented in Fig 3. Hence we have the relation

$$\left(\sum_q \frac{\chi''_\perp(q,\omega_0)}{\omega_0} \right)_{x,t} = f(t)/T_c(x). \tag{2.8}$$

This relation means that T_c is intimately correlated with the Cu-AF spin fluctuation that governs $^{63}(1/T_1)$. This is a direct evidence that the attractive force of high-T_c superconductivity is magnetic in origin.

When the dynamical susceptibility is dominated by the Cu-AF spin fluctuation around $Q = (\pi/a, \pi/a)$, and the energy distribution is assumed to be of a Lorentzian form, $\sum_q \chi''_\perp(q,\omega_0)/\omega_0$ is reduced to $\chi_Q/\Gamma_Q\xi^2$[22], where $\chi(Q)$, Γ_Q and ξ are the staggered susceptibility, the characteristic energy of the Cu-AF spin fluctuation around Q and the magnetic correlation length, respectively (MMP model). Then from eq.(2.8), we have the relation of

$$T_c(x) \propto \left(\frac{\Gamma_Q \xi^2}{\chi_Q} \right)_{x,t} f(t) \propto \Gamma_Q(x,t) f(t) \tag{2.9}$$

since $\chi(Q) \propto \xi^2$ is expected as discussed for the optimum and overdoped compounds such as $YBCO_7$ [9], $HgBa_2Ca_2Cu_3O_8$ [23] and $TlSr_2CaCu_2O_7$ [24]. Thus it is demonstrated that the x dependence in T_c is contained in the spin fluctuation energy scale, Γ_Q.

From the theoretical point of view, the strong coupling calculations of spin-fluctuation-induced superconductivity were developed by Moriya, Takahashi and Ueda[25], and Monthoux and Pines[26] independently. In both theories, T_c scales to $\Gamma_Q\xi^2$. Especially the latter authors derived the following relation,

$$T_c = \Gamma_Q \left(\frac{\xi}{a} \right)^2 \frac{(1-\delta)}{0.79} \exp(-1/\lambda) \qquad (0.42 \leq \lambda \leq 0.48), \tag{2.10}$$

where δ and λ are the doping level and the dimensionless coupling constant, respectively.

In order to confirm the relation of $T_c \propto \Gamma_Q\xi^2$, we have to combine the present novel relation $T_c \propto \Gamma_Q$ with the relation between the magnetic correlation length, ξ and Ni content or T_c. The expression for $^{63}T_{2G}$ can be simplified considerably by using the MMP form for the susceptibility in the limit $\xi \gg a$,

$$\frac{1}{^{63}T_{2G}} \propto \frac{\chi_Q}{\xi(T)}. \tag{2.11}$$

As shown in Fig.2.11, we have found that the T dependence of $1/T_{2G}$ also undergoes a universal scaling with a single parameter, $t = T/T_c(x)$ above T_c regardless of Ni contents.

Hence we have the relation,

$$\frac{1}{T_{2G}} \propto \frac{\chi_Q}{\xi(t)} = g(t) \tag{2.12}$$

where $g(t)$ is a universal function of t and independent of Ni contents. ξ is constant with x when t is fixed.

Now we combine $1/T_1T$ and $1/T_{2G}$ results. As discussed above, they are expressed as

$$\frac{1}{T_1T} \propto \frac{\chi_Q}{\Gamma_Q(x)\xi^2} = \frac{f(t)}{T_c(x)} \tag{2.13}$$

and

$$\left(\frac{1}{T_{2G}} \right)^2 \propto \left(\frac{\chi_Q}{\xi} \right)^2 = g(t)^2 \tag{2.14}$$

Because both are proportional to ξ^{-2}, one then has

$$\frac{T_1T}{T_{2G}^2} \propto \chi_Q\Gamma_Q = \frac{g(t)^2}{f(t)} T_c(x) \tag{2.15}$$

The temperature dependence of T_1T/T_{2G}^2 is plotted in Fig.2.12. T_1T/T_{2G}^2 is temperature independent above T_c regardless Ni content, indicating that the universal function $g(t)^2/f(t)$ is constant with temperature. In the inset of Fig.2.12, the constant values of $T_1T/T_{2G}^2 \propto \chi_Q\Gamma_Q$ are plotted against T_c . As expected in eq.(2.15), $\chi_Q\Gamma_Q \propto T_c$ is obtained.Since $\chi_Q \propto \xi^2$ is expected in optimally doped $YBa_2Cu_3O_7$, this result gives directly evidence for the relation, $T_c \propto \Gamma_Q\xi^2$, which is proposed by the strong coupling calculations of spin-fluctuation-induced superconductivity

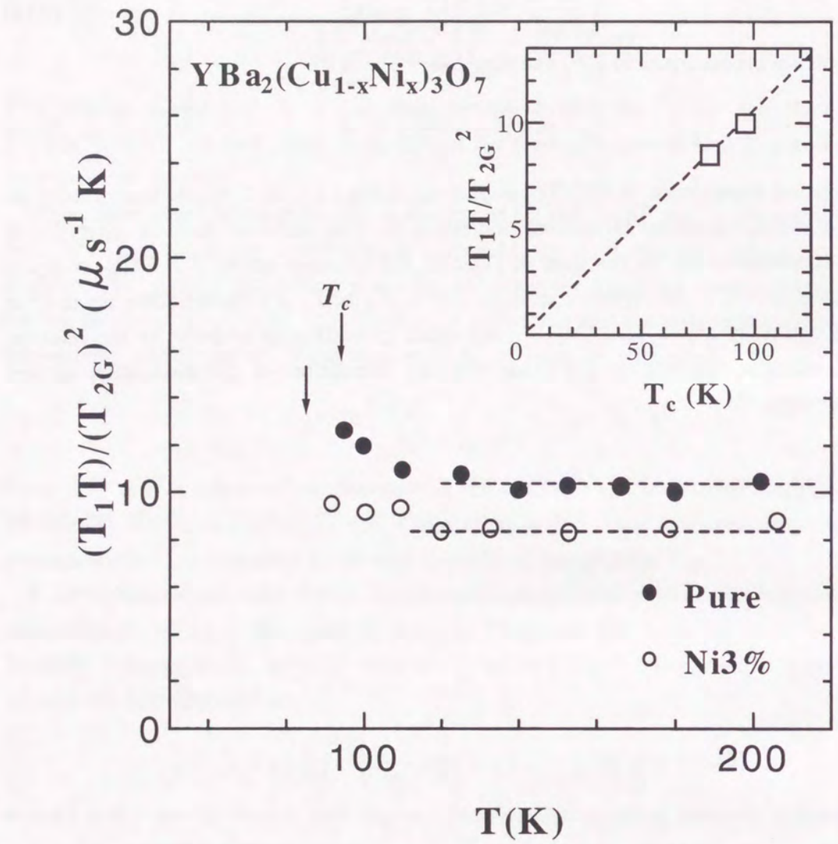

Figure 2.12: T-dependence of T_1T/T_{2G}^2 at Cu(2) sites in $YBa_2(Cu_{1-x}Ni_x)_3O_7$. The inset shows the constant values of $T_1T/T_{2G}^2 \propto \chi_Q\Gamma_Q$ plotted against T_c

2.5 Summary

It has been found from the T_1 and T_{2G} measurement for Cu(2) that T_c is intimately correlated with the Cu-AF spin fluctuation that governs $1/^{63}T_1$ and $1/^{63}T_{2G}$. In the normal state, we found that all the $1/T_1$ and $1/T_{2G}$ data are on a universal curve, when they are plotted against $t = T/T_c(x)$ in the normal state and even just below T_c. From the universal scaling formula of $1/T_1T$ against $t = T/T_c$, we have the novel relation between T_c and the characteristic energy of the Cu-AF spin fluctuation, Γ_Q;$T_c \propto \Gamma_Q(x,t)$. Furthermore, by combining with the universal scaling of $1/T_{2G}$, we can obtain the relation, $T_c \propto \Gamma_Q\xi^2$, which has been proposed by the theoretical model based on the spin-fluctuation-induced mechanism for the d-wave superconductivity. It is concluded that the suppression of T_c with Ni substitution in $YBa_2Cu_3O_7$ is caused by the decrease in Γ_Q rather than by either magnetic or potential impurity scattering.

Our results provides *a direct experimental evidence for the attractive force to be magnetic in origin* irrespective of the theoretical model, furthermore the analysis supports strongly spin fluctuation mediated mechanism for superconductivity.

Bibliography

[1] Y. Kitaoka, S. Hiramatsu, T. Kondo and K. Asayama, J. Phys. Soc. Jpn. **57**, 30 (1988).

[2] T. Imai, T. Shimizu, H. Yasuoka, Y. Ueda and K. Kosuge, J. Phys. Soc. Jpn. **57**, 2280 (1988).

[3] J. A. Martindale, S. E. Barrett, K. E. O'Hara, C. P. Slicher, W. C. Lee and D. M. Ginsberg, Phys. Rev. B **47**, 9155 (1993).

[4] P. C. Hammel, M. Takigawa, R. H. Heffner, Z. Fisk and K. C. Ott, Phys. Rev. Lett. **63**, 1992 (1989).

[5] M. Takigawa: in Dynamics of Magnetic Fluctuations in High Temperature Superconductors, eds. G. Reiter, P. Horsch and G. Psaltakis (Plenum, New York).

[6] S. Ohsugi Y. Kitaoka, K. Ishida and K. Asayama, J. Phys. Soc. Jpn. **60**, 2351 (1991).

[7] Y. Kitaoka, K. Fujiwara, K. Ishida, K. Asayama, Y. Shimakawa, T. Manako and Y. Kubo, Physica **C179**, 107 (1991).

[8] C.H. Pennington, D.J.Durand, C.P. Slichter, J.P. Rice, E.D. Bukowski and D.M. Ginsberg, Phys. Rev. B**39**, 274 (1989): C.H. Pennington and C.P. Slichter, Phys. Rev. lett. 66, 381 (1991).

[9] T. Imai, C. P. Slichter, A. P. Paulikas and B. Veal, Phys. Rev. B**47**, 9158 (1993).

[10] R. E. Walstedt and S-W. Cheong, Phys. Rev. B**51**, 3163 (1995).

[11] K. Ishida, Y. Kitaoka, T. Yoshitomi, N. Ogata, T. Kamino and K. Asayama, Physica **C179** (1991) 29.
K. Ishida, Y. Kitaoka, N. Ogata, T. Kamino, K. Asayama, J. R. Cooper and N. Athanassopoulou, J. Phys. Soc. Jpn **62**, 2803 (1993).

[12] K. Ishida, Y. Kitaoka, K. Asayama, K. Kadowaki and T. Mochiku, J. Phys. Soc. Jpn **63**, 1104 (1994).

[13] Y. Kitaoka, K. Ishida and K. Asayama, J. Phys. Soc. Jpn. **63**, 2052 (1994).

[14] R. Dupree, A. Gencten and D. McK. Paul, Physica **C193**, 81 (1992).

[15] T. Kajitani, K. Kusaba, M. Kikuchi, Y. Syono and M. Hirabayashi, Jpn. J. Appl. Phys. **27**, L354 (1988).

[16] S. A. Hoffman, M. A. Castro, G. C. Follis and S. M. Durbin, Phys. Rev. **B49**, 12170 (1994).

[17] H. Shaked *et al.*, Solid State Commun. **75**, 445 (1990).

[18] P. Mendels, H. Alloul, G. Collin, N. Blanchard, J. F. Marucco and J. Bobroff: Physica **C235**, 1595 (1994).

[19] H. Yamagata *et al*, Physica **C185** 1101 (1991)

[20] Y. Tokunaga, K. Ishida, Y. Kitaoka and K. Asayama, Czech. J. Phys. 46 suppl. S2 1139 (1996).

[21] K. Kumagai and F. Y. Fradin, Phys. Rev. **B27**, 2770 (1983).

[22] A. J. Millis, H. Monien and D. Pines, Phys. Rev. **B42**, 167 (1990) .

[23] K. Magishi, Y. Kitaoka, G.-q. Zheng, K. Asayama, K. Tokiwa, A. Iyo and H. Ihara, J. Phys. Soc. Jpn. **64**, 4561 (1995) .

[24] K. Magishi, Y. Kitaoka, G.-q. Zheng, K. Asayama, T. Kondo, Y. Shimakawa, T. Manako and Y. Kubo, Phys. Rev. B **54**, 10131 (1996).

[25] T. Moriya, Y. Takahashi and K. Ueda, J. Phys. Soc. Jpn. **59**, 2905 (1990); T. Moriya and K. Ueda, J. Phys. Soc. Jpn. **63**, 1871 (1994).

[26] D. Pines, Physica **B163**, 78 (1990); P. Monthoux and D. Pines, Phys. Rev. **B49**, 4261 (1994).

[27] T. Nakano, N. Momono, T. Nagata, M. Oda and M. Ido, Phys. Rev. B**58** 5831 (1998)

[28] R.L. Corey, N.J. Curro, K. O'Hara, T. Imai, C.P. Slichter, K. Yoshimura, M. Katoh and K. Kosuge, Phys. Rev. B**53**, 5907 (1996); N. J. Curro, T. Imai, C. P. Slichter and B. Dabrowski, Phys. Rev. B**56**, 877 (1997).

Chapter 3

^{63}Cu -NMR Study in $Bi_2Sr_2CaCu_2O_{8+\delta}$

3.1 Introduction

In underdoped cuprates, there is considerable evidence that the pseudogap in the magnetic and electronic excitation spectra is already formed in the normal state above T_c. From studies of the magnetic excitation spectrum [1, 2, 3, 4, 5], the spin-gap behavior was first reported and the pseudogap in the electronic excitation spectrum later from a variety of other probes [6, 7, 8, 9, 10, 11]. Recent studies by Ding*et al* and Harris*et al* of angle-resolved photoemission spectroscopy (ARPES) in underdoped $Bi_2Sr_2CaCu_2O_{8+\delta}$ (Bi2212) revealed that the pseudogap with d-wave symmetry opens below $T^*_{\rm ARPES} \sim 170$K and 225K respectively, and these authors suggested that the pseudogap develops into the d-wave superconducting gap once phase coherence is established below T_c [7, 8, 9]. The result was interpreted as evidence in favor of a preformed d-wave gap. The $T^*_{\rm ARPES}$ seems to increase above $\sim$ 300 K in the underdoped Bi2212 with T_c=10 K [7].

It was reported on underdoped $YBa_2Cu_3O_{6.6}$ ($YBCO_{6.6}$) that the Knight shift $K(T)$ decreases upon cooling from $T_{\rm mK}$[4], whereas the spin-lattice relaxation rate divided by temperature, $1/T_1T$ has a broad maximum around $T^* \sim$ 150 K far above T_c but below T_{mK} [1, 2, 3]. Recently, this behavior was also found in underdoped Hg-based compounds with mono- and three CuO_2 layers[12, 13, 14]. The anomalous suppression in the spectral weight of the low-energy spin-dynamics below T^* is referred as a *spin-gap* behavior[1] and was confirmed by subsequent neutron experiments[5]. However, the $1/T_1T$ in underdoped $La_{2-x}Sr_xCuO_4$ (LSCO) [15] does not show the spin-gap behavior, but increases continuously close to T_c, whereas the spin susceptibility deduced from the $K(T)$ in underdoped LSCO undergoes a continuous decrease below T_{mK}[15, 16, 17]. On the other hand, Loram *et al* suggested from susceptibility and high-resolution specific heat measurements that *pseudogap* is developed below T_{mK} upon cooling in the normal state quasiparticle spectrum[18]. The anomalies around T_m is also shown from measurements of Hall coefficients and thermoelectric power in LSCO[19]. There is as yet no general consensus on a consistent interpretation of these magnetic anomalies related to the Knight shift and $1/T_1T$.

Even in the NMR community, there is no consensus about this issue. As a matter of fact,

Yasuoka *et al* insisted that the decrease in $1/T_1T$ below T^* is ascribed to an opening of a pseudogap in the antiferromagnetic(AF) spin excitation spectrum, and estimated from the rapid decrease in $1/T_1T$ between T_c and T^* that an *activated-gap* size, Δ_{T_1} is in a range of 13$\sim$18 meV for various underdoped compounds[20]. Although they stressed that this spin gap should not be directly related to the superconducting gap, they considered that the appearance of the spin gap is likely to be related to the mechanism of high-T_c superconductivity. On the other hand, Williams et al. claimed that the reduction in Knight shift from T_{mK} is due to the presence of a pseudogap with the *d-wave symmetry* in the quasiparticle density of states (DOS) in the normal state [21]. They analyzed the decreasing behavior of $K(T)$ over the entire temperature range by assuming a gap comprising the pseudogap (E_g) and the superconducting gap (Δ_s), $\Delta^2 = \Delta_s^2 + E_g^2$ and claimed that since E_g scales to a maximum value of T_c in various cuprates, the pseudogap and the superconducting gap have a similar energy scale. In their analyses, however, the spin-gap behavior in $1/T_1T$ was ignored completely. In addition, Bobroff et al. claimed from the ^{17}O Knight shift, $^{17}K(T)$ measurement on underdoped $HgBa_2CuO_{4+\delta}$ that $^{17}K(T)$ extrapolates to zero at $T > 0$, which indicates the opening of a pseudogap at $T^* > T_c$[12]. They considered that the pseudogap temperature T^* may be defined as a crossover temperature between the decreasing behavior and the flat high temperature part in $^{17}K(T)$. The different temperature dependence of $1/T_1T$ and $K(T)$ has never been interpreted in a consistent manner on a same footing.

In this chapter, we present the NMR results in the single crystal $Bi_2Sr_2CaCu_2O_{8+\delta}$ for a doping range from underdoping to overdoping . In the normal state, $1/T_1T$ has a broad maximum around T^*, showing the spin-gap behavior. We found that the ^{63}Cu Knight shift, $K(T)$, also exhibits the steep decrease below $T_K^* \sim T^*$, indicating that the pseudogap opens not only in the AF spin excitation spectrum at low energy around $\boldsymbol{Q} = (\pi, \pi)$ but also in the quasiparticle DOS. In all the samples, we found that $1/T_{2G}$ starts to decrease at a certain temperature, T_c^*, which is higher than the bulk superconducting temperature (T_c) and lower than T^*. These diminution of $1/T_{2G}$ as well as K and $1/T_1T$ below T_c^* suggest that the formation of local Cooper pairing without global phase coherency. Based on our NMR results, we develop the phase diagram in the Bi2212 system which is sketched by three crossover temperature, T_{mK}, T^* and T_c^* below which K, $1/T_1T$ and $1/T_{2G}$ start to decrease, respectively. The magnetic scaling behaviors between $1/T_1T$ and $1/T_{2G}$ will be also discussed.

3.2 Experimental Procedures

Single crystals of Bi2212 were synthesized by the FZ method. Underdoped (T_c=79 K) and overdoped (T_c=77.3 K) single crystals were prepared by annealing at 600 °C under $P(O_2)=4.67\times10^{-4}$ (atm) for one day and under $P(O_2)$=2.1 (atm) for three days, respectively. The temperature width in the superconducting transition is about 3 K for both samples. The superconducting fraction in the underdoped and overdoped samples is nearly the same, since the size of the diamagnetic shielding signal for each is comparable. From the dependence of T_c on carrier-hole concentration p per the CuO_2 plane[36], p in the underdoped and overdoped samples is estimated to be $\sim$ 0.125 and $\sim$ 0.225, respectively. The ^{63}Cu Knight shift, K, and the nuclear spin-lattice relaxation time, T_1, were measured at the frequency of 178.1 MHz using a 16 T (4.2 K) superconducting magnet. T_1 was measured by the saturation recovery method. Above 40 K, a single component of T_1 was determined by fitting the recovery of the nuclear magnetization, $M(t)$ after saturation pulses to the theoretical relaxation function $[M(\infty) - M(t)]/M(t) = 0.1\exp(-t/T_1) + 0.9\exp(-6t/T_1)$. The $1/T_{2G}$ of ^{63}Cu was measured at the frequency range between 49.1 and 85.1 MHz ($H = 4.3 \sim 7.5$ T) for the central transition line ($I_z = 1/2 \leftrightarrow -1/2$) to obtained the narrow NMR linewidth. To investigate an evolution of magnetic behavior with respect to hole content, we include the previous results of the $1/T_1T$, $1/T_{2G}$ and the Knight shift in optimally-doped Bi2212 ($T_c \sim$ 86 K, $p \sim$ 0.20)[24, 25]. NMR data in overdoped Bi2212 (T_c=77 K) have already been reported by Walstedt *et al*[26]. The present NMR results in the overdoped Bi2212 is found to be consistent with their results.

Spin-echo amplitude E was recorded as a function of the time τ between the first and second pulses, and the Gaussian part of decay, T_{2G} , was extracted by fitting to the function,[27, 28]

$$E(2\tau) = E_0 \exp\left[-\left(\frac{2\tau}{T_{2L}}\right) - \frac{1}{2}\left(\frac{2\tau}{T_{2G}}\right)^2\right] \tag{3.1}$$

where $1/T_{2L}$ is the Lorentzian spin-echo decay rate associated with the T_1 process. $1/T_{2L}$ was determined using the relation $1/T_{2L} = (3 + R)/T_1$, where R is the anisotropy ratio.[29]

Since T_{2G} arises through a magnetic interaction between a nuclear spin and nuclear spins in neighbors because of the change in precession frequency of a nucleus resulting from the inversion of neighbor spin, it is needed to measure $1/T_{2G}$ in the condition when these neighbors are uniformly flipped by the rf pulse. Therefore, one must pay attention to the size of the rf excitation amplitude (H_1) compared to the width of the resonance line, ΔH, in NMR measurement of $1/T_{2G}$. In the case of $H_1 \gg \Delta H$, it is sure that the rf pulse flips the most part of the neighbors. On the other hand, in the case of $H_1 \leq \Delta H$ there is no such an assurance, however the effect of line converge can be tested by measuring T_{2G} as a function of the magnitude of H_1. The relation between $H_1/\Delta H$ and $1/T_{2G}$ obtained at 90K, where ΔH has the maximum value for underdoped Bi2212, is shown in Fig.3.1, where H_1 is estimated from the width of the 1st excitation pulse. $1/T_{2G}$ is hardly dependent upon H_1 for $H_1/\Delta H \geq 0.6$ under magnetic field $H_0 \sim 5$ T (57.1 MHz) where ΔH are $\sim$ 175 Oe. We checked that this relation between $H_1/\Delta H$ and $1/T_{2G}$ also holds under the different magnetic filed, $H_0 \sim 7.5$ T (85.1 MHz) with

$\Delta H \sim 230$ Oe. The results in Fig.3.1 shows that we can reduce H_1 to small values compared to the line width: e.g. $H_1/\Delta H \geq 0.6$ at 90K for underdoped Bi2212. This indicates that the field gradients which give rise to the line width are slowly varying with position in the crystallites relative to the range of the spin-spin coupling, as discussed by Corey *et al.* in $YBa_2Cu_4O_8$.[37] All of our $1/T_{2G}$ measurements were carried out in this H_1 range where $1/T_{2G}$ is not dependent on the magnitude of H_1.

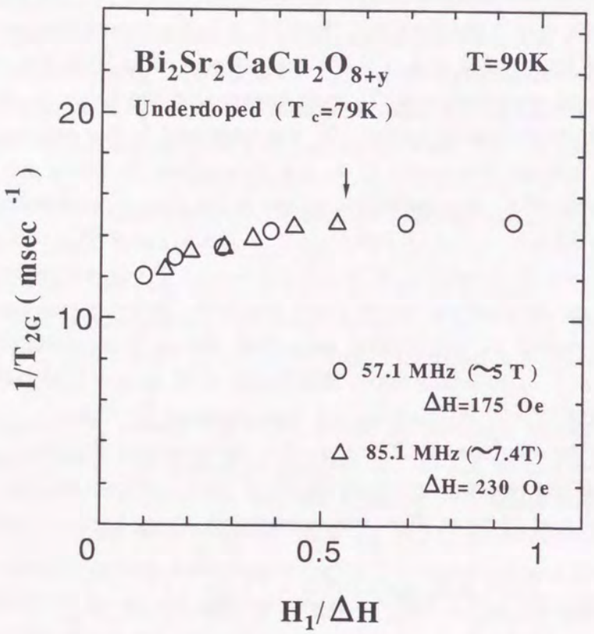

Figure 3.1: The relation between $H_1/\Delta H$ and $1/T_{2G}$ obtained at 90K for underdoped Bi2212

3.3 Experimental Results

3.3.1 Knight shift

T-dependent part of the Knight shift $\Delta K(T) = K_{obs} - K(4.2\text{ K})$ is shown in Fig.3.2, together with the data in the optimally-doped Bi2212 reported previously [24, 25]. In the optimally-doped Bi2212, since the accuracy of the ^{63}Cu Knight shift is poor, the $\Delta^{17}K(T)$ deduced from the ^{17}O Knight shift data reported by Takigawa et al, are also plotted for comparison[25]. The ΔK_c in the underdoped Bi2212 decreases linearly in the range of 200 K$-$300 K, whereas it undergoes a marked decrease below $T_K^* \sim 200$ K, exhibiting a small anomaly at T_c. In contrast, the ΔK_c in the optimally doped and the overdoped Bi2212 decreases gradually below $T_{mk} \sim 203$ and ~ 100 K from a constant value in temperatures higher than T_{mk} and steeply decrease below $T_k^* \sim 123$ K and $T_c \sim 77.3$ K, respectively.

For each compound, the decreasing behavior in $\Delta K(T)$ is different, reflecting their different doping level.

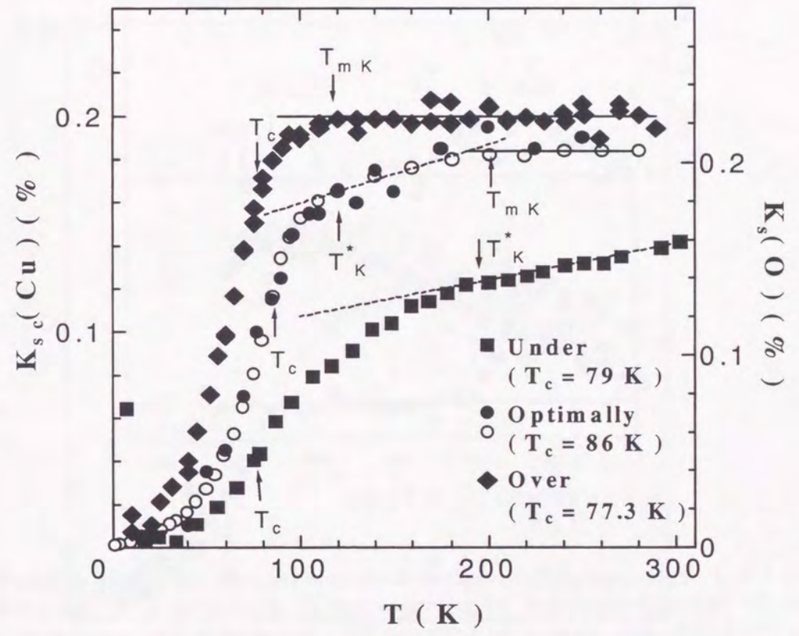

Figure 3.2: T-dependent spin part K_{cs}(Cu) in K_c in under-, optimally- and over-doped Bi2212. The T-dependent spin part K_s(O) in the ^{17}O Knight shift in optimally-doped Bi2212 reported by Takigawa et al. is also plotted by open circles ([25]).
The anomalies at T_c, T_K^* and T_{mK} are indicated by arrows. (see text.)

In order to characterize the respective T variation in $\Delta K(T)$ upon cooling, we plot in Fig.3.3

the temperature-derivative change in $\Delta K(T)$, $dK(T)/dT$ as a function of temperature. From the respective behavior for the underdoped and optimally-doped Bi2212 in Fig.3.3, two characteristic temperatures of T_{mK} and T_K^* are defined as the temperatures where $dK(T)/dT$ begins to increase from zero and increase steeply from a finite value, respectively. In the optimally-doped Bi2212, $T_{mK} \sim 203$ K and $T_K^* \sim 123$ K are deduced. In the underdoped Bi2212, T_{mK} shifts to a temperature higher than room temperature and $T_K^* \sim 200$ K. By contrast, T_K^* and T_{mK} in the overdoped Bi2212 can not be exactly distinguished from one another as seen in Fig.3.3.

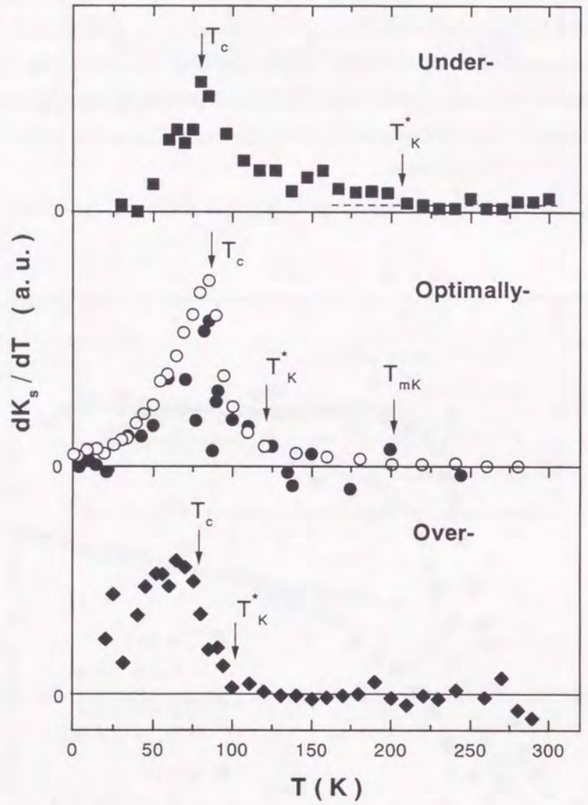

Figure 3.3: T dependence of T-derivatives of the spin part in ^{63}Cu Knight shift for (a) underdoped, (b) optimally-doped and (c) overdoped Bi2212. Open circle in (b) is the T-derivatives in the ^{17}O Knight shift reported by Takigawa([25]). Arrows show the anomalies at T_c, T_K^* and T_{mK}.

3.3.2 Nuclear spin-lattice relaxation rate, $1/T_1$

Figure 3.4 shows the T dependence of $1/T_1T$ in the underdoped and overdoped Bi2212 together with the data in the optimally-doped Bi2212[24]. The $1/T_1T$ in the underdoped Bi2212 reveals a broad maximum around $T^* \sim 210$ K and continues to decrease without any clear change at T_c. The value of $1/T_1T$ at T_c has decreased to 34% of its value at T^*, which is lower than the underdoped $YBa_2Cu_3O_{6.6}$ (63%)[3] and $YBa_2Cu_4O_8$(57%)[30], and is comparable with that in the underdoped $HgBa_2CuO_{4+\delta}$ with T_c=80K (27%)[13]. In the optimally-doped and the overdoped Bi2212, T^* is reduced to $\sim$ 130 K and $\sim$ 100 K, respectively. In contrast to the underdoped Bi2212, the steep decrease in $1/T_1T$ is clear below T_c for both the samples. A striking result is that T^* is close to T_K^* for the underdoped and optimally-doped Bi2212. Even in the overdoped Bi2212, T^* is close to $T_{mK} \sim T_K^*$. These results provide evidence that the spin-gap behavior in $1/T_1T$ below T^* has the same origin as the pseudogap behavior in the quasiparticle DOS below T_K^*.

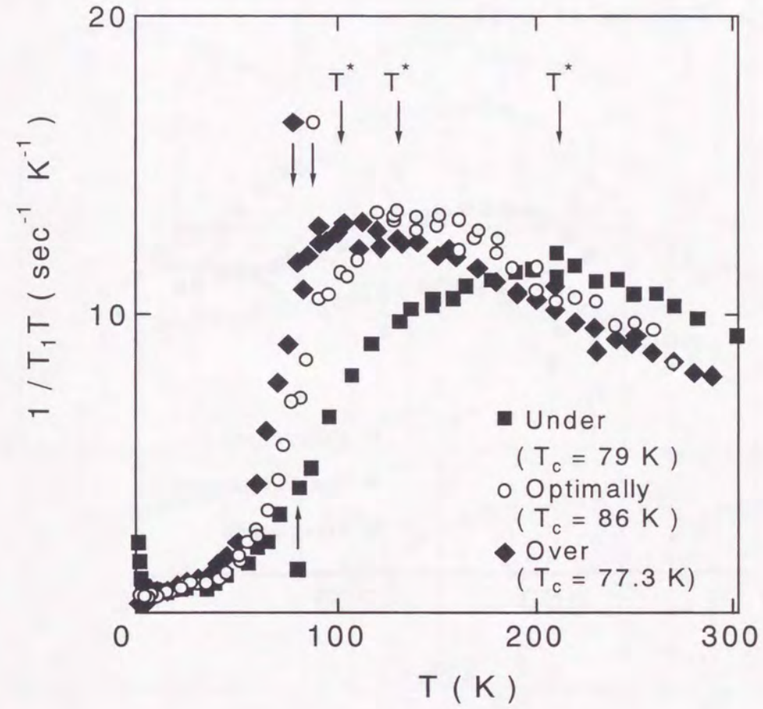

Figure 3.4: T dependence of $1/T_1T$ in under-, optimally- and overdoped Bi2212. Arrows indicate T_c and T^* for each compound.

3.3.3 Gaussian spin-echo decay rate, $1/T_{2G}$

In Figs.3.5, we plot the T dependence of $1/T_{2G}$ for under, optimally and overdoped Bi2212, respectively. We can see that $1/T_{2G}$ in three samples shows the following characteristic behavior. Below 300K, $1/T_{2G}$ increases gradually with decreasing T, and saturates with nearly T-independent value at T^*_{TG}. With further decreasing T, $1/T_{2G}$ starts to decrease at a certain temperature denote as T^*_c, which is higher than T_c. In the under-(optimum-)doped Bi2212, it is estimated that T^*_{TG} is $\sim$ 180 (140) K, and T^*_c is $\sim$ 120 (115) K, respectively. In the overdoped Bi2212, we can identify that $T^*_c \sim 95K$, however the saturation temperature, T^*_{TG} ($\sim$ 120 K) is not obvious due to the dull increase of $1/T_{2G}$. The enhancement of $1/T_{2G}$ with decreasing T is progressively suppressed with hole- doping. This suggests that the AFM correlation length ξ, which governs $1/T_{2G}$, decreases with increasing hole content, in consistent with other experimental results.

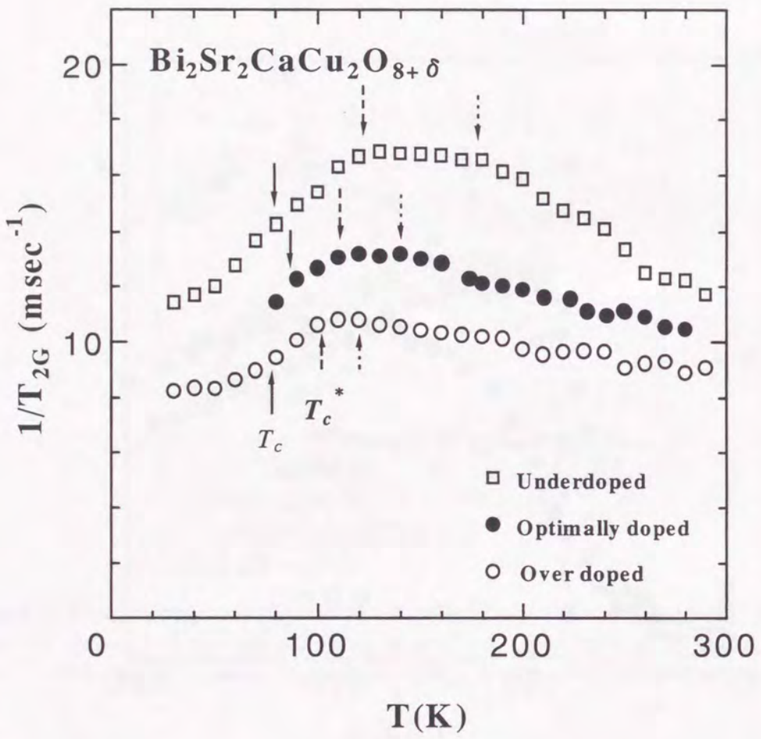

Figure 3.5: Temperature dependence of $1/T_{2G}$ for under, optimally and overdoped Bi2212.

3.4 Discussion

In order to consider the implication of the characteristic temperatures seen in K, $1/T_1T$ and $1/T_{2G}$ and to investigate the evolution of the normal-state magnetic excitation, we plot together their temperature dependence in the normal state in Fig.3.6.

Since $1/T_1T$ and $1/T_{2G}$ continues to increase between T_{mK} and T^* where K decreases gradually as seen in Figs.3.6, the likely cause for the gradual decrease in $K(T)$ is associated with the development of AF-spin correlations towards T^*, which is also suggested from the recent theoretical studies[31, 32]. In the gapless quantum-spin systems such as one dimensional S=1/2 linear spin-chain Sr_2CuO_3[33] and three-leg spin-ladder $Sr_3Cu_2O_5$[34], the gradual decrease in susceptibility was observed as temperature decreases. This means that the gradual decrease in static susceptibility in the underdoped and optimally-doped Bi2212 is not always related with the opening of the pseudogap.

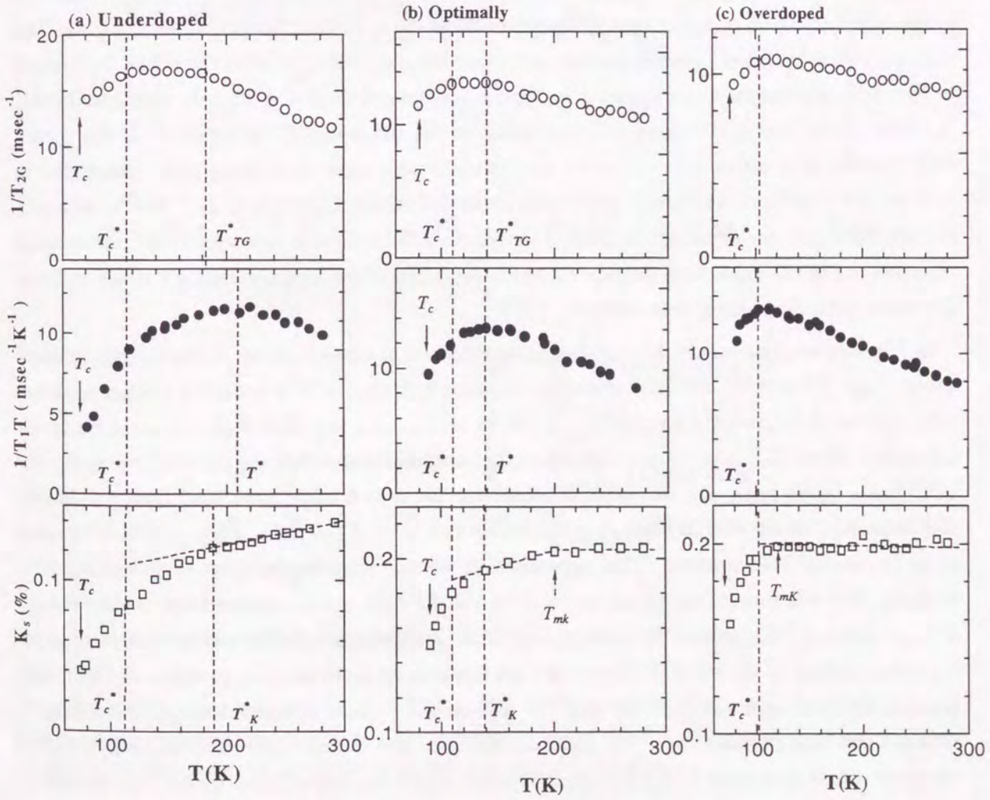

Figure 3.6: T-dependence of $1/T_{2G}$ is plotted together with $1/T_1T$, K_s for (a)underdoped (b)optimally doped (c)overdoped Bi2212, respectively.

Rather, the sharp decrease in $^{63}K(T)$ below T_K^*, where $1/T_1T$ starts to decrease, should be ascribed to the opening of the pseudogap. We note that an extrapolation of pronounced decrease in $K(T)$ in the normal state near T_c intercepts to the temperature axis at $T > 0$ in the $\Delta K(T)$ vs T plot in Fig.3.2. This feature is consistent with the ^{17}O Knight shift data in underdoped $HgBa_2CuO_{4+\delta}$ single-layer cuprates [12]. It is obvious that the saturation temperature of $1/T_{2G}$, T_{TG}^* is also close to T^* in underdoped and optimally doped Bi2212, implying that the development of AFM correlation length ξ is restricted below T^* by the formation of the spin-gap. The qualitatively similar relation between $1/T_1T$ and $1/T_{2G}$ was also observed in the spin-ladder systems with the spin-gap in the magnetic excitation.

The striking result is that the lower characteristic temperature T_c^* can be defined by not only $1/T_{2G}$ but also $1/T_1T$ and K_s as the temperature below which all physical quantities steeply decrease toward T_c . This result suggests the existence of a second crossover in the pseudogap state below T^*. T_c^* is observed at $T \sim 120K$ in underdoped Bi2212, and then decrease with doping to $\sim$ 115 K in optimally doped and to $\sim$ 100 K in overdoped Bi2212. A possible explanation for this significant reduction decreases of $1/T_{2G}$ as well as K and $1/T_1T$ below T_c^* is that the formation of a the local Cooper pairing without global phase coherency. Indeed, the temperature separation between pairing and phase coherency arising from the phase fluctuation of the order parameter was suggested by several theoretical studies in high-T_c cuprates.[43, 44] In these phase fluctuation scenario, the crossover temperature, T_c^* is regarded as the mean-field transition temperature where the amplitude of the superconducting order parameter is well established but there is no long-range phase coherence until below T_c . Furthermore, it is suggested that the effect of the phase fluctuation will be mostly pronounced for underdoped cuprates, since the superfluid density n_s which determines the superconductor's phase stiffness decreases with decreasing hole content.

In Fig.3.7, we show results for the doping dependence of three different characteristic temperature, T_{mK}, T^* and T_c^* obtained from the present NMR studies in the Bi2212 system together with various characteristic temperature at which an anomaly was observed by other experimental probe. Here, $T_{m\chi}$ and T_ρ^* are defined as the temperatures where the uniform susceptibility $\chi(T)$ has a broad peak and the in-plane resistivity starts to deviate downward from a T-linear-like behavior.[23] As seen in Fig.3.7, it is obvious that $T^* \sim T_K^* \sim T_\rho^* \sim T_{\rm ARPES}^*$, which increase with decreasing hole content. This agreement in various characteristic temperatures suggests strongly that the pseudogap opens not only in the AF-spin excitation spectrum at low energy around $\mathbf{Q}=(\pi,\pi)$ but also in the quasiparticle DOS. Furthermore, the tunneling spectroscopy on the same optimally-doped Bi2212 reveals that the normal-state pseudogap opens in the quasiparticle DOS around 120 K close to $T^* \sim$ 130 K [22]. Convincing evidence is increasing to indicate that the pseudogap in the quasiparticle DOS and the spin gap observed in $1/T_1T$ has the same origin in a series of Bi2212 single crystals where the doping level varies from underdoping to overdoping. By contrast, other characteristic temperatures, T_{mK} and $T_{m\chi}$, below which the Knight shift and the susceptibility decrease gradually, respectively, have nothing to do with the pseudogap formation, but provide signature for the development of AF-spin correlations.

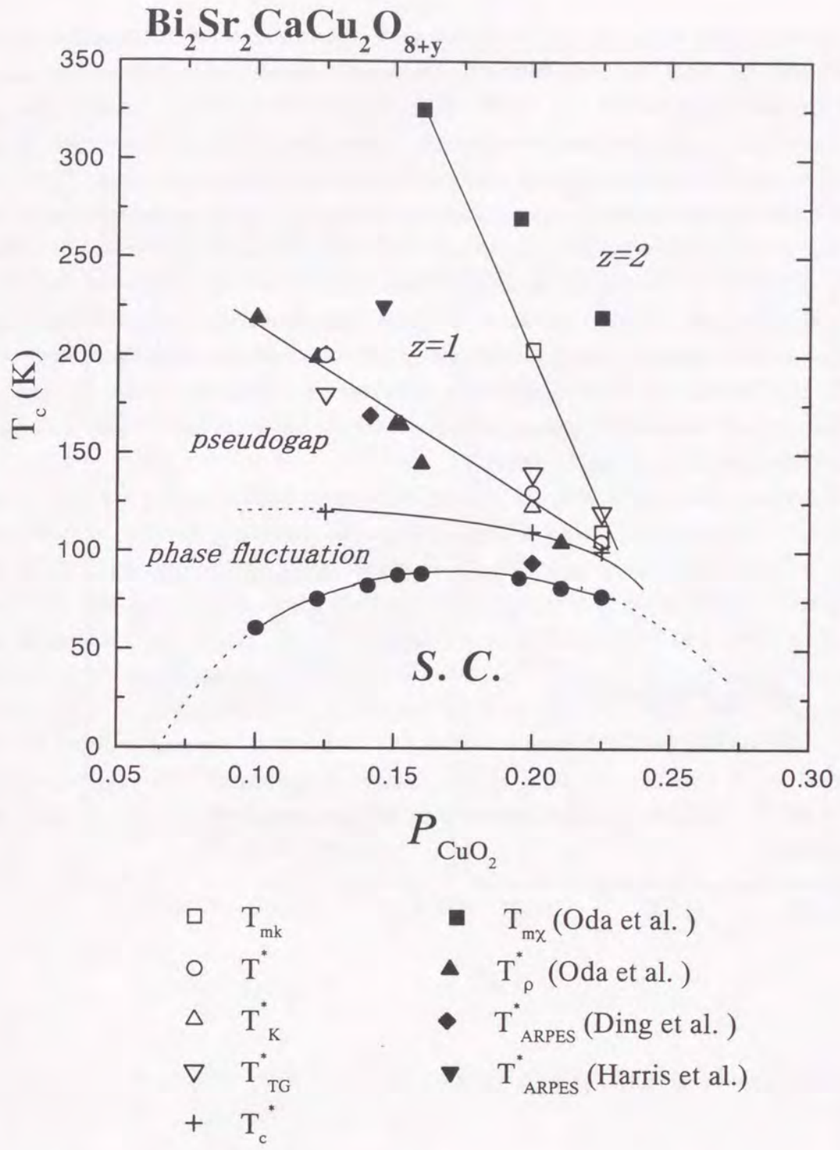

Figure 3.7: The characteristic temperatures, T_{mk}, T^* and T_c^* obtained from NMR study are plotted against hole content P_{CuO2} together with various characteristic temperature at which an anomaly was observed by other experimental probe in Bi2212.

The lower crossover temperature T_c^* appears in the pseudogap state, below which all the physical quantities steeply decrease toward T_c . It should be noted that the doping dependence of T_c^* is different from those of T_{mK} and T^*. Both T_{mK} and T^* drastically increases when the holes are decreased toward the phase boundary, providing the evidence that these crossovers are intimately correlate to the development of AFM correlations. On the other hand, T_c^* has the saturate tendency below optimum concentration, which is reasonably consistent with the doping dependence of the mean-field value of transition temperature calculated by several authors from the point of the AFM spin-fluctuation-induced mechanism.[44, 47, 48] We propose that T_c^* is the mean-field transition temperature below which the amplitude of the order parameter is well established, however phase fluctuations cause the global superconducting transition occur at T_c below T_c^*. It is, however, still open question how three characteristic crossover temperatures, T_c^*, T^* and T_{mK} behave near the phase boundary. The NMR studies in the underdoped compounds near the phase boundary are highly desired.

Finally we comment on the magnetic scaling behavior in Bi2212 derived from $1/T_1T$ and $1/T_{2G}$ results. The magnetic scaling is often employed to characterize the normal-state magnetic excitation in high-T_c cuprates.[37, 38, 39, 40, 41, 42] In Fig.3.8, the rations $T_1T/(T_{2G})$ and T_1T/T_{2G} are plotted together as a function of temperature for under, optimally and overdoped Bi2212. It is found that T-independent behavior in $T_1T/(T_{2G})^2$, that is $z = 2$ scaling characteristic of the mean-field non-universal regime is observed above the temperature of $\sim$ 180(120) K in optimally-(over-)doped Bi2212, which is close to $T_{mK} \sim$ 203 (120) K. It is also found that T_1T/T_{2G} becomes constant above $T \sim$ 240 (140) K in under- (optimally-) doped Bi2212, as expected in $z = 1$ scaling, signalling to the quantum critical regime. The magnetic scaling behaviors seen in Bi2212 are quite consistent with the results reported by Curro *et al.*[42] and Pines *et al.*[38].

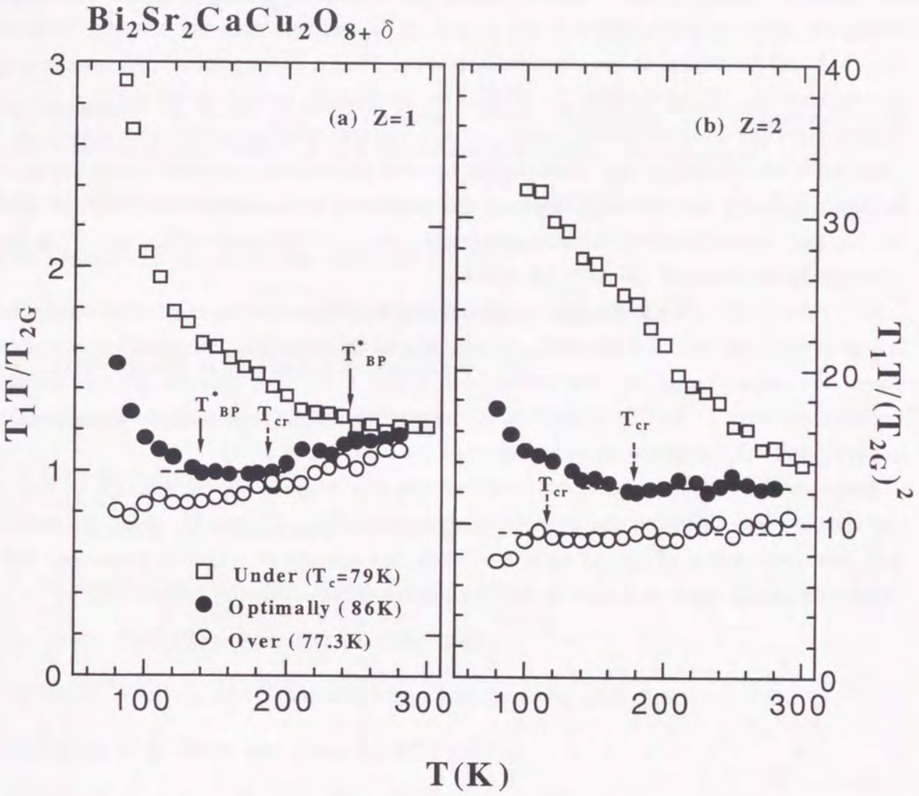

Figure 3.8: T dependencies of (a) $(T_1T)_c/T_{2G}$ and (b) $(T_1T)_c/(T_{2G})^2$ for under, optimally and overdoped Bi2212.

3.5 Summary

In the underdoped Bi2212, a broad peak in $1/T_1T$ was observed at $T^* \sim 210$ K where the steep decrease in $K_s(T)$ occurred, deviating from a T-linear-like gradual decrease below a much higher temperature T_{mk} from which $K(T)$ starts to decrease. This result verified that the antiferromagnetic (AFM) spin excitation spectrum at low energy around $Q = (\pi, \pi)$ is correlated with the static susceptibility at $q = (0, 0)$, and that spin-gap behavior observed in $K_s(T)$ should be defined as the steep decrease from T^*, not as the gradual decrease from T_{mK}. It was noted that T^* agrees with the ARPES results that the gap opens below $T^*_{ARPES} \sim 170K$ reported by Ding *et al* and 225K by Harris *et al* for samples with the same doping level[7, 9]. The remarkable coincidence among these gaplike features led us to the conclusion that the spin-gap behavior in $1/T_1T$ has the same origin as the pseudogap in DOS evidenced from the ARPES results, and hence that the gradual decrease observed in $K(T)$ between T_{mK} and T^* is related with the development of the AFM correlation.

In addition, from the systematic measurement of $1/T_{2G}$, we found the low temperature crossover at T_c^* below T^* but above T_c , which suggests the formation of the incoherent preformed pairs. We propose from the relation between $1/T_1T$ and $1/T_{2G}$ that the gradual pseudogap behavior between T^* and T_c^* is ascribed to the magnetic origin, and that the sharp pseudogap behavior below T_c^* is to the precursor effect of the superconductivity.

Based on these NMR results, we developed the new magnetic phase diagram of Bi2212 in the normal state, including the crossover temperatures, T_{mK}, T^* and T_c^*, which are associated with the development of the AF-spin correlation, the opening of magnetic pseudogap and the phase-fluctuating superconductivity with incoherent preformed pairs, respectively.

Bibliography

[1] H. Yasuoka, T. Imai and T. Shimizu, *Strong Correlation and Superconductivity* (H.Fukuyama, S.Maekawa and A.P.Malozemoff eds.) p.254, Springer-Verlag.

[2] W. W. Warren *Jr. et al.*, Phys. Rev. Lett. **62**, 1193 (1989).

[3] M. Takigawa *et al.*, Phys. Rev. B**43**, 247 (1991).

[4] H. Alloul, T. Ohno and P. Mendels, Phys. Rev. Lett. **63**, 1700 (1989).

[5] J. Rossat-Mignod *et al*, Physica B **186-188**, 1 (1993).

[6] for exmaple, see Physica C **282-287**, (1997).

[7] H. Ding *et al*, Nature **382**, 51 (1996).

[8] A. G. Loeser *et.al.*, Science **273**, 325 (1996).

[9] J. M. Harris *et al*, Phys. Rev. B, **54**, R15665 (1996).

[10] J. Loram *et al.*, Phys. Rev. Lett.**71**, 1740 (1993).

[11] T. Ito, K. Takenaka and S. Uchida, Phys. Rev. Lett. **70**, 3995 (1993).

[12] J. Bobroff *et al.*, Phys. Rev. Lett. **78**, 3757 (1997).

[13] Y. Itoh *et al.*, J. Phys. Soc. Jpn. **65**, (1996) 3751; *ibid*, J.Phys. Soc. Jpn. **67** (1998).

[14] M. -H. Julien *et al.*, Phys. Rev. Lett. **76**, 4238 (1996).

[15] S. Ohsugi *et al.*, J. Phys. Soc. Jpn. **63**, 700 (1993).

[16] K. Ishida *et. al.*, J. Phys. Soc. Jpn. **60**, 3516 (1991).

[17] G.-q. Zheng *et. al.*, Physica C **208** 339 (1993).

[18] J.W.Loram, K.A.Mirza, J.M.Wada, J.R.Cooper and W.Liang, Physica C **235-240** 134 (1994).

[19] T. Nishikawa *et al.*, J. Phys. Soc. Jpn. **63**, 1441 (1994).

[20] H.Yasuoka, Physica C **282-287**, 119 (1997).

[21] G. V. M. Williams *et al.*, Phys. Rev. Lett **78**, 721 (1997).

[22] N. Nishida *et. al.*, private communication (to be published in Physica C)

[23] M. Oda *et al.*, Physica C **281**, 135 (1997).

[24] K. Ishida *et.al.*, J. Phys. Soc. Jpn. **63**, 1104 (1994); *ibid* Physica C **263**, 371 (1996).

[25] M. Takigawa and D. B. Mitzi, Phys. Rev. Lett. **73**, 1287 (1994).

[26] R. E. Walstedt, R. F. Bell, and D. B. Mitzi, Phys. Rev. B **44**, 7760 (1991).

[27] C.H. Pennington, D.J.Durand, C.P. Slichter, J.P. Rice, E.D. Bukowski and D.M. Ginsberg, Phys. Rev. B**39**, 274 (1989).

[28] C.H. Pennington and C.P. Slichter, Phys. Rev. lett. 66, 381 (1991).

[29] R. E. Walstedt and S-W. Cheong, Phys. Rev. B**51**, 3163 (1995).

[30] H. Yasuoka, S. Kambe, Y. Itoh and T. Machi, Physica B **199-200**, 278 (1994).

[31] K. Miyake and O. Narikiyo, J.Phys. Soc. Jpn. **63**, 3821 (1994).

[32] J. Jaklic and P. Prelovsek, Phys. Rev. Lett. **77**, 892 (1996).

[33] T. Ami *et al.*, Phys. Rev. B **51**, 5994 (1995). N.Motoyama *et al.*, Phys. Rev. Lett. **76**, 3212 (1996).

[34] M. Azuma *et al.*, Phys. Rev. Lett. **73**, (1994) 3463. K. Ishida *et. al.*, Phys. Rev. B **53**, 2827 (1996).

[35] K.Kadowaki: in *the proc. of the Int. Workshop on Electronic Properties and Mechanism in High-T_c Superconductors.*

[36] W.A.Groen, D.M. de Leeuw, and L.F.Feiner, Physcica C**165**, 55 (1990).

[37] R.L. Corey, N.J. Curro, K. O'Hara, T. Imai, C.P. Slichter, K. Yoshimura, M. Katoh and K. Kosuge, Phys. Rev. B**53**, 5907 (1996).

[38] V. Barzykin and D. Pines, Phys. Rev. B**52** 13585 (1995)

[39] S. Chakravarty, B. I. Halperin and D. R. Nelson, Phys. Rev. B**39** 2344(1989).

[40] A. Chubukov and S. Sachdev, Phys. Rev. Lett. **71** 169 (1993)

[41] A. Sokol and D. Pines, Phys. Rev. Lett. **71** 2813 (1993)

[42] N. J. Curro, T. Imai, C. P. Slichter and B. Dabrowski, Phys. Rev. B**56** 877 (1997)

[43] V.J.Emery and S.A.Kivelson, Nature **374**, 434 (1995); Phys. Rev. Lett. **74** 3253 (1995); B.Batlogg and V. J. Emery, Nature **382**, 20 (1996)

[44] J. schmalian, S. Grabowski and K. H. Benemann, Phys. Rev. B56 R509 (1997)

[45] K. Miyake and O. Narikiyo, J. Phys. Soc. Jpn. **63**, 3821 (1994).

[46] O. Narikiyo and K. Miyake, submitted to Physica C

[47] H.Hotta, J. Phys. Soc. Jpn. **62**, 4126 (1994)

[48] T. Takimoto and T Moriya, J.Phys. Soc. Jpn. **66** 2459 (1997)

Chapter 4

^{63}Cu -NMR Study in $HgBa_2Ca_3Cu_4O_{10+\delta}$

4.1 Introduction

Extensive NMR and NQR experiments on various high-T_c cuprates have uncovered magnetic behaviors depending on their doping level. The product of the nuclear spin-lattice relaxation time T_1 and the temperature T, T_1T and the Gaussian spin-echo decay rate T_{2G}^{-1} are related to the energy of the AF relaxational mode, Γ_Q and the AF correlation length, ξ, respectively. Optimally doped [1, 2, 3] and overdoped [4] (underdoped [6, 7, 8]) cuprates exhibit $T_1T/T_{2G}^2 \propto \Gamma_Q \cdot \xi^2$=const. ($T_1T/T_{2G} \propto \Gamma_Q \cdot \xi$=const.) behavior, which was denoted as z=2 (z=1) behavior. Furthermore in $YBa_2Cu_4O_8$ (Y1248) where the pseudogap temperature T^* defined by the maximum of $1/T_1T$ is 150 K, a temperature crossover from the z=2 to the z=1 behavior around $\sim$ 500 K was reported.[9] The magnetic scenario for the pseudogap was proposed to describe the temperature crossover from the z=2 to the z=1 behavior in the normal state.[10] It is, however, not yet clear whether the pseudogap is associated with a *spin gap* signaling a non-Fermi liquid state based on a concept of a spin-charge separation,[11] or a normal-state precursor of the d-wave superconducting gap [12] or a precursor to an SDW state.[10, 13] In order to settle these underlying issues, it is desired to accumulate further systematic experimental works.

A series of mercury-based cuprate superconductors, $HgBa_2Ca_{n-1}Cu_nO_{2n+2+y}$ are of great interest. The n =1 compound with T_c =52 K is the first single layer cuprate where the large spin gap opens below the record high temperature $T^* \sim$ 280 K to date.[14] The underdoped n=3 compound with T_c=115 K shows the pseudogap behavior below $T^* \sim$ 200 K,[8] whereas the optimally doped n=3 compound exhibit a record high T_c=134 K to date. This Hg1223 consists of three CuO_2 sheets where Cu in two outer CuO_2 planes is surround by five oxygens (denoted as 5-fold) and that in one inner CuO_2 plane by four oxygens (4-fold). The 4-fold CuO_2 plane is sandwiched by two Ca layers (see Fig.4.1(a)). The z=2 behavior was observed for both the 4- and 5-fold Cu sites in the optimally doped Hg1223.[3]

In this section, we report systematic Cu-NQR and -NMR studies in order to inspect magnetic behaviors for the 4- and 5-fold Cu sites in Hg1234 comprising the four CuO_2 planes. We have

found that the 4-fold (5-fold) Cu sites are underdoped (optimally doped), exhibiting the z=1 (z=2) behavior. Regardless of their marked difference in magnetic correlations, the pseudogap behavior has been observed for both Cu sites based on measurements of Knight shift (K) and $1/T_1T$. The pseudogap temperature defined by the Knight shift is found to be $T_K^* \sim 220$ K, which is somewhat higher than $T^* \sim 190$ K defined by the maximum of $1/T_1T$. We reproduce the T dependence of K between T_K^* and T_c by a model which assumes d-wave symmetry on the pseudogap. Based on this model, the value of the pseudogap is suggested to increase linearly as the temperature is lowered from $T_K^* = 220$ K to $T_c = 123$ K.

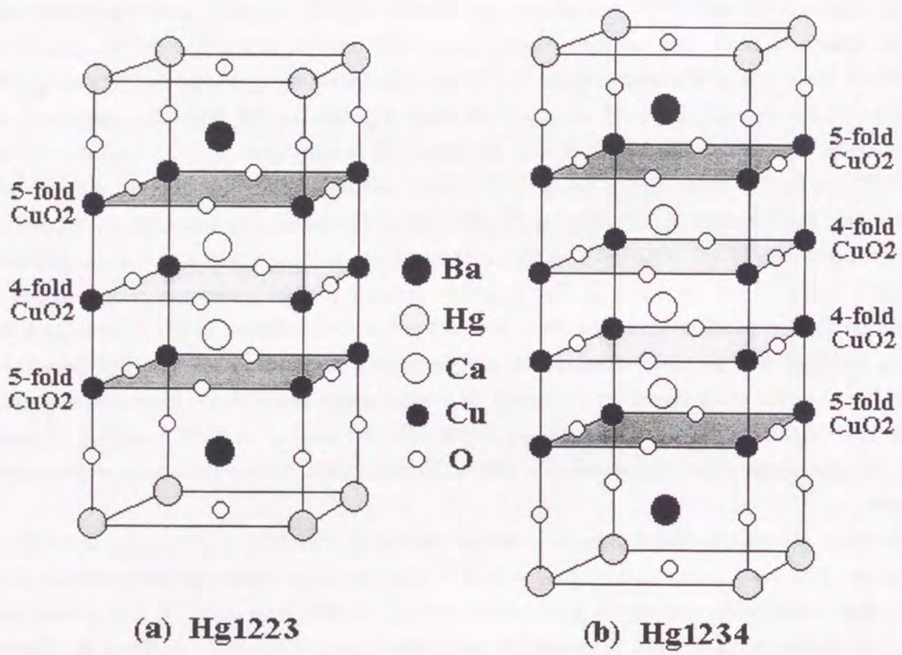

Figure 4.1: Crystal structures of $HgBa_2Ca_2Cu_3O_{8+y}$ and $HgBa_2Ca_3Cu_4O_{10+y}$.

4.2 Experimental Procedures

Polycrystal Hg1234 was prepared by the synthesis technique under high pressure as described elsewhere.[15] T_c was determined as 123 K from the ac-susceptibility measurement. The sample was confirmed to be almost of single-phase by the x-ray diffraction experiment. Pellet was crushed into powder with diameters smaller than $20\mu m$. The powder was magnetically aligned along the c axis and fixed with the stycast 1266 epoxy under the external magnetic field (H) of 16 T.

The Cu-NQR spectrum was obtained at H=0 and 4.2 K by plotting a spin-echo intensity as a function of frequency with an interval of 0.1 MHz. The Cu-NMR measurement was carried out by a conventional phase-coherent laboratory-built pulsed-NMR spectrometer using a superconducting magnet (16 T at 4.2 K). Field-swept ^{63}Cu-NMR spectrum was obtained for $H\|$ c axis and $H \perp$ c axis using a boxcar integrator. The K, $1/T_1$, and $1/T_{2G}$ of ^{63}Cu were measured at 174.2 MHz ($H \sim 15.3$ T) in a T range of 4.2−300 K. A single component of T_1 was obtained by the saturation recovery method. The nuclear-relaxation function, $R(t)$, for the central transition ($1/2 \leftrightarrow -1/2$) for $I = 3/2$ is given by [16]

$$R(t) = \frac{M(\infty) - M(t)}{M(\infty)} = 0.9\exp(-\frac{6t}{T_1}) + 0.1\exp(-\frac{t}{T_1}) \tag{4.1}$$

where $M(t)$ is the nuclear magnetization at a time t after saturation pulses. Spin-echo amplitude E recorded as a function of the time τ between the first and second pulses was well fitted to the expression [17, 18]

$$E(2\tau) = E_0\exp\left[-(\frac{2\tau}{T_{2L}}) - \frac{1}{2}\left(\frac{2\tau}{T_{2G}}\right)^2\right] \tag{4.2}$$

where $1/T_{2L}$ is the Lorentzian spin-echo decay rate associated with the T_1 process. $1/T_{2L}$ was determined using the relation $1/T_{2L} = 3(1/T_1)_{\|} + (1/T_1)_{\perp}$.[19]

4.3 Experimental Results

4.3.1 Cu-NQR and -NMR spectra

Upper panel in Fig. 4.2 shows Cu-NQR spectra at zero field and 4.2 K. From the analysis of NQR spectra, the $^{63}\nu_Q$ for the 4-hold (5-fold) Cu site in Hg1234 is estimated as 9.65 (17.8) MHz which is close to 10.2 (16.1) MHz in Hg1223.[3] The lower panel in Fig. 4.2 indicates the ^{63}Cu-NMR spectra for the central transition $(1/2 \leftrightarrow -1/2)$ at 174.2 MHz and 180 K for $H\|$ c axis (left) and $H \perp$ c axis (right). The NMR spectrum for $H \perp$ c axis is affected by the second-order quadrupole shift, but that for $H\|$ c axis is not. From the magnitude of ν_Q for $H \perp$ c axis, the sharp ^{63}Cu spectrum at higher field side is assigned to the 4-fold Cu sites and the broad one to the 5-fold Cu sites. Their full width at the half maximum (FWHM) for $H\|$ c axis are about $\sim$ 85 Oe and $\sim$ 155 Oe for the 4- and 5-fold Cu sites, respectively.

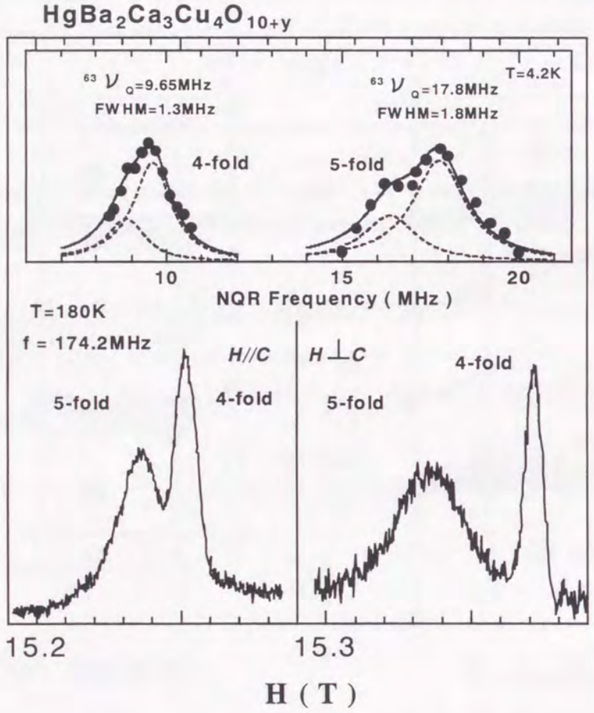

Figure 4.2: The ^{63}Cu NMR spectra for the central transition $(1/2 \leftrightarrow -1/2)$ at f=174.2 MHz and T=180 K in the aligned powder with the c-axis parallel and perpendicular to the external magnetic field, H. The full-width at the half-maximum (FWHM) of the NMR spectra for $c \parallel H$ are about $\sim$ 85 Oe and $\sim$ 155 Oe for 4- and 5-fold, respectively. Inset shows the Cu NQR spectra at T=4.2 K. ν_Q's and FWHM's are estimated to be 9.65MHz and 1.3MHz for 4-fold, and 17.8MHz and 1.8MHz for 5-fold, respectively.

4.3.2 Knight shift

Figure 4.3 shows the T dependence of Knight shifts K_{ab} for $H \perp$ c axis and K_c for $H\|$ c axis for both the Cu sites. In general, Knight shift $K(T)$ consists of the spin part, $K^s(T)$ and the T-independent orbital part, K^{orb} as

$$K_\alpha(T) = K^s_\alpha(T) + K^{orb}_\alpha(\alpha = ab, c). \tag{4.3}$$

As indicated in Fig. 4.3, $K^s_{ab}(T)$ decreases gradually upon cooling in the normal state for both the Cu sites.

According to the Mila-Rice Hamiltonian,[20] $K^s_\alpha(T)$ is expressed as,

$$K^s_\alpha(T) = \frac{(A_\alpha + 4B)}{N\mu_B}\chi_s(T)(\alpha = ab, c), \tag{4.4}$$

where A_α and B are the on-site and the supertransferred hyperfine-coupling constant of ^{63}Cu, respectively. χ_s is assumed to be isotropic. N is the Avogadoro' number. A_α contains anisotropic dipole, spin-orbit, and isotropic core polarization contributions for the Cu-3d$_{x^2-y^2}$ orbit and B originates from the isotropic 4s-spin polarization produced by the neighboring four Cu spins through the Cu($3d_{x^2-y^2}$)-O($2p\sigma$)-Cu($4s$) hybridization. The value of B increases from B = 40 kOe/μ_B in underdoped cuprates [5, 21, 22] to 80 $\sim$ 120 kOe/μ_B in overdoped cuprates.[4, 23] From the slope of $K_c(T)$ vs $K_{ab}(T)$ plot indicated in the inset in Fig. 4.3, we obtain $(A_c + 4B)/(A_{ab} + 4B) = 0.14$ (0.39) for the 4-fold (5-fold) Cu sites. By assuming that A_c and A_{ab} are the same as those in $YBa_2Cu_3O_7$ (Y123),[5] $B \simeq 50$ (75) kOe/μ_B is estimated for the 4-fold (5-fold) Cu sites in Hg1234. In the optimally doped Hg1223, $B \simeq 80$ (90) kOe/μ_B is estimated for the 4-hold (5-fold) Cu sites.[3] B for optimally doped and overdoped cuprates becomes larger than B = 40kOe/μ_B for underdoped cuprates. Therefore, the fact that $B \sim 75$ kOe/μ_B for the 5-fold Cu sites is larger than B=50 kOe/μ_B for the 4-fold Cu sites provides evidence that the doping level for the former is greater than for the latter in Hg1234.

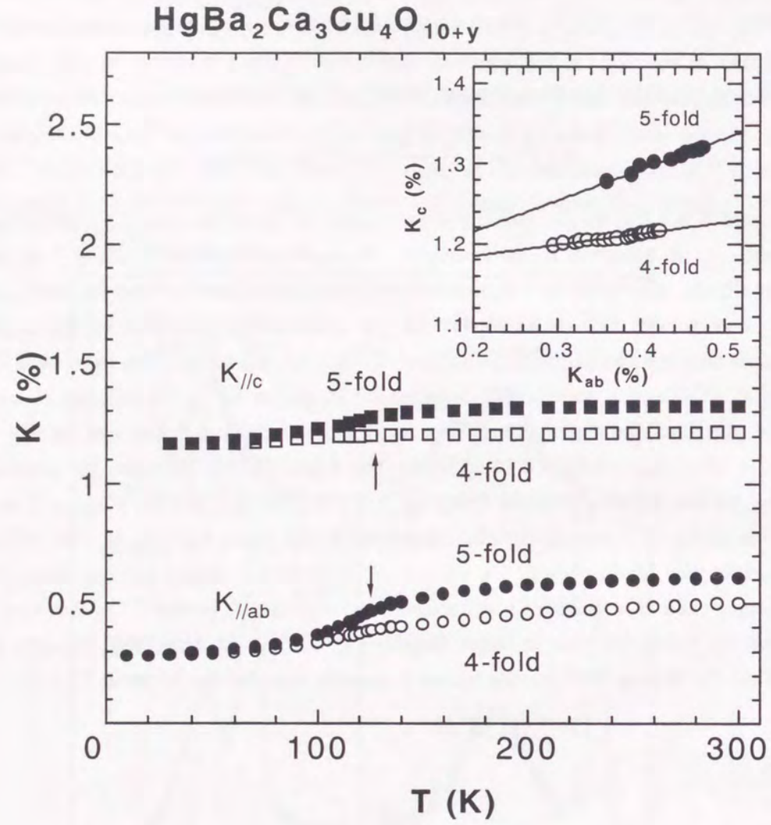

Figure 4.3: T dependence of the Knight shifts perpendicular, K_{ab}, and parallel, K_c, to the c-axis for 4-fold and 5-fold at magnetic field of $\sim$ 15T. Inset indicates the $^{63}K_c$ vs $^{63}K_{ab}$ with T as an implicit parameter. Solid lines are obtained from the least squares fitting.

4.3.3 Nuclear spin-lattice relaxation rate, $1/T_1$

According to the Mila-Rice Hamiltonian,[20] $1/T_1$ is given by

$$^{63}(1/T_1)_c = \frac{\gamma_N^2 k_B T}{2\mu_B^2} \sum_q F_{ab}(q)^2 \frac{\chi''(q,\omega)}{\omega} \tag{4.5}$$

$$^{63}(1/T_1)_{ab} = \frac{\gamma_N^2 k_B T}{4\mu_B^2} \sum_q [F_{ab}(q)^2 + F_c(q)^2] \frac{\chi''(q,\omega)}{\omega} \tag{4.6}$$

where $\chi''(q,\omega)$ is the imaginary part of the dynamical susceptibility and ω is the NMR frequency. The form factors are given by

$$F_{ab}(q) = A_{ab} + 2B[\cos(q_x a) + \cos(q_y a)] \tag{4.7}$$

$$F_c(q) = A_c + 2B[\cos(q_x a) + \cos(q_y a)] \tag{4.8}$$

where a is the distance between Cu atoms.

A $(1/T_1T)_c/(A_{ab} - 4B)^2$ vs T plot for both the Cu sites in Hg1234 is shown in Fig. 4.4 along with plots in underdoped[7] and optimally doped cuprates.[5, 3] Here $(1/T_1T)_c$ is divided by $F(Q)^2 = (A_{ab} - 4B)^2$ with $\mathbf{Q}$=$(\pi/a, \pi/a)$ for comparison of $\chi''(q,\omega)/\omega$ with those in other cuprates. The magnitude of $(1/T_1T)_c/(A_{ab} - 4B)^2$ for the 4-fold Cu sites is similar to that for the underdoped Y1248 with T^*= 150 K,[7] whereas that for the 5-fold Cu sites to those for the 4- and 5-fold Cu sites in the optimally doped Hg1223.[3] It should be noted that the maximum in $1/T_1T$ is observed for both the Cu sites in Hg1234, allowing us to define T^* to be $\sim$ 190 K.

Assuming that $\chi''(q,\omega)$ is described in terms of the Lorentzian forms in energy and momentum distributions as

$$\frac{\chi''(q,\omega)}{\omega} = \frac{\chi_Q}{1 + (q-Q)^2\xi^2} \frac{\Gamma_q}{\omega^2 + \Gamma_q^2}, \tag{4.9}$$

$$\Gamma_q = \Gamma_Q[1 + (q-Q)^2\xi^2],$$

Provided that $\chi''(q,\omega)$ has a maximum around $\mathbf{Q}$=$(\pi/a, \pi/a)$, $1/T_1T$ is expressed as follows,

$$^{63}(1/T_1T)_c/(A_{ab} - 4B)^2 \propto \frac{\chi_Q}{\Gamma_Q \xi^2} \propto \frac{\alpha}{\Gamma_Q}, \tag{4.10}$$

where χ_Q, Γ_Q and ξ are the AF staggered susceptibility, the characteristic energy of AF spin relaxational mode and the AF spin correlation length, respectively. In the case that instantaneous spin-spin correlation function decays exponentially as $\exp(-r_{ij}/\xi)$, $\chi(Q) = \alpha\xi^2$ is derived. We remark that the Γ_Q for the 5-fold Cu sites are larger than that for the 4-fold Cu sites. This assures that the doping level in the former is larger than in the latter.

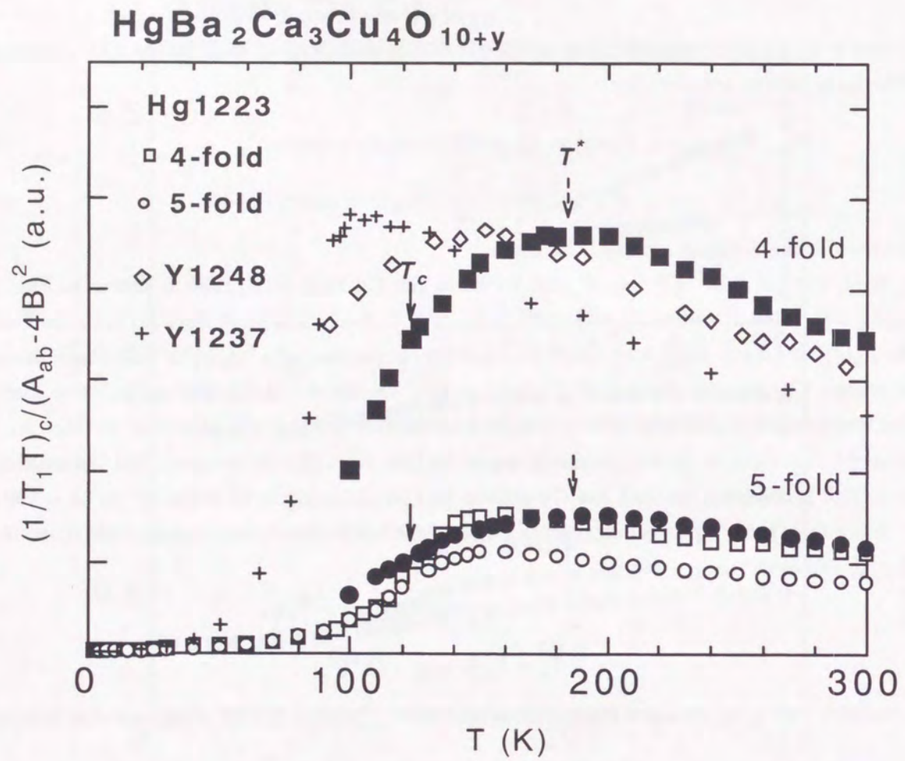

Figure 4.4: T dependence of $^{63}(1/T_1T)_c/(A_{ab}-4B)^2$ ($\propto \alpha/\Gamma_Q$) along with the results of various high-T_c cuprates.

4.3.4 Gaussian spin-echo decay rate, $1/T_{2G}$

$1/T_{2G}$ originating from the indirect nuclear spin-spin coupling in most high-T_c cuprates is generally derived as [6, 17, 18, 24]

$$(\frac{1}{T_{2G}})^2 = \frac{0.69(\gamma_N\hbar)^4}{8\mu_B^4\hbar^2}[\sum_q F_{\parallel}(q)^4\chi(q)^2 - [\sum_q F_{\parallel}(q)^2\chi(q)]^2]. \quad (4.11)$$

As a consequence, $1/T_{2G}$ is given for $\xi > a$ by

$$\frac{1}{T_{2G}} \simeq (\frac{0.69}{32\pi})^{1/2}\frac{\gamma_N^2\hbar}{\mu_B^2}\cdot(A_{\parallel}-4B)^2\frac{\chi_Q}{\xi}(\propto \alpha\xi). \quad (4.12)$$

Accordingly, $1/T_{2G} \propto \xi(T) \propto \sqrt{\chi_Q(T)}$ is deduced. Spin-echo decay curve is well fitted to eq.(4.2). Figure 4.5 shows the T dependence of $1/T_{2G}$ for both the Cu sites together with the results for optimally doped [1, 3] and underdoped cuprates.[6, 9] Here $1/T_{2G}$ is divided by $F(Q)^2 = (A_{\parallel}-4B)^2$ at $\mathbf{Q}$=$(\pi/a, \pi/a)$ for comparison of ξ with those in other cuprates.

The ξ for the 4-fold Cu sites reveals a stronger T dependence with a larger value than for underdoped cuprates, whereas that for the 5-fold Cu sites is similar to those in optimally doped cuprates with a comparable value. The ξ just above T_c for the 4-fold Cu sites is three times larger than that for the 5-fold sites . Noting that ξ is determined by a mean distance among doped holes, it is obvious that the doping level in the 5-fold Cu sites is greater than in the 4-fold Cu sites.

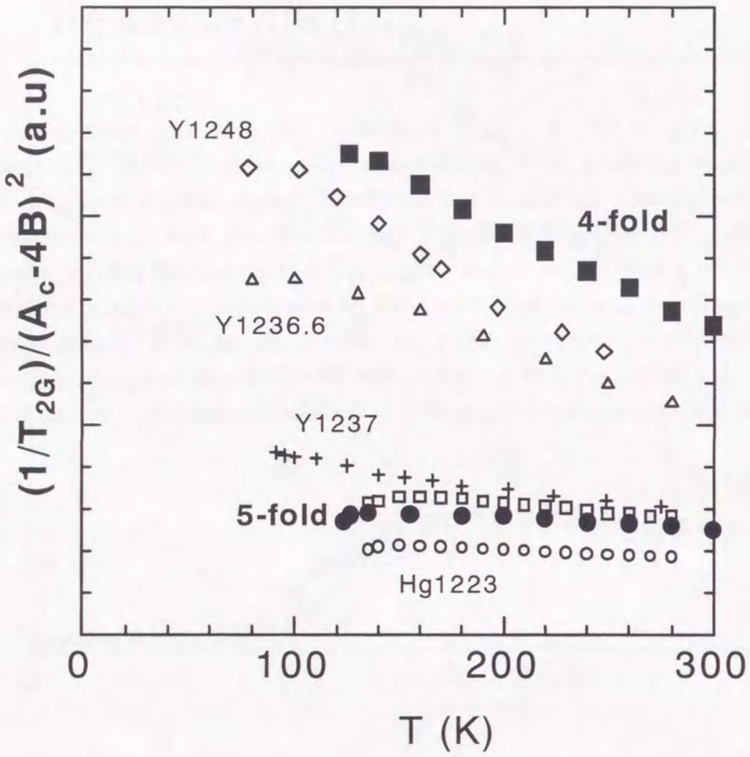

Figure 4.5: T dependence of $1/T_{2G}/(A_c - 4B)^2$ ($\propto \xi$) along with the results of various high-T_c cuprates.

4.4 Discussion

For underdoped cuprates, magnetic correlations are characterized by the T_1T/T_{2G}=const. (z=1) behavior, followed by the spin gap behavior. In fact, the T_1T/T_{2G} for the 4-fold Cu sites stays constant between $T^* \sim 190$ K and 300 K as indicated in Fig. 4.6a. The pseudogap emerges below $T^* \sim 190$ K. By contrast, the 5-fold Cu sites exhibit the T_1T/T_{2G}^2=const. (z=2) behavior above $T^* \sim 190$ K as seen in Fig. 4.6b, which is typical behavior for optimally doped and overdoped cuprates. The inset in Fig.4.7 shows the T dependence of the ratio $(T_1T)_{5-fold}/(T_1T)_{4-fold}$, which stays constant between $T_c = 123$ K and $T_K^* \sim 220$ K. This shows that the pseudogap temperature $T^* \sim 190$ K is defined for both the Cu sites by the maximum of $1/T_1T$ regardless of their marked difference in magnetic correlations. The pseudogap opens up for both the optimally doped 5-fold and underdoped 4-fold Cu sites.

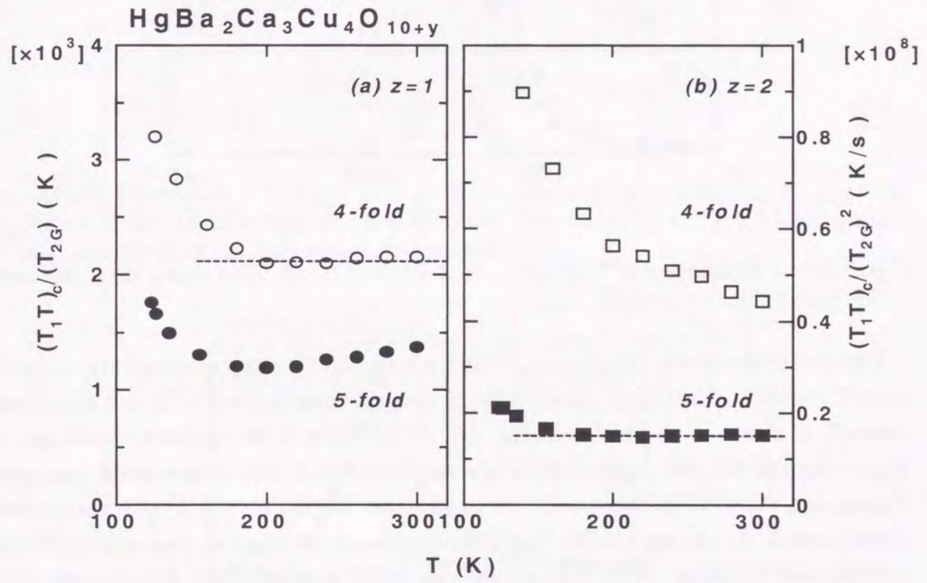

Figure 4.6: T dependence of $(T_1T)_c/T_{2G}$ and $(T_1T)_c/(T_{2G})^2$ for both 4- and 5-fold.

As indicated in Fig. 4.8, $K_{ab}^s(T)$'s for both the Cu sites decreases moderately as the temperature decreases from $T_K^* \sim 220$ K to 300 K, and with further decreasing T below T_K^* its decrease becomes more significant. The T-derivative change in $K_{ab}^s(T)$, $dK_{ab}^s(T)/dT$ is plotted as a function of temperature in Fig. 4.9. From this plot, T_K^* is defined as the temperature below which $dK^s(T)/dT$ begins to increase from a finite value. In $Bi_2Sr_2CaCu_2O_{8+\delta}$ (Bi2212),[25] this T_K^* was reported to be comparable to T_{ARPES}^* below which the normal-state pseudogap with the $d_{x^2-y^2}$ symmetry opens up at the Fermi surface.[28, 29] Therefore, the reduction in $K_{ab}^s(T)$ below T_K^* signals the pseudogap opening in the quasiparticle density of states at the Fermi level. It is not clear whether a difference between $T^* \sim 190$ K and $T_K^* \sim 220$ K is intrinsic or should

be ascribed to some experimental error.

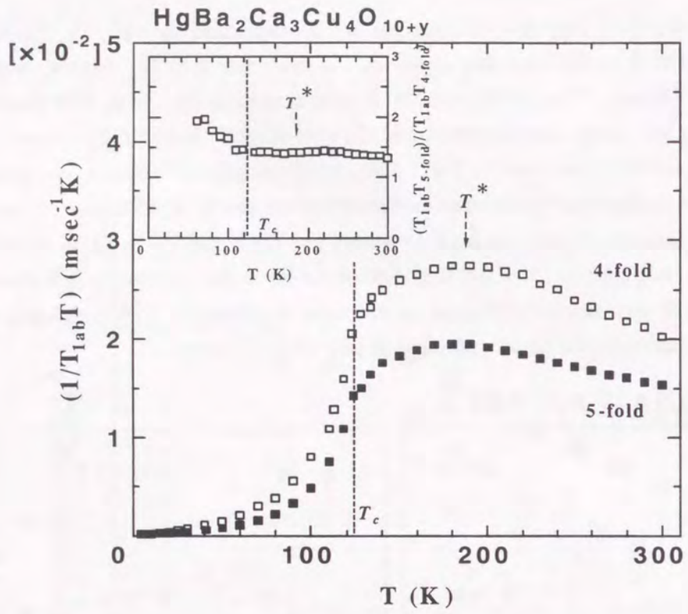

Figure 4.7: T dependence of $^{63}(1/T_1T)_{ab}$ for 4-fold and 5-fold. Inset shows the T dependence of the ratio of $(T_1T_{5\text{-}fold})/(T_1T_{4\text{-}fold})$.

Figure 4.10 shows the $(K^s_{ab}(T)/K_n(T))$'s for both the Cu sites, which exhibit almost the same T variation. Here $K_n(T)$ is assumed to decrease linearly down to T_c and stay constant below T_c as drawn by dotted line in Fig. 4.8. $K^s(T)$ below T_c for optimally doped and over-doped cuprates was well reproduced by the two-dimensional (2D) d-wave model proposed by Monien and Pines.[26] In this model, the gap function has the form $\Delta(\phi) = \Delta\cos 2\phi$ where ϕ is the angle in the ab plane.[4, 27] The T dependence of the SC order parameter, $\Delta(T)/\Delta(0)$ was assumed to follow the BCS form. We may apply a model which assumes d-wave symmetry on the pseudogap observed for both the Cu sites in Hg1234. Eventually we reproduce $K^s_{ab}(T)/K_n(T)$ between T_c =123 K and $T^*_K \sim 220$ K. The solid line in Fig.4.10 is a calculation on the model which assumes that $\Delta(T)/\Delta(0)$ increases linearly as the temperature is lowered from $T^*_K \sim 220$ K to T_c=123 K and follows the mean-field BCS form below T_c. The agreement between the experiment and the calculation seems to be satisfactory with a zero temperature gap $2\Delta(0)/k_BT_c = 8.3$. This T dependence of $\Delta(T)/\Delta(0)$ displayed in the inset in Fig.4.10 appears to be consistent with that suggested from ARPES on Bi2212.[28] It is noteworthy that the pseudogap for both the Cu sites is reproduced by the model which assumes the same T dependence of $\Delta(T)/\Delta(0)$ with $2\Delta(0)/k_BT_c = 8.3$ below $T^*_K \sim 220$ K.

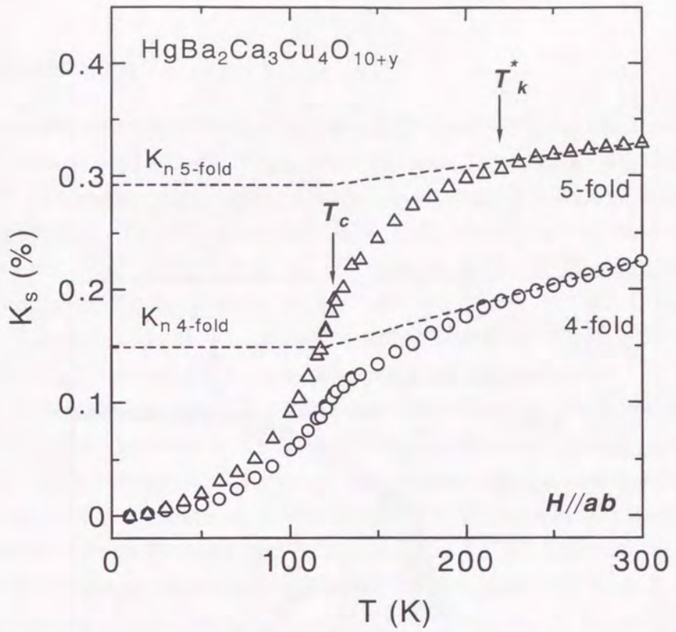

Figure 4.8: T dependence of the spin part in the Knight shifts perpendicular, $K_{s,ab}$, to the c-axis for 4-fold and 5-fold at magnetic field of $\sim$ 15T. The K_n for $T_c < T < T^*$ (dotted lines) is an extrapolation from the least square fitting above $220K$.

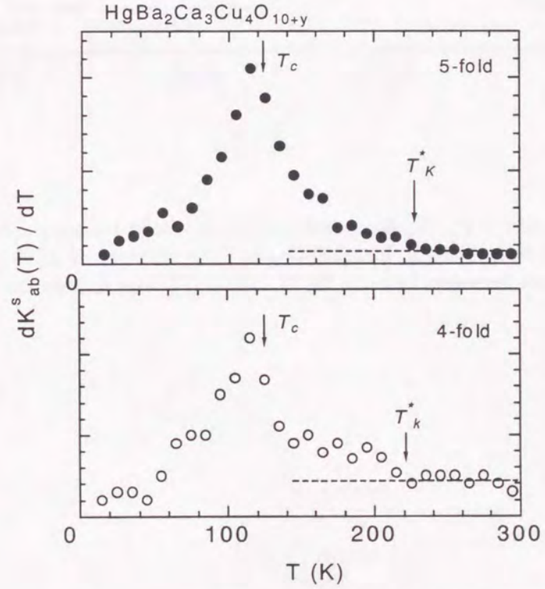

Figure 4.9: T-derivative change in $K^s_{ab}(T)$, $dK^s_{ab}(T)/dT$ for 4-and 5-fold are plotted as a function of temperature.

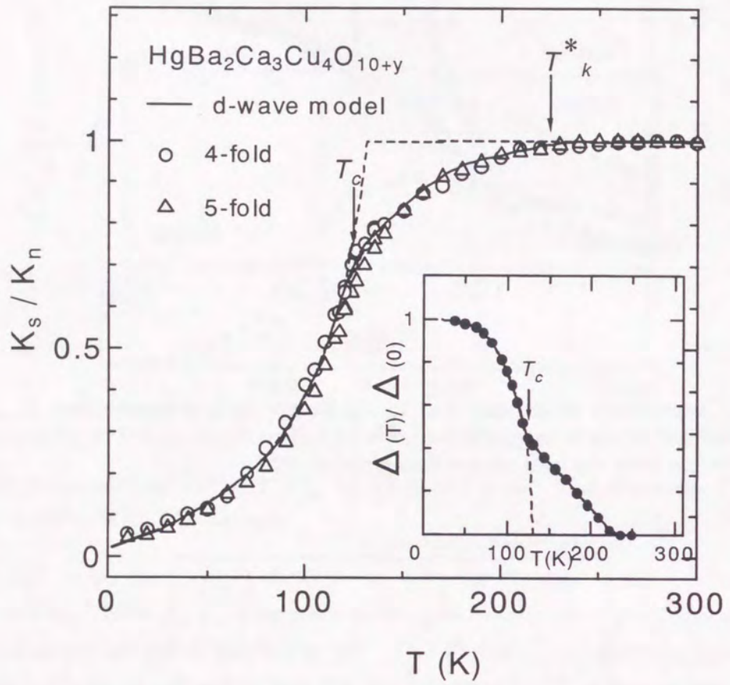

Figure 4.10: T dependence of K_s/K_n for 4-fold and 5-fold. Solid lines are calculated by using the d-wave model with $2\Delta/k_BT_c$=8.3. Inset shows the T-dependence of $\Delta(T)/\Delta(0)$ used in the d-wave calculation, which increases linearly for $T_c < T < T_K^*$ and follows the mean-field BCS type belowT_c.

4.5 Summary

We have measured the ^{63}Cu Knight shift, $1/T_1T$ and $1/T_{2G}$ for the inner 4-fold and outer 5-fold Cu sites in $HgBa_2Ca_3Cu_4O_{10+y}$ (Hg1234) with T_c = 123 K. We found that the 4-fold (5-fold) CuO_2 plane is underdoped (optimally doped). This is in striking contrast to the case of $HgBa_2Ca_2Cu_3O_{8+y}$ (Hg1223) where the doping level was almost the same for both the 4- and 5-fold Cu sites. The 4-fold (5-fold) Cu site revealed the T_1T/T_{2G}=const. (T_1T/T_{2G}^2=const.) behavior characteristic for underdoped (optimally doped and overdoped) cuprates. The pseudogap temperature T^* ~190 K was defined by the maximum of $1/T_1T$ for both the Cu sites regardless of their marked difference in magnetic correlations.

The pseudogap temperature T_K^* ~220 K was also defined by the more significant reduction in $K_{ab}^s(T)$ for both the Cu sites. The Knight shift data between T_c and T_K^* was well reproduced by a model which assumed $d_{x^2-y^2}$ symmetry on the pseudogap. From this analysis, we propose that the value of the pseudogap increases linearly with decreasing T from T_K^* ~ 220 K to T_c=123 K and follows the mean-field BCS form below T_c. We note that the T variation of the normal-state pseudogap is similar to the result obtained from ARPES on Bi2212.[28, 29]

The present experiment has thus provided a new clue to the clarification of the origin of the normal-state pseudogap which suppresses not only the spectral weight of the AF-spin fluctuation spectrum at low energy but also the quasiparticle particle density of states at the Fermi level.

Bibliography

[1] T. Imai, C.P. Slichter, A.P. Paulikas and B. Veal, Phys. Rev. B**47**, 9158 (1993).

[2] G.-q. Zheng, Y. Kitaoka, K. Asayama, K. Hamada, H. Yamauchi and S. Tanaka, J. Phys Soc. Jap. **64** 3184 (1995); Physica C**260**, 197 (1996).

[3] K. Magishi, Y. Kitaoka, G.-q. Zheng, K. Asayama, K. Tokiwa, A. Iyo and H. Ihara, J. Phys. Soc. jpn. **64**, 4561 (1995).

[4] K. Magishi, Y. Kitaoka, G.-q. Zheng, K. Asayama, T. Kondo, Y. Shimakawa, T. Manako and Y. Kudo, Phys. Rev. B**54**, 10131 (1996).

[5] M. Takigawa, A.D. Reyes, P.C. Hammel, J.D. Thompson, R.H. Heffner, Z. Fisk and K.C. Ott, Phys Rev B**43**, 247 (1991).

[6] M. Takigawa, Phys. Rev. B**49**, 4158 (1994).

[7] I. Tomeno, T. Machi, K. Tai, N. Koshizuka, S. Kambe, A. Hayashi, Y. Ueda, and H. Yasuoka, Phys. Rev. B**49**, 15327 (1994).

[8] M.-H. Julien, P. Carretta, M. Horvatic, C. Berthier, Y. Berthier, P. Segransan, A. Carrington, and D. Colson, Phys. Rev. lett. **76**, 4238 (1996).

[9] R.L. Corey, N.J. Curro, K. O'Hara, T. Imai, C.P. Slichter, K. Yoshimura, M. Katoh and K. Kosuge, Phys. Rev. B**53**, 5907 (1996); N. J. Curro, T. Imai, C. P. Slichter and B. Dabrowski, Phys. Rev. B**56**, 877 (1997).

[10] A. V. Chbukov, D. Pines and B. P. Stojkovic, J. Phys. Condens. Matter **8**, 10017 (1996).

[11] T. Tanamoto, H. Kohno, and H. Fukuyama, J. Phys. Soc. Jpn. **63**, 2739 (1994).

[12] V.J.Emery and S.A.Kivelson, Nature (London) **374**, 434 (1995).

[13] K. Miyake and O. Narikiyo, J. Phys. Soc. Jpn. **63**, 3821 (1994).

[14] Y. Itoh. T. Machi, A. Fukuoka, K. Tanabe and H. Yasuoka, J. Phys. Soc. Jpn. **65**, 3751 (1996).

[15] H. Ihara, M. Hirabayashi, H, Tanino, K. Tokiwa, H. Ozawa, Y. Akahama and H. Kawamura, Jpn. J. Appl. Phys. **32**, L1732 (1993).

[16] A. Narath, Phys. Rev. **13**, 3724 (1976).

[17] C.H. Pennington, D.J.Durand, C.P. Slichter, J.P. Rice, E.D. Bukowski and D.M. Ginsberg, Phys. Rev. B**39**, 274 (1989).

[18] C.H. Pennington and C.P. Slichter, Phys. Rev. lett. 66, 381 (1991).

[19] R. E. Walstedt and S-W. Cheong, Phys. Rev. B**51**, 3163 (1995).

[20] F. Mila and T.M. Rice, Phys. Rev. B**40**, 11382 (1989); Physica C**157**, 561 (1989).

[21] S. Ohsugi, Y. Kitaoka, K. Ishida, G.-q. Zheng and K.Asayama, J. Phys. Soc. Jpn. **63**, 700 (1994).

[22] H. Zimmerman, M. Mali, M. Bamky and D. Brinkmann, Physica C**185-189**, 9574 (1990).

[23] Y. Kitaoka, K. Fujiwara, K. Ishida, K. Asayama, Y. Shimakawa, T. Manako and Y. Kubo, Physica C**179**, 107 (1991).

[24] D. Thelen and D.Pines, Phys. Rev. B**49**, 3528 (1994).

[25] K. Ishida, Y. Yoshia, T.Mito, Y. Tokunaga, Y. Kitaoka, K. Asayama, Y. Nakayama, J. Shimoyama and K. Kishio, Phys. Rev. **B 58**, R5960 (1998)

[26] H. Monien and D. Pines, Phys. Rev. B **41**, 6297 (1990).

[27] K. Ishida, Y. Kitaoka, N. Ogata, T. Kamino, K. Asayama, J.R. Cooper and N. Athanassopoulou, J.Phys. Soc. Jpn. 62, 2803 (1993).

[28] H. Ding, T. Yokoya, J. C. Campuzano, T. Takahashi, M. Randeria, M. R. Norman, T. Mochiku, K. Kadowaki and J. Giapintzakis, Nature **382**, 51 (1996); Phys. Rev. Lett. **78**, 2628 (1997).

[29] A. G. Loeser, Z. -X. Shen, D. S. Marshall, C. H. Park, P. Fournier and A. Kapitulnik, SCIENCE **273**, 325 (1996).

Chapter 5

^{63}Cu -NMR Study in $CuBa_2Ca_3Cu_4O_{12+\delta}$

5.1 Introduction

A newly discovered a Cu-based (CuC)$Ba_2Ca_3Cu_4O_{12+y}$(Cu1234) system has the least anisotropic superconductivity($\gamma = 1.6$) among the cuprate superconductors and a long coherence length along c-axis($\xi_c = 10\mathring{A}$) at the longest level[5]. The low superconducting anisotropy (γ) and the long coherence-length along c-axis (ξ_c) are very important for high J_c under high field, high irreversible field and Josephson device fabrication.

Fig.5.1 shows the crystal structure of (CuC)-1234 refined from neutron-powder-diffraction data.[2] (CuC)-1234 consists of three kind of Cu sites in a unit cell, i.e. four coordination Cu sites in the inner CuO_2 layers,(4-fold), five coordination Cu sites in the outer one,(5-fold) and six coordination Cu sites in $(CuO)O_{1+y}$ block layer. C atoms in CO_3 groups substitute at the Cu site in $(CuO)O_{1+y}$ layers leading to a chemical composition of $(Cu_{1-x}C_x)Ba_2Ca_3Cu_4O_{12+y}$. The presence of the CO_3 groups in block-layer unit induces the variation in apical Cu$-$O distance for the 5-fold CuO_5 unit. This means that there are two inequivalent Cu sites with the apical oxygens on ideal and displaced position in the 5-fold CuO_2 layers.

For understand the mechanism of high-T_c superconductivity for the multilayer cuprates which consist inequivalent kinds of CuO_2 layers, it is important to take the difference of local character for each layer into consideration. The local magnetic properties at each layer can be extracted separately from NMR measurement. In NMR study for a mercury-based cuprate superconductors, $HgBa_2Ca_2Cu_3O_{8+y}$(Hg1223) which has a inner square (4-fold) and two outer pyramidal (5-fold) CuO_2 layers, Magishi *et al.* showed that the product of the staggered susceptibility and the characteristic energy of spin fluctuation around a zone boundary, $\chi_Q\Gamma_Q$ for 4-fold was larger than $YBa_2Cu_3O_7$($YBCO_7$), although that for 5-fold was almost the same. They proposed that this enhancement of $\chi_Q\Gamma_Q$ for 4-fold was responsible for the higher T_c of 133K in Hg1223 than $YBCO_7$.[12] On the other hands, in four layers $HgBa_2Ca_3Cu_4O_{10+y}$(Hg1234), it was revealed that the magnetic characters for 4-fold were analogue to those in underdoped cuprates, whereas for 5-fold to those in overdoped cuprates, as discussed in the chapter 4. However it was unique that the pseudogap has been observed in 4- and 5-fold below the temperature, T^* where $1/T_1T$

has a peak. It is suggested that the pseudogap is common for 4- and 5-folds despite of respective contrasting magnetic properties analogous to the under and over doped cuprates. The value of $\chi_Q \Gamma_Q$ for 5-fold was larger than that for 4-fold, therefore T_c was considered to be determined by 5-fold.

In this chapter, we report systematic Cu-NMR studies in order to characterize local magnetic behaviors inherent to 4- and 5-fold and elucidate possible control parameters for T_c in Cu1234. From the Cu Knight shift, K and the nuclear relaxation rate, $1/T_1$ measurements, it is revealed that 4- and 5-fold layers are in the different in-plane doping level, i.e. 4-fold is in the underdoped, whereas 5-fold in the widely overdoped regime. In the normal state, the pseudogap behavior is evidenced in 4-fold below $T^* \sim 150K$ ($T_K^* \sim 180K$) from the decrease in $1/T_1T$ and K. On the other hand, $1/T_1$ and K for 5-fold show a behavior typical for the overdoped cuprate without the pseudogap above T_c. In the superconducting state, it is revealed that the conventional superconducting state is not established above 60K in 5-fold site. This proposes that the superconductivity in the outer 5-fold layers are degraded by the over-carrier doping, however higher T_c of 117K is maintained by the inner 4-fold layers which are less corrugated and near the optimum doping.

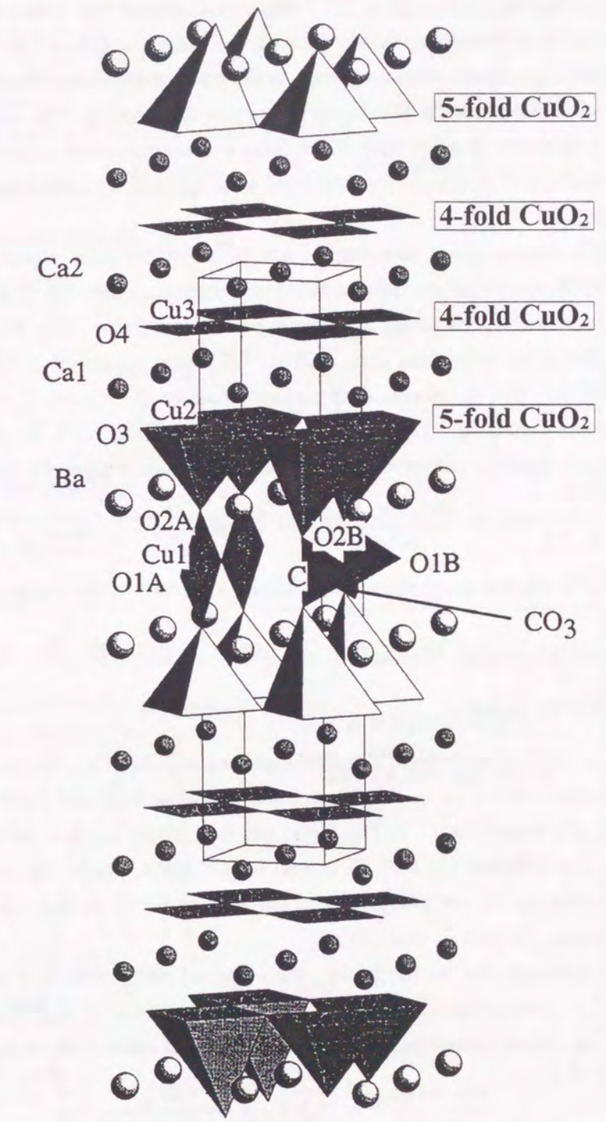

Figure 5.1: Crystal structures of (Cu,C)$Ba_2Ca_3Cu_4O_{12+y}$[2]

5.2 Experimental Procedures

A $(Cu_{1-x}C_x)Ba_2Ca_3Cu_4O_{12+y}$(Cu1234) polycrystal sample was prepared by a high pressure synthesis technique as described elsewhere.[5] T_c was determined as 117 K from the temperature below which the diamagnetic signal appears in the ac-susceptibility. The sample was confirmed to be almost of single-phase by the X-ray diffraction experiment. The pellet was crushed into powder with a diameter smaller than $20\mu m$, and was magnetically aligned along the c axis by use of the anisotropy of susceptibility and fixed with the stycast 1266 epoxy under the external magnetic field of 16 T.

The Cu-NMR measurement was carried out by a conventional phase-coherent laboratory-built pulsed NMR spectrometer using a superconducting magnet (16 T at 4.2 K). Field-swept ^{63}Cu-NMR spectrum was obtained by using a boxcar integrator. The Knight shift, $K(T)$ and the nuclear-spin-lattice relaxation rate, $1/T_1$ of ^{63}Cu were measured at 174.2 MHz ($\sim$ 15.5 T) in a T range of 4.2−300 K parallel and perpendicular to the c axis. T_1 was measured by the saturation recovery method. The nuclear-relaxation function, $R(t)$, for the central transition $(1/2 \leftrightarrow -1/2)$ for $I = 3/2$ among the quadrupole-split lines is given by [10]

$$R(t) = \frac{M(\infty) - M(t)}{M(\infty)} = 0.9\exp(-\frac{6t}{T_1}) + 0.1\exp(-\frac{t}{T_1}) \tag{5.1}$$

where $M(t)$ is the nuclear magnetization at time t after saturation pulses.

5.3 Experimental Results

5.3.1 Cu NMR spectra

Figure 5.2 (a) and (b) show the ^{63}Cu NMR spectra in $(Cu_{0.6}C_{0.4})Ba_2Ca_3Cu_4O_{12+y}$ at 130 K for the central transition $(1/2 \leftrightarrow -1/2)$ with the c-axis parallel and perpendicular to external magnetic field, H, respectively. In Fig.5.2(a) for $H \| c$, there are two well resolved peaks corresponding to two different Cu sites in 4- and 5- fold CuO_2 plane. However in Fig.5.2(b) for $H \perp c$, the spectra exhibit one sharp peak at higher field region (4-fold) and two broader peaks at lower field region (5-fold(A) and (B)).

When H is perpendicular to the c-axis, the obtained shift consists of the Knight shift and the second-order quadrupoler shift. The Knight shift component, K_{ab} and ν_Q of ^{63}Cu can be expressed for the central transition according to the second-order perturbation theory as follows,

$$\frac{\omega - \gamma_N H_{res}}{\gamma_N H_{res}} = K_{ab} + \frac{3\nu_Q^3}{16(1+K_{ab})(\gamma_N H_{res})^2} \tag{5.2}$$

where H_{res} is the field where the resonance is observed, γ_N is the nuclear gyromagnetic ratio and ω is the NMR frequency, respectively. Therefore, K_{ab} and ν_Q are determined from the extrapolation to zero of $(\gamma_N H_{res})^{-2}$ and the slope of line respectively. In Fig.5.3, we plot the value of $(\omega - \gamma_N H_{res})/(\gamma_N H_{res})$ against $(\gamma_N H_{res})^{-2}$. As expected, 5-fold(A) and (B) have the same magnetic knight shift, $\sim 0.75\%$ but the different nuclear quadrupole frequency, ν_Q, $\sim$ 14.7 and 30.0MHz, respectively. On the other hands, the ν_Q value for 4-fold are estimated to be

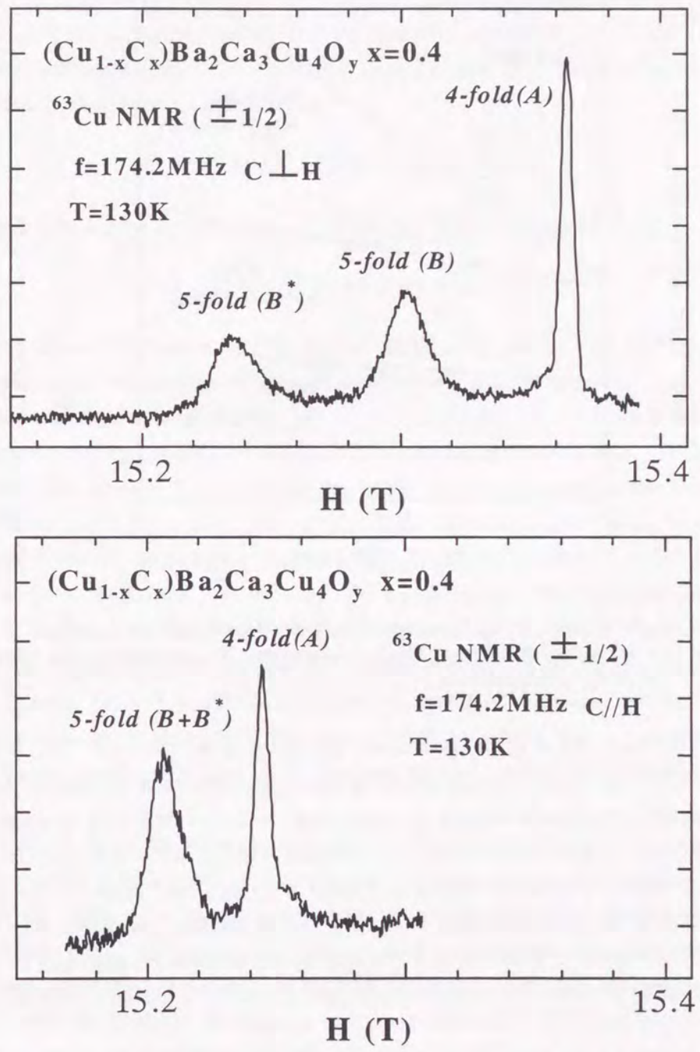

Figure 5.2: The ^{63}Cu NMR spectra for the central transition $(1/2 \leftrightarrow -1/2)$ at f=174.2 MHz and T=130 K in the aligned powder with the c-axis parallel (a) and perpendicular (b) to the external magnetic field, H.

11.1MHz. In Hg1234 system which has the same crystal structure, ν_Q were estimated to be 9.7 and 17.8MHz for 4- and 5-fold sites.

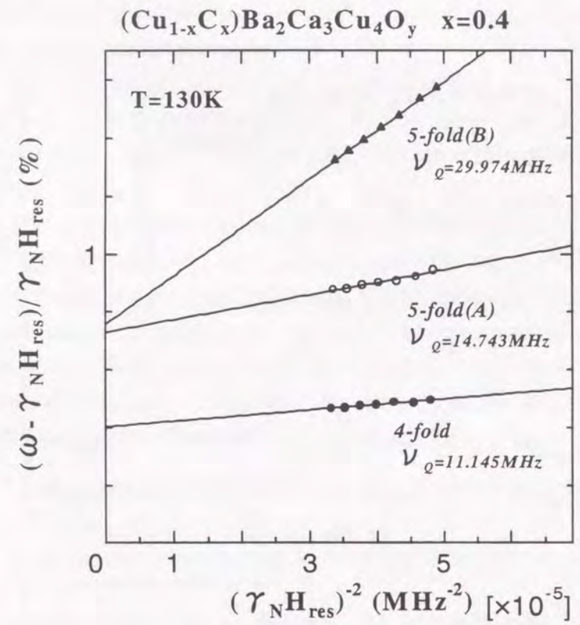

Figure 5.3: The value of $(\omega - \gamma_N H_{res})/(\gamma_N H_{res})$ is plotted against $(\gamma_N H_{res})^{-2}$ in the field perpendicular to the c-axis for different NMR frequencies. H_{res} is the field for resonance corresponding to 4- and 5-fold, respectively.

The integrated intensity of three spectra for $H \perp c$ are in the ratio 1.0 : 0.6 : 0.4 for 4-fold , 5-fold(A) and (B), in $x = 0.4$ $(Cu_{0.6}C_{0.4})Ba_2Ca_3Cu_4O_{12+y}$. This ratio change to 1.0 : 0.55 : 0.45 in $x = 0.5$ sample. From these results, the sharp peak at higher field sites is assigned to Cu in the 4-fold layers and the broad peaks at lower field sites to Cu in the 5-fold layers, since 5-fold has two inequivalent Cu sites with the apical oxygens on ideal and displaced position and the ratio of the number of those sites (0.6 : 0.4 in $x = 0.4$) are well consistent with the ratio of the intensity. Furthermore, 5-fold(A) and (B) exhibit an identical K_s and $1/T_1$ in the whole T ranges, which also provides evidence that these peaks arise from Cu sites existing on the same CuO_2 layers.

Unfortunately, the NMR signal from Cu sites in $(CuO)O_{1+y}$ block layers have not been observed, which suggests that the large distortion is introduced in this layer due to the partial substitution of CO_3 groups.

5.3.2 Knight shift

The local susceptibility at each atomic site can be extracted separately from the Knight shift measurement without any appreciable influence impurity spin. In order to extract an intrinsic magnetic property for each CuO_2 plane, the Knight shift measurement carried out for perpendicular, K_{ab}, and parallel, K_c, to the c axis for 4-fold and 5-fold.

In general, the Knight shift $K(T)$ consists of the spin part, $K_s(T)$ and the orbital part, K_{orb} which is generally temperature independent,

$$K_\alpha(T) = K_{s,\alpha}(T) + K_{orb,\alpha}(\alpha = ab, c). \tag{5.3}$$

According to the Mila-Rice Hamiltonian,[7] the K_s of ^{63}Cu is expressed as,

$$K_{s,\alpha}(T) = (A_\alpha + 4B)\chi_s(T)(\alpha = ab, c), \tag{5.4}$$

where A_α and B are the on-site and the supertransferred hyperfine field of ^{63}Cu, respectively and χ_s is assumed to be isotropic. A_α contains anisotropic dipole, spin-orbit, and isotropic core polarization contributions for the Cu $3d_{x^2-y^2}$ orbit and B originates from the isotropic $4s$-spin polarization produced by the neighboring four Cu spins through the Cu($3d_{x^2-y^2}$)-O($2p\sigma$)-Cu($4s$) hybridization. The value of B increases as the carrier density increases in the CuO_2 plane, i.e. from $B = 40\text{kOe}/\mu_B$ in the underdoped cuprates [8, 9, 11] to $80 \sim 120\text{kOe}/\mu_B$ in the overdoped cuprates.[6, 3] From the slope of the K_c vs K_{ab} plot, we have obtained $(A_c+4B)/(A_{ab}+4B) =$ 0.30 and 0.45 for 4- and 5-fold, respectively. By assuming that the on-site hyperfine coupling constants, A_c and A_{ab} are the same as in Y123, $B \simeq 65$ and 85 kOe/μ_B are obtained for 4-fold and 5-fold, respectively. Noting that the B-term becomes larger for the optimally and the overdoped cuprates than $B = 40\text{kOe}/\mu_B$ for the underdoped cuprates, the fact that $B \sim 85$ kOe/μ_B in 5-fold is larger than B=65 kOe/μ_B in 4-fold provides evidence that the doping level in 5-fold is larger than in 4-fold for Cu1234, which will be verified by T_1 results as mentioned below.

Figure 5.4 shows the T dependence of $K_{s,ab}$. K_s decreases gradually upon cooling for 4-fold, by contrast, K_s for 5-fold largely enhanced and T-independent in the normal state. In the superconducting state, 4-fold shows a strong reduction just below T_c, however 5-fold shows a gradual decrease with T-decreasing just below T_c and a strong reduction below $60K$.

As discussed in NMR study for Hg1234 [Chap.4] and Bi2212 [Chap.3], the pseudogap behavior is evidenced not only from the appearance of the maximum in $1/T_1T$, but also from the steep decrease of the spin contribution in Knight shift. In Fig.5.4, K_s in 4-fold decreases moderately down to near $T_K^* \sim 180$ K, and decreases more steeply below T_K^* to T_c. It is reasonable to consider that the gradual decrease of $K_s(T)$ upon cooling to T_K^* is due to the development of AF correlation, which is also suggested from the recent theoretical studies [15, 16]. However, the decrease of $K_s(T)$ below T_K^* is so steep that an extrapolation of pronounced decrease in $K_s(T)$ near T_c intercepts to the temperature axis at $T \geq 0$ in K_s vs T plot. This suggests that the additional decrease below $T_K^* \sim 180K$ is due to the opening of pseudogap which is evident

from the decrease of $1/T_1T$ below $T \sim 150K$ as discussed later. On the other hands, 5-fold shows a T-independent K_s above T_c. This indicates that the pseudogap do not open in 5-fold above T_c, which is also consistent with the monotonically increase in $1/T_1T$ in the normal state.

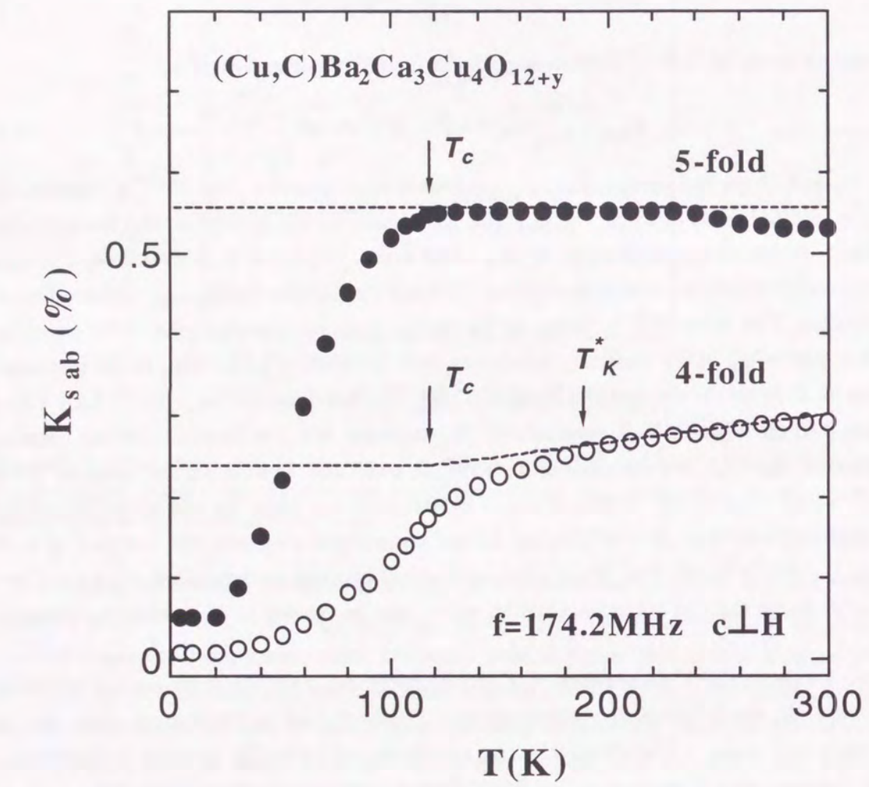

Figure 5.4: T dependence of the Knight shifts perpendicular, K_{ab}, to the c-axis for 4-fold and 5-fold at $H \sim 15$T.

5.3.3 Nuclear-spin lattice relaxation rate, $1/T_1$

Fig.5.5 shows the T-dependence of $1/T_1$ with the c-axis parallel and perpendicular to external magnetic field, H. $1/T_1T$ for 5-fold is more suppressed than 4-fold in the normal state, suggesting that Γ_Q in 5-fold are larger than in 4-fold. T-dependence of $1/\mathrm{T_1T}$ for 4-fold shows the broad maximum around $T^* \sim 150K$, that is, shows the pseudogap behavior. On the other hand, $1/T_1T$ for 5-fold increase monotonically with T-decreasing, which indicates the development of AF fluctuation without the opening of the pseudogap in the normal state.

Fig.5.6 shows the T-dependence of $1/T_1$ in the superconducting state. $1/T_1$ for 4-fold shows a strong reduction and T^3 like behavior just below T_c due to the opening of the d-wave superconducting gap. However, the decrease of $1/T_1$ for 5-fold is gradual for $60K < T < T_c$ and T^3 like behavior is observed only below $\sim 60K$. $1/T_1$ for 5-fold behaves $1/T_1T =$ const. below $10K$, indicative of the gapless nature of superconductivity such as Zn-doped $YBCO_7$ [4].

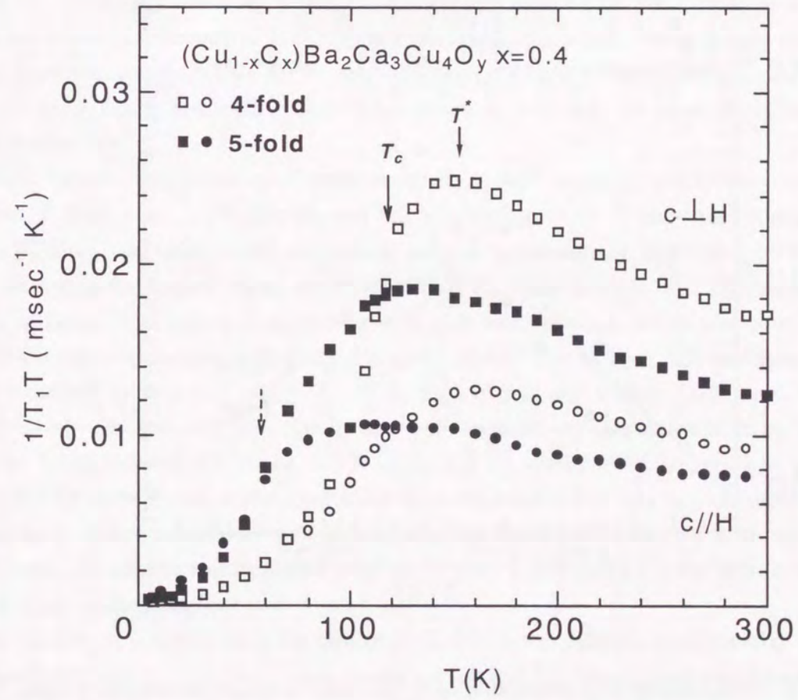

Figure 5.5: T dependence of $1/T_1T$ perpendicular and parallel to the c-axis for 4-fold and 5-fold.

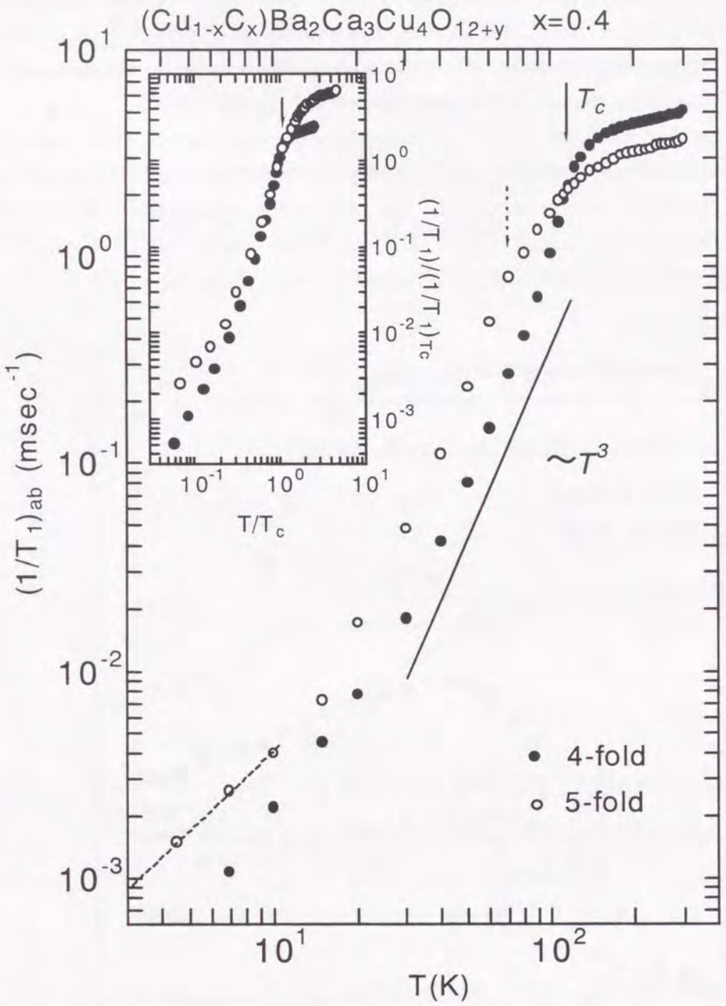

Figure 5.6: T dependence of $1/T_1$ perpendicular to the c-axis in the superconducting state. The inset show $(1/T_1)/(1/T_1)_{T_c}$ plotted against T/T_c for 4- and 5-fold (for 5-fold, we adopts 60K as T_c.)

5.4 Discussion

5.4.1 Carrier content in 4- and 5-fold layers.

In high-T_c cuprate, the T dependence of $^{63}K_s$ and $^{63}1/T_1T$ in the normal state are sensitive to the changes of the carrier content in CuO_2 layer, therefore, give an information of doping level in CuO_2 layers. Generally, in the underdoping region, K_s which is proportional to the static spin susceptibility is small at T_c and decrease with T-decreasing, associated with the development of AF spin correlations and the opening of pseudogap. In overdoped region, K_s is enhanced and shows a T-independent behavior. $1/T_1T$ at plane Cu sites is inversely proportional to the energy of AF spin fluctuation, Γ_Q which get progressively enhanced by increasing the carrier content in CuO_2 layer. Hence, $1/T_1T$ above T_c monotonically decreases with increasing doping level.

In Cu1234 system, 4-fold layer has smaller χ_s and Γ_Q than 5-fold in the normal state. T-dependence of K_s and $1/T_1$ for 4-fold sites are described within the slightly underdoped cuprate with the pseudogap behavior below $T^* \sim 150K$, in contrast to the T-independent K_s and the monotonically increase of $1/T_1T$ with T-decreasing for 5-fold. Those results indicate that multilayer compound Cu1234 is a structure containing planes of the different doping level, that is, the inner 4-fold layers are in slightly underdoping level and the outer 5-fold layers are in overdoping level.

Fig.5.7 shows the hole content dependence of K_s at 300K perpendicular to the c-axis for overdoped $Tl_2Ba_2CuO_{6+y}$, $YBa_2Cu_3O_7$ and $La_{2-x}Sr_xCuO_4(x = 0.15)$ and underdoped $YBa_2Cu_3O_{6.6}$.[3] Since the underdoped compounds show a monotonically decreasing of K_s with T-decreasing in the normal state, we estimated all K_s value at 300K for the comparison. As seen in figure, K_s increase progressively with hole concentration, which allows us to roughly estimate the local in-layer hole content in CuO_2 layers. The in-layer hole contents in Cu1234 are estimated to be ~ 0.27 and ~ 0.73 from $K_{s,ab}$ of 0.24 and 0.50 at $300K$ for 4- and 5-fold, respectively. By the same way, the in-layer hole contents are also estimate to be ~ 0.30 and ~ 0.47 in Hg1223 and ~ 0.18 and ~ 0.35 in Hg1234 for 4- and 5-fold, respectively, as shown in fig.5.8. The lower doping of the inner 4-fold than the outer 5-fold may be a common feature for multilayers compounds. However it should be noted that 5-fold in Cu1234 is widely overdoped and hence the difference of local hole contents between 4- and 5-fold is quite large in comparison with other compounds.

In Cu1234, it is known that the change in T_c due to the different stoichiometry of the constituent elements in $(CuC)O_{2+y}$ block layers is small and T_c's for all those samples were around 117K, although the magnitude of R_H is different.[1] The partial doping between the 4- and 5-fold layers may give an answer to this problem. Namely, it is considered that 5-fold mainly changes the in-layer carrier content with the variation of total carrier content and that 4-fold which mainly contribute to T_c around 117K as discussed later is kept near the optimum doped level for higher-T_c.

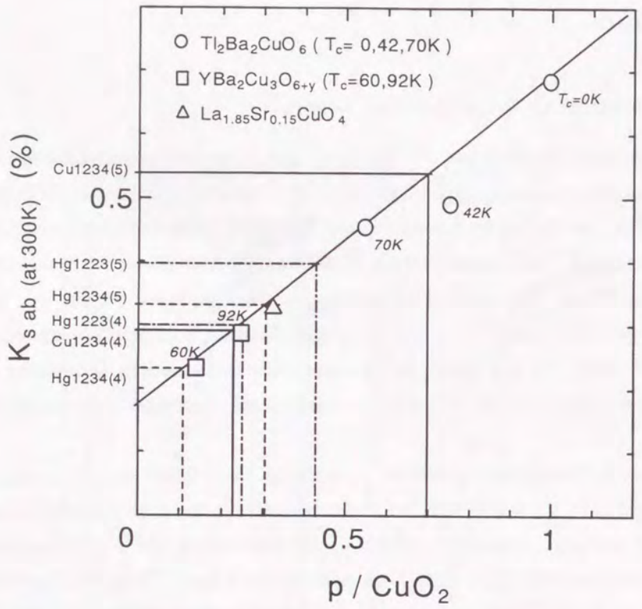

Figure 5.7: T dependence of $1/T_1T$ perpendicular and parallel to the c-axis for 4-fold and 5-fold.

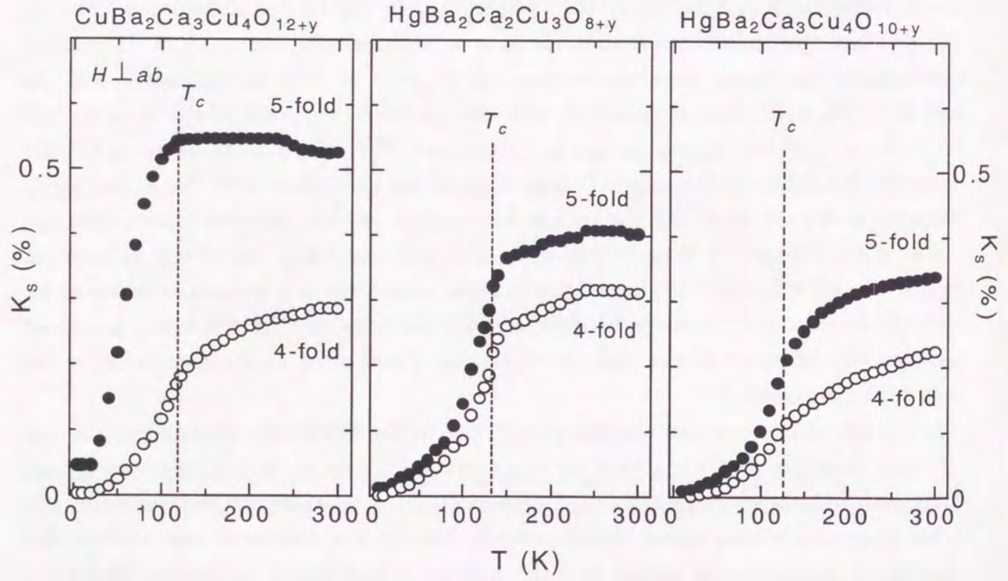

Figure 5.8: T dependence of $1/T_1T$ perpendicular and parallel to the c-axis for 4-fold and 5-fold.

5.4.2 Superconductivity in 5-fold layers.

In high T_c compounds, it is well known that K_s of the plane copper has a strong reduction just below T_c due to the spin-singlet formation in the superconducting state. $1/T_1$ also decrease strongly and shows a T^3 like behavior associating with the opening of d-wave superconducting gap below T_c. In Cu1234, both K_s and $1/T_1$ for 4-fold actually show the strong reduction and T^3 like behavior just below T_c. However the decreases of K_s and $1/T_1$ for 5-fold are gradual just below T_c and T^3 like behavior in $1/T_1$ is observed only below $\sim 60K$ as seen in Fig.5.4,5.5 and 5.6. This indicates that the d-wave superconducting state is established only in 4-fold just below T_c, therefore the superconductivity with $T_c = 117K$ is maintained only by 4-fold.

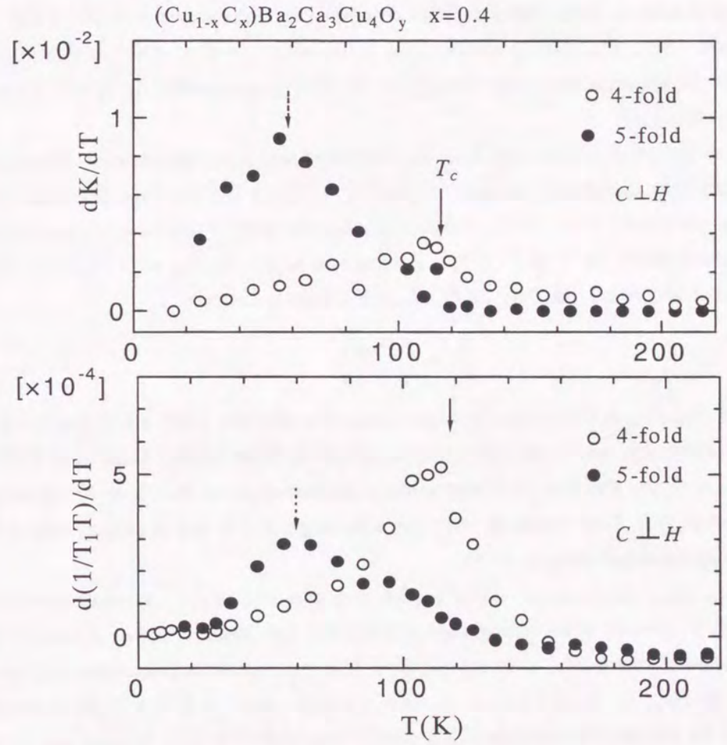

Figure 5.9: T dependence of $1/T_1T$ perpendicular and parallel to the c-axis for 4-fold and 5-fold.

In order to characterize this T dependence of K_s and $1/T_1$, the temperature-derive change in K_s and $1/T_1$, dK_s/dT and $d1/T_1/dT$ are plotted as function of temperature in Fig.5.9(a) and (b). As discussed above, both K_s and $1/T_1$ generally have a strong reduction with the superconducting transition, therefore both dK_s/dT and $d1/T_1T/dT$ show a peak just below T_c. As seen in Fig.5.9, both dK_s/dT and $d1/T_1/dT$ for 4-fold actually have peaks just below T_c. However those for 5-fold show peaks around 60K, indicating that 5-fold has the transition to

the superconducting state at this temperature. In addition, T^3 behavior in $1/T_1$ in 5-fold below 60K also indicates that the conventional d-wave superconducting state is established anew below $60K$ in 5-fold layers.

It should be noted that 5-fold is in widely overdoped level, moreover the estimated value of in-layer hole content, ~ 0.73 is similar to that for Tl1212 with $T_c = 52K$ as shown in Fig.5.7. This suggests that the over carrier doping suppresses the in-layer superconducting transition around $60K$ in 5-fold. On the other hands, the hole content in 4-fold is estimated to be ~ 0.27. This value is suitable for $T_c \sim 117K$ as compared with ~ 0.30 in 4-fold for Hg1223($T_c = 133K$) and ~ 0.35 in 5-fold for Hg1234($T_c = 123K$) which layers have the larger $\Gamma_Q \chi_Q$ values, hence determine T_c for each compounds. In addition, the inner 4-fold layers exhibit a structure very similar to those of infinite-layer compounds as discussed by Shimakawa et al.[2] In the infinite-layer compounds, $(Sr_{1-x}Ca_x)CuO_2$ shows T_c of 110K with $x = 0.3$, which also supports the possibility that the superconductivity with $T_c \sim 117K$ is maintained only by the inner 4-fold layers in this system.[18]

The structural distortion associated with the displaced apical oxygen sites may also suppress the superconductivity in 5-fold. As seen in Fig.5.6, $1/T_1$ for 5-fold shows the $1/T_1T$=const. behavior at low temperature below T_c, which indicates the gapless nature of superconductivity due to the inhomogeneity in 5-fold. $1/T_1T$ normalized at T_c, $R_s/R_n = (1/T_1T)/(1/T_1T)_n$ is related to the fraction of the residual DOS, N_{res}/N_0, from a formula

$$\frac{R_s}{R_n} = \left(\frac{N_{res}}{N_0}\right)^2. \tag{5.5}$$

The function of N_{res}/N_0 is a measure to what extent the effective DOS is lost due to the onset of the superconductivity, and is estimated to be about 0.15 for 5-fold. From this DOS value, the suppression in T_c by the impurity scattering is estimated to be less than 3K based on the *dirty* d-wave model.[17] This indicates that the inhomogeneity is not principal reason for the suppression of superconductivity in 5-fold.

Fig.5.10 shows the T dependence of K_s/K_n for 4- and 5-fold. $K_n(T)$ is assumed to decrease linearly down to T_c, which is an extrapolation from the least square fitting above $150K$, and stay constant below T_c for 4-fold, whereas K_n for 5-fold is assumed to T-independent, as shown by dotted line in Fig.5.3. $K_s(T)$ below T_c for optimally doped and overdoped cuprates was well reproduced by the two-dimensional (2D) d-wave model proposed by Monien and Pines.[19] In this model, the gap function has the form $\Delta(\phi) = \Delta \cos 2\phi$ where ϕ is the angle in the ab plane.[6, 20] The T dependence of the SC order parameter, $\Delta(T)/\Delta(0)$ was assumed to follow the BCS form.

In order to reproduce $K_s(T)$ below T_c for 5-fold sites, we may apply a model in which $\Delta(T)/\Delta(0)$ is assumed to increase linearly for $60K < T < T_c$ and to follow the mean-field BCS type below $60K$. A solid line is a calculation on the assumption of a temperature dependent order parameter, $\Delta(T)/\Delta(0)$ in the inset in Fig.5.10 with a gap parameter, $2\Delta/k_BT_c = 8.3$ which is adjusted so as to explain the experiment. The agreement between the experiment and the calculation seems to be satisfactory.

Interestingly, the pseudogap behaviors in K below T^* for 4- fold is also reproduced by assuming d-wave symmetry on the pseudogap with the same T-linear increase of $\Delta(T)/\Delta(0)$ for $T_c < T < T_K^*$, as discussed in the chapter.4. The agreement between the experiment and the calculation seems to be satisfactory, as shown by the solid line in Fig.5.10. The T dependence of $\Delta(T)/\Delta(0)$ used in the calculation is also displayed in the inset in Fig.5.10.

It is noteworthy that both the T-dependence of K in the unconventional superconducting state for 60K $< T < T_c$ in 5-fold layers, which is considered to be induced by the superconductivity in 4-fold layers, and in the pseudogap state for $T_c < T < T_K^*$ in 4-fold layers are well reproduced by assuming the same T-linear increase of the order parameter, $\Delta(T)/\Delta(0)$. This similarity indicates the possibility that these two states have the similar origin.

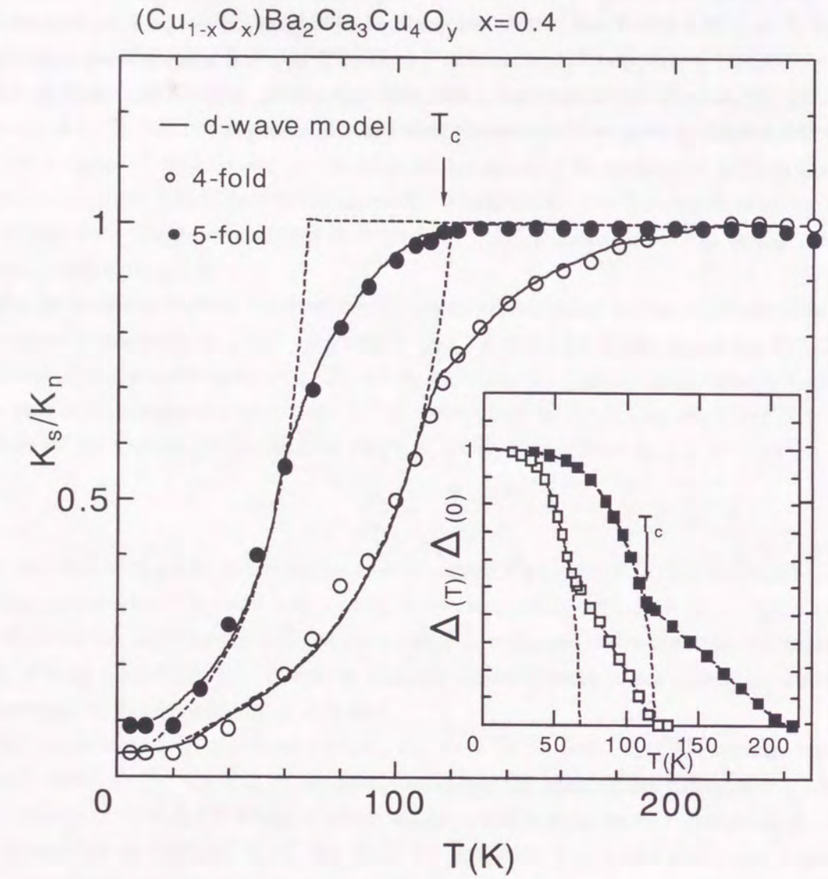

Figure 5.10: T dependence of $1/T_1T$ perpendicular and parallel to the c-axis for 4-fold and 5-fold.

5.5 Summary

The ^{63}Cu Knight shift and $1/T_1T$ have been separately measured for the inner square (4-fold) and the outer pyramidal (5-fold) CuO_2 planes in $(Cu_{0.6}C_{0.4})Ba_2Ca_3Cu_4O_{12+y}$ (Cu1234) with $T_c = 117$ K. It is revealed that multilayer compound Cu1234 is a structure containing layers of the different doping level, that is 4-fold is near the slightly underdoped, whereas 5-fold in the widely overdoped region. The in-layer hole content for 4- and 5-fold are estimated from K_s at 300K to be 0.27 and 0.73, respectively.

From T-dependence of K_s and $1/T_1$ in the superconducting state, it is revealed that the d-wave superconducting state is established in 4-fold, but not in 5-fold for $60K < T < T_c$. This indicates that the superconductivity with T_c of $117K$ is maintained only by the inner two 4-fold layers which are near the optimum carrier condition. The conventional d-wave superconducting state in 5-fold is established anew below $60K$. This temperature is considered to be the inherent transition temperature in 5-fold originating from the widely overdoped carrier content.

In 4-fold, the Knight shift data between T_c and T_K^* was well reproduced by a model which assumed that the value of the pseudogap with $d_{x^2-y^2}$ symmetry increases linearly with decreasing T from $T_K^* \sim 220$ K to T_c=117 K and follows the mean-field BCS form below T_c. Furthermore, this model can be applied to the temperature dependence of K below T_c for 5-fold by assuming the linear increase of a size of superconducting gap between T_c and 60K with the $d_{x^2-y^2}$ symmetry. This similarity indicates the possibility that these two states have the similar origin.

Bibliography

[1] M. Ogino, T. Watanabe, H. Tokiwa, A. Iyo and H. Ihara, Physica **C 258** (1996) 384

[2] Y. Shimakawa, J. D. Jorgensen, D. G. Hinks, H. Shaked, R. L. Hitterman, F. Izumi, T. Kawashima, E. Takayama, Muromachi and T. Kamiyama, Phys. Rev. **B 50** (1994)16008

[3] Y. Kitaoka, K. Fujiwara, K. Ishida, K. Asayama, Y. Shimakawa, T. Manako and Y. Kubo, Physica**C 179** (1991) 107

[4] K. Ishida, Y. Kitaoka, N. Ogata, T. Kamino, K. Asayama, J.R. Cooper and N. Athanassopoulou, J.Phys. Soc. Jpn. 62, 2803 (1993).

[5] H. Ihara, K. Tokiwa, H. Ozawa, M. Hirabayashi, A. Negishi, H. Matuhata and Y. S. Song, Jpn. J. Appl. Phys. 33 (1994) 503., H. Ihara, K Tokiwa, H. Ozawa, M. Hirabayashi, M. Matsuhata, A. Negishi, Y. S. Song, Jpn.J.Appl.Phys. 33 (1994) L300, H. Ihara, A. Iyo, K. Tokiwa, M. Hirabayashi, N. Terada, M. Tokumoto, Y. S. Song, Physica **C 235-240** (1994) 981

[6] K. Magishi, Y. Kitaoka, G.-q. Zheng, K. Asayama, T. Kondo, Y. Shimakawa, T. Manako and Y. Kudo, Phys. Rev. B**54**, 10131 (1996).

[7] F. Mila and T.M. Rice, Phys. Rev. B**40**, 11382 (1989); Physica C**157**, 561 (1989).

[8] S. Ohsugi, Y. Kitaoka, K. Ishida, G.-q. Zheng and K.Asayama, J. Phys. Soc. Jpn. **63**, 700 (1994).

[9] H. Zimmerman, M. Mali, M. Bamky and D. Brinkmann, Physica C**185-189**, 9574 (1990).

[10] A. Narath, Phys. Rev. **13**, 3724 (1976).

[11] M. Takigawa, A.D. Reyes, P.C. Hammel, J.D. Thompson, R.H. Heffner, Z. Fisk and K.C. Ott, Phys Rev B**43**, 247 (1991).

[12] K. Magishi, Y. Kitaoka, G.-q. Zheng, K. Asayama, K. Tokiwa, A. Iyo and H. Ihara, J. Phys. Soc. jpn. **64**, 4561 (1995).

[13] Y. Tokunaga, K. Ishida, K. Magishi, S. Ohsugi, G. -q. Zheng, Y. Kitaoka, K. Asayama, A. Iyo, K. Tokiwa and H. Ihara, submitted to Phys. Rev. **B**. Y.Tokunaga, K. Ishida, K. Magishi, S, Ohsugi, G.-q. Zheng, Y. Kitaoka, K. Asayama, A. Iyo, K. Tokiwa and H. Ihara, preprint in SCES98.

[14] K. Ishida, Y. Yoshia, T.Mito, Y. Tokunaga, Y. Kitaoka, K. Asayama, Y. Nakayama, J. Shimoyama and K. Kishio, Phys. Rev. **B 58** (1998)

[15] K. Miyake et al., J. Phys. Soc. Jpn. **63**, 3821 (1994)

[16] J.Jaklic et al., Phys. Rev. Lett. **77**, 892 (1996)

[17] K. Miyake (private communication), T. Hotta (private communication), Y. Kitaoka, K. Ishida and K. Asayama, J.Phys. Soc. Jpn. **63** (1994) 2052

[18] M. Takano et al. Mechanisms of superconductivity (1992) p3-13

[19] H. Monien and D. Pines, Phys. Rev. B **41**, 6297 (1990).

[20] K. Ishida, Y. Kitaoka, N. Ogata, T. Kamino, K. Asayama, J.R. Cooper and N. Athanassopoulou, J.Phys. Soc. Jpn. 62, 2803 (1993).

Chapter 6

Discussion

6.1 Relation between T_c and Spin Fluctuation

The spin fluctuation mechanism gives a consistent explanation of the anomalous physical properties above T_c and the high values of T_c in high-T_c cuprates on the same physical basis. The mechanism is also successful in estimating the relative values of T_c for various cuprates from their spin fluctuation spectra. Moriya, Takahashi and Ueda,[1] and Monthoux and Pines (MP)[2] proposed that the cutoff energy or the effective bandwidth of correlated quasiparticles, $\Gamma_0 \propto \Gamma_Q \xi^2$ is proportional to T_c in the spin-fluctuation-induced superconducting mechanism. In MP's expression,

$$T_c = \Gamma_Q \xi^2 [(1-\delta)/0.79] \exp(-1/\lambda) \tag{6.1}$$

with $0.42 \ll \lambda \ll 0.48$ based on the strong-coupling calculation.

As discussed in the section 1.2.6, the value of $\chi_Q \hbar \Gamma_Q$ is obtained experimentally from the constant value of $T_1 T / T_{2G}^2$ by using the following relation for $\xi > a$:

$$\frac{(T_1T)c}{(T_{2G})^2} \simeq \frac{0.69(^{63}\gamma_N \hbar)^2 F_c(Q)^2}{16\pi \mu_B^2 \hbar \kappa_B} (2 \times^{63} R - 1)(\chi_Q \hbar \Gamma_Q). \tag{6.2}$$

In Fig.6.1, we present the temperature dependence of $(T_1T)c/(T_{2G})^2$ for the optimally doped $YBa_2(Cu_{1-x}Ni_x)_3O_7$ [Chap.2], $HgBa_2Ca_3Cu_4O_{10+\delta}$ [Chap.4], $HgBa_2Ca_2Cu_3O_{8+y}$[3] and $Tl_2Ba_2Ca_2Cu_3O_{10}$[4], and the overdoped $Tl_2Ba_2CuO_{6+y}$[6] and $TlBa_2CaCu_2O_7$[5]. As shown in figure, $(T_1T)c/(T_{2G})^2$ =const. behaviors are observed in a wide temperature range above T_c for the overdoped and optimally doped high-T_c cuprates. These constant behaviors allow us to estimate the value of $\chi_Q \hbar \Gamma_Q$ for those cuprates.

In Fig.6.2, we present the relation between T_c and $\chi_Q \hbar \Gamma_Q$ estimated from the constant values of $(T_1T)c/(T_{2G})^2$. As discussed in the chapter 2, the relation $\Gamma_Q \propto T_c$ is directly derived from the universal scaling formula of $1/T_1T$ against $t = T/T_c$ in Ni substituted $YBa_2Cu_3O_7$. Furthermore, by combining with the universal scaling of $1/T_{2G}$, we can obtain the relation, $T_c \propto \Gamma_Q \hbar \Gamma_Q$, indicating that the decrease of $\chi_Q \hbar \Gamma_Q$ induced by Ni substitution to planer Cu sites is directly proportional to the decrease of T_c in $YBa_2(Cu_{1-x}Ni_x)_3O_7$. The relation $T_c \propto \Gamma_Q \hbar \Gamma_Q$ observed in $YBa_2(Cu_{1-x}Ni_x)_3O_7$ is shown in figure by the solid arrow.

For $HgBa_2Ca_3Cu_4O_{10+y}$[Chap.4], we can estimate the values of $\chi_Q\hbar\Gamma_Q$ in 5-fold to be ~ 4.9 from the constant value of T_1T/T_{2G}^2. However for 4-fold, $T_1T/(T_{2G})^2$ continues to decrease upon heating below 300 K. Therefore, we could not evaluate the value of $\chi_Q\hbar\Gamma_Q$ for 4-fold. For $YBa_2Cu_4O_8$, $T_1T/(T_{2G})$ = constant behavior observed above T^* undergoes a crossover to $T_1T/(T_{2G})^2$ = constant behavior at much higher temperature $T_{cr} \sim 500$ K. (see Fig.1.5)[7]. Thus, $\chi_Q\hbar\Gamma_Q$ is evaluated from the $T_1T/(T_{2G})^2$=constant above 500K.

As shown in Fig.6.2, all the results seem to support that T_c is proportional to $\chi_Q\hbar\Gamma_Q$ in the overdoped and the optimally doped regions. Since $\chi_Q \propto \xi^2$ is expected in these regions, this gives evidence for the relation, $T_c \propto \Gamma_Q\xi^2$. This relation allows us to conclude that the decrease of $\Gamma_Q\xi^2$ reduces T_c in the overdoped region, and thus the spin-fluctuation-induced mechanism is most promising for the high-T_c superconductivity.

We note here that in Fig.6.2 the data of $Bi_2Sr_2CaCu_2O_{8+\delta}$ is particularly deviated from the linear relation between T_c and $\chi_Q\hbar\Gamma_Q$. The observed T_c in $Bi_2Sr_2CaCu_2O_{8+\delta}$ is lower than the expected value from the linear relation between T_c and $\chi_Q\hbar\Gamma_Q$. This suggests that the inherent superconducting temperature induced by the AF spin-fluctuation mechanism is not $T_c \sim 86$ K but $T_c^* \sim 120$ K in this sample, as discussed in the following section.

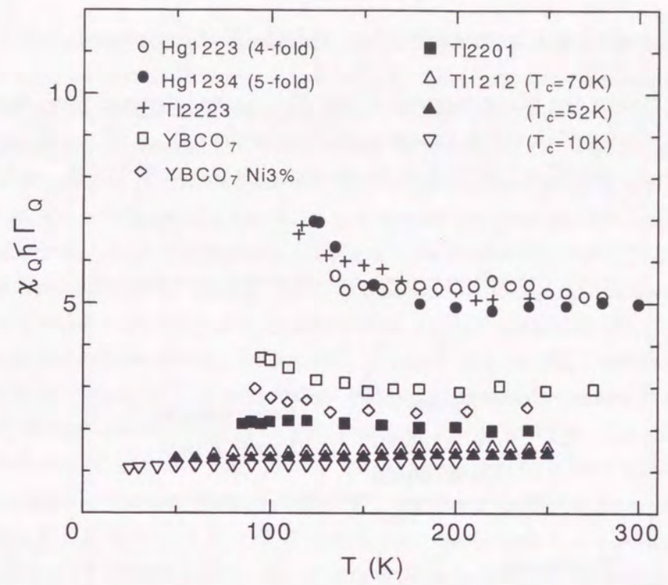

Figure 6.1: Temperature dependence of $\chi_Q\hbar\Gamma$ for the optimally doped $YBa_2(Cu_{1-x}Ni_x)_3O_7$, $HgBa_2Ca_3Cu_4O_{10+\delta}$ and $HgBa_2Ca_2Cu_3O_{8+y}$, and the overdoped $Tl_2Ba_2CuO_{6+y}$ and $TlBa_2CaCu_2O_7$

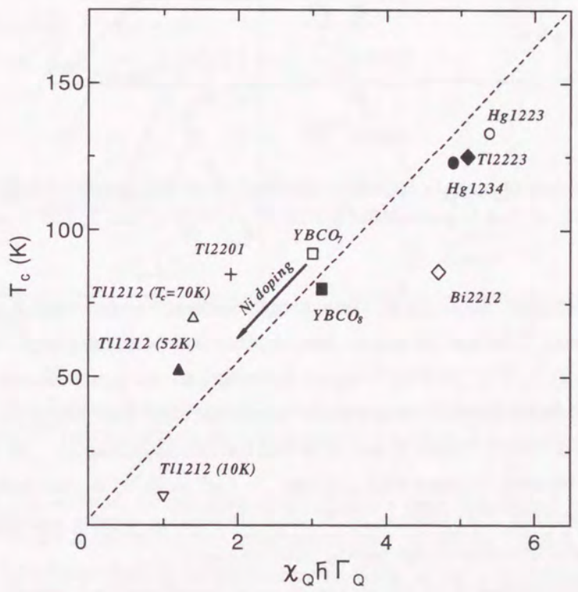

Figure 6.2: The relation between T_c and $\chi_Q\hbar\Gamma_Q$ estimated from the constant values of $(T_1T)c/(T_{2G})^2$

6.2 Temperature Crossovers in High-T_c Cuprates

In Fig.6.3, we present the phase diagram of high-T_c cuprates obtained from NMR study in Bi2212 [Chap.3], which contains three characteristic temperature, T_{mK}, T^* and T_c^* in the normal state. Here $T_{mk}*$, T^* and T_c^* are defined as the temperature where K, $1/T_1T$, and $1/T_{2G}$ start to decrease, respectively.

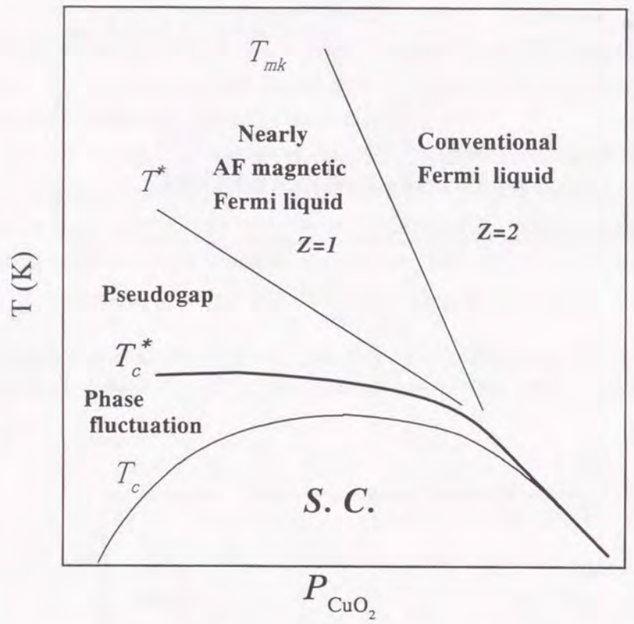

Figure 6.3: Phase diagram of high-T_c cuprates obtained from the present NMR studies. $T_{mk}*$, T^* and T_c^* are defined as the temperature where K, $1/T_1T$, and $1/T_{2G}$ start to decrease, respectively.

In the overdoped cuprates, the normal state properties can be understood in terms of the conventional Fermi liquid. One find an almost temperature independent Knight shift and mean-field behavior of $\chi(\boldsymbol{q},\omega)$ ($1/T_1T$ $/1/T_{2G}$ ^{2}=const behavior) at all temperatures in the normal state, and thus no evidence for the temperature crossover until just above T_c (refer to the results in the overdoped Bi2212 [Chap.3] and in 5-fold for Cu1234[Chap.5]). In this regime, we can obtain the linear relation between this increase T_c and $\chi Q h \Gamma Q$, as discussed in the above section. This indicates that the increase of T_c with decreasing doping concentration in this regime is ascribed to the increase of the pairing interaction.

On the other hand, the normal state properties in underdoped cuprates is characterized by the sequence of temperature crossovers at T_{mk}, T^* and T_c^*, as discussed in the chapter 3. Below the highest crossover temperature, T_{mK}, the Knight shift and the uniform susceptibility decrease gradually while $1/T_1T$ and $1/T_{2G}$ continue to increase. The likely cause for the gradual decrease

in $K(T)$ is associated with the development of AF-spin correlations towards T^*, which is also suggested from the recent theoretical studies[8, 9]. One finds the quantum critical z=1 scaling behavior in $\chi(\boldsymbol{q},\omega)$ in this temperature regime. At lower temperature, magnetic property enters the pseudogap regime around the characteristic temperature T^*. The decreases of $1/T_1T$ and K_s with T-decreasing provide a evidence that the pseudogap opens in the AF spin excitation spectrum at low energy around Q=(π,π) and also in the quasiparticle density of state in this regime. The temperature dependence of Knight shift between T_c and T_K^* shows that the value of the pseudogap increases linearly with decreasing T with $d_{x^2-y^2}$ symmetry[Chap.4 and 5], which is consistent with the result obtained from ARPES on Bi2212.[10, 11, 12] Furthermore, the temperature independent $1/T_{2G}$ between T^* and T_c^* where $1/T_1T$ decrease, implies that the origin of the pseudogap in this temperature regime is the energy transfer of the spectral weight from lower energy spin fluctuation to spin waves at higher energies. The one-particle spectral weight is considered to follow this spectral weight transfer of spin fluctuation.[13]

With decreasing the temperature below T^*, the lower crossover temperature T_c^* appears, below which $1/T_{2G}$ as well as K, $1/T_1T$ steeply decrease toward T_c . A possible explanation for these significant reduction of all the physical quantities below T_c^* is relevant to a develpoment of S. C. fluctuation without global phase coherency. In this scenario, the crossover temperature, T_c^* is regarded as the mean-field transition temperature where the amplitude of the superconducting order parameter is well established, but there is no long-range phase coherence until below T_c .

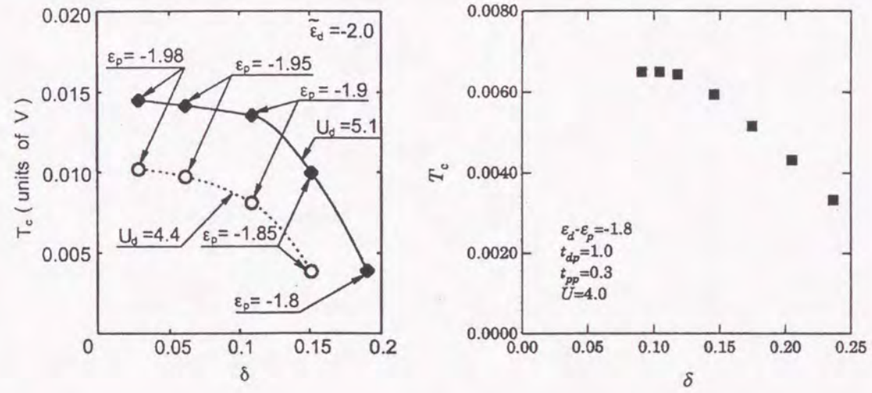

Figure 6.4: The doping dependence of the mean-field T_c calculated by Hotta *et al* [14] and Takimoto *et al* [15] using a strong coupling theory based on a two-dimensional $d-p$ model.

The doping dependence of the mean-field T_c have been calculated by several authors from the point of the AF spin-fluctuation mechanism.[15, 14, 16] In Fig.6.4, we present the doping dependence of the mean-field T_c calculated by Hotta *et al* [14] and Takimoto *et al* using a strong coupling theory based on a two-dimensional $d-p$ model. Many of their results suggest the increase of the mean-field T_c with hole decreasing in the overdoped regime, but not reproduced the reduction of $1/T_{2G}$ in the underdoped regime. The saturate tendency in T_c^* with hole decreasing

below optimum concentration is reasonably consistent with these theoretical suggestion.

Finally, we present the NMR results in $HgBa_2CaCu_2O_{6+y}$(Hg1212) reported by Y.Ito *et al*[17] in Fig.6.5. It is observed that $1/T_1T$ starts to decreases at $T^* \sim 240, 200$ and 110 K, while $1/T_{2G}$ starts to decrease at $T_c^* \sim 140, 145$ and 100 K in the underdoped ($T_c \sim 103$ K) and optimally (127K) and overdoped (93K) Hg1212, respectively. From the doping dependence of these characteristic temperature, we can derive the phase diagram in Hg1212, which is quite consistent with that in Bi2212, as shown in Fig.6.6. This suggests that the sequence of temperature crossovers at T_{mK}, T^* and T_c^* is intrinsic in the underdoped high-T_c cuprates.

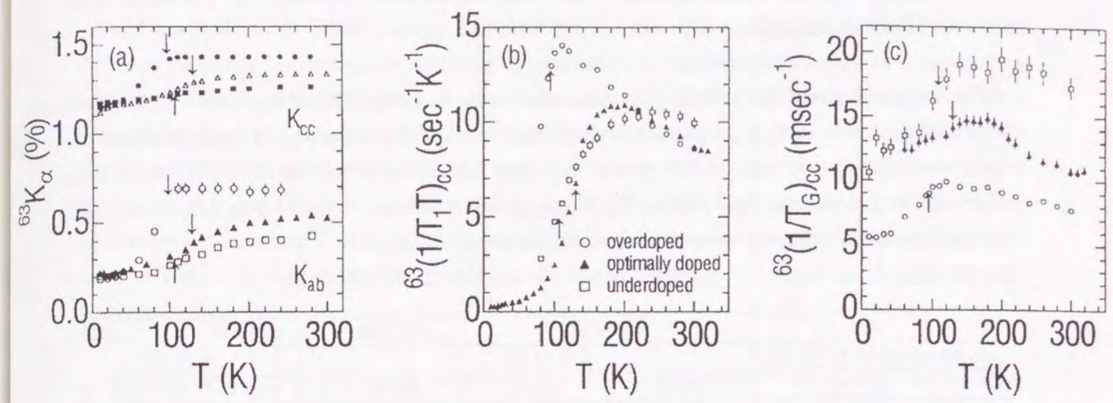

Figure 6.5: (a)The doping dependence of $^{63}K_\alpha$ ($\alpha = cc$ and ab), (b) $^{63}(1/T_1T)_{cc}$ and (c) $^{63}(1/T_G)_{cc}$ as a function of T are presented for $HgBa_2CaCu_2O_{6+y}$. The arrows indicate the T_c in each case. The squares, triangles and circles indicate the data for the underdoped, optimally doped and overdoped compounds, respectively.

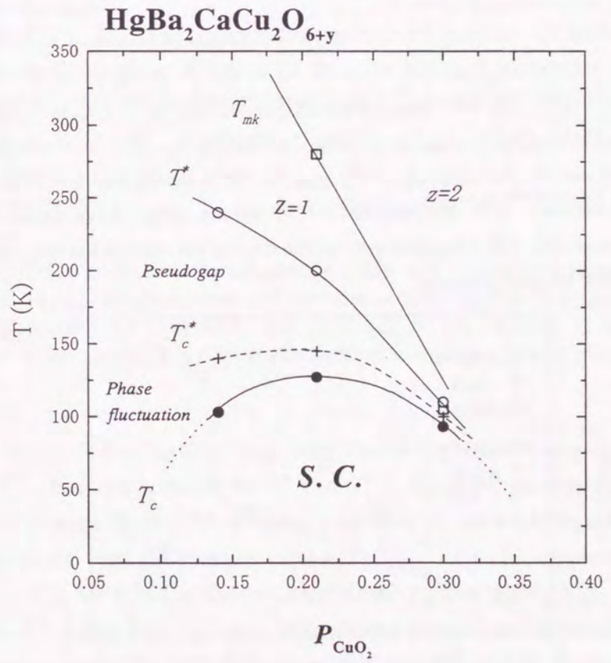

Figure 6.6: Doping dependence of the characteristic temperature, T_c, T_c^*, T^* and T_{mk} in $HgBa_2CaCu_2O_{6+y}$. $T_{mk}*$, T^* and T_c^* are defined as the temperature where K, $1/T_1T$, and $1/T_{2G}$ start to decrease, respectively.

6.3 Carrier distribution and Superconductivity in Multilayer Compounds

For understand the mechanism of superconductivity in the multilayer cuprates which consist inequivalent kinds of CuO_2 layers, it is important to take the difference of local character for each layer into consideration. There are one inner 4-fold and two outer 5-fold layers in three Cu-O layers systems such as $HgBa_2Ca_2Cu_3O_{8+y}$, while two inner 4-fold and two outer 5-fold layers in four Cu-O layers systems such as $HgBa_2Ca_3Cu_4O_{10+\delta}$.

	Hg1223		Cu1223	Hg1234	Cu1234
layers number n(4f/5f)	3 (1/2)			4 (2/2)	
T_c	115 K	133 K	95 K	123 K	117 K
P_{4fold}/CuO_2	0.15	**0.25**	0.31	0.11	**0.22**
P_{5fold}/CuO_2	0.23	0.42	0.56	**0.30**	0.70
Total carriers δ	0.61	1.09	1.43	0.82	1.84
$P_{4fold}/\delta(\%)/n_{4f}$	0.25% /1	0.23% /1	0.22% /1	0.27% /2	0.24% /2
$P_{5fold}/\delta(\%)/n_{5f}$	0.75% /2	0.77% /2	0.78% /2	0.73% /2	0.76% /2

Table 6.1: The comparison of the doping concentration in 4- and 5-fold layers.

In Table6.1, we show the values of the doping concentration per CuO_2, P/CuO_2, at each layer, which is extracted separately from the value of K_s at 300 K using the liner relation between K_s and P/CuO_2 in Fig.5.7 for the three layers $HgBa_2Ca_2Cu_3O_8$[18, 19], $(Cu,Tl)Ba_2Ca_2Cu_3O_8$ and the four layers $HgBa_2Ca_3Cu_4O_{10+\delta}$, $CuBa_2Ca_3Cu_4O_{12+\delta}$. The total carrier contents, δ is estimated by the equation, $\delta = 2P_{5-fold} + P_{4-fold}$ for three layers and $\delta = 2P_{5-fold} + 2P_{4-fold}$ for four layers, respectively. It is obvious that 4-fold layer is rather underdoped than the 5-fold in all the samples, and that the inequivalency of the doping concentration between 4- and 5-fold become larger in four layered systems.

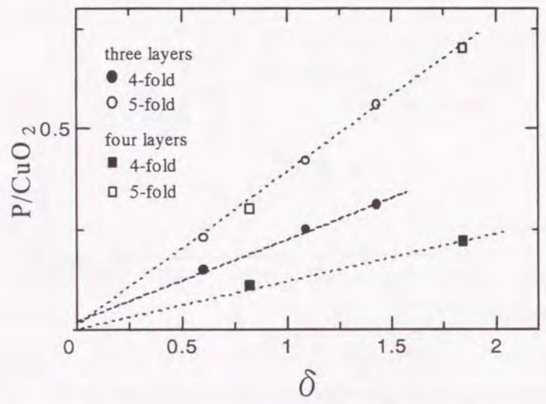

Figure 6.7: Carrier distribution among the 4- and 5-fold CuO_2 layers in a layered structure with three and four CuO_2 layers per unit cell.

A striking results is that P increase linearly with δ in both 4- and 5-fold layers, moreover, the rate of which do so in 5-fold is independent of the number of layers, as shown in Fig.6.7. This indicates that the percentages of the doping concentration in two 5-fold layers as compared to the total carrier content, δ, are kept at a certain value, $\sim$ 75% in all the sample, in spite of the difference of the total number of layers and the total carrier content, δ, as shown in the table.6.1. The difference is that the rest carrier $\sim$ 25% is divided by one 4-fold layers in three layers, while it is divided by two 4-fold in four layers. Therefore, the inequivalency of the doping concentration between 4- and 5-fold become larger in four layered systems. These results teach us that the outer 5-fold has the priority to decide the doping concentration in multilayered system.

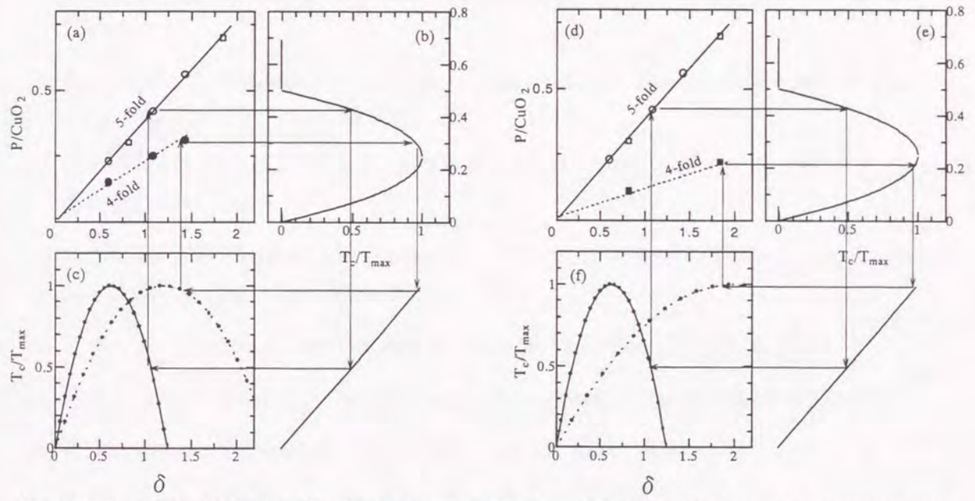

Figure 6.8: (a) [(d)] Carrier distribution among the 4- and 5-fold CuO_2 layers in a layered structure with three [four] CuO_2 layers per unit cell, respectively. (b)[(e)] Parabolic dependence upon the carrier concentration, P needed to calculate. (c)[(f)] the intrinsic T_c 's of the inequivalent CuO_2 layers as a function of δ in a layered structure with three [four] CuO_2 layers per unit cell, respectively.

In the overdoped $CuBa_2Ca_3Cu_4O_{12+\delta}$, the d-wave superconducting state is established in 4-fold below T_c , but not in 5-fold for $60K < T < T_c$, which provide the evidence that the superconductivity with T_c of $117K$ is maintained only by the 4-fold layers. From the value of the $\chi_Q\hbar\Gamma_Q$ estimated from the constant value of T_1T/T_{2G}, it is also suggested that T_c is ascribed to the larger $\chi_Q\hbar\Gamma_Q$ for 4-fold in the optimally-doped $HgBa_2Ca_2Cu_3O_{8+\delta}$, while that for 5-fold in the underdoped $HgBa_2Ca_3Cu_4O_{10+\delta}$. These behaviors can be explained in term of a model which has been suggested by D.Tristan Jover *et al* to explain their pressure dependence of T_c in Hg1223 and Hg1234.[20]. The model is based upon the assumption that each CuO_2 layer behaves as a superconducting structural unit with a well defined intrinsic T_c which depends on the charge carrier density, P of the layer under consideration. In the simplest case, the

intrinsic T_c as a function of P in each CuO_2 layer follow the inverted parabolic dependence as shown in Fig.6.8(b). Since in Fig.6.8(a) P_{4fold} and P_{5fold} are given as a function of δ, a relation for the intrinsic T_c as a function of δ can be calculated for the 4-fold and 5-fold CuO_2 layers, respectively. The result is a different parabolic function of T_c vs δ for each kind of layer, as seen in Fig.6.8(c), and T_c will be the maximum of these two curves.

The result shows that T_c is determined by the outer 5-fold in underdoped regime, while by the inner 4-fold in the optimally and the overdoped regimes, which is consistent with our experimental results. Furthermore, the result also give a explanation for the dull reduction of T_c in overdoped region for the four layered system, i.e. $CuBa_2Ca_3Cu_4O_{12+\delta}$.

Bibliography

[1] T. Moriya, Y. Takahashi and K. Ueda, J. Phys. Soc. Jpn. **59**, 2905 (1990); T. Moriya and K. Ueda, J. Phys. Soc. Jpn. **63**, 1871 (1994).

[2] D. Pines, Physica **B163**, 78 (1990); P. Monthoux and D. Pines, Phys. Rev. **B49**, 4261 (1994).

[3] K. Magishi, Y. Kitaoka, G.-q. Zheng, K. Asayama, K. Tokiwa, A. Iyo and H. Ihara, J. Phys. Soc. Jpn. **64**, 4561 (1995) .

[4] G.q.Zheng, Y.Kitaoka, K.Asayama, K.Hamada, H.Yamauchi and S.Tanaka, J. Phys. Soc. Jpn. **64**, 2524 (1995)

[5] K. Magishi, Y. Kitaoka, G.-q. Zheng, K. Asayama, T. Kondo, Y. Shimakawa, T. Manako and Y. Kubo, Phys. Rev. B **54**, 10131 (1996).

[6] Y. Ito, H. Yasuoka, A. Hayashi and Y. Ueda, J. Phys. Soc. Jpn. **63** 22 (1994)

[7] N. J. Curro, T. Imai, C. P. Slichter and B. Dabrowski, Phys. Rev. B**56** 877 (1997)

[8] K. Miyake and O. Narikiyo, J.Phys. Soc. Jpn. **63**, 3821 (1994).

[9] J. Jaklic and P. Prelovsek, Phys. Rev. Lett. **77**, 892 (1996).

[10] H. Ding *et al*, Nature **382**, 51 (1996).

[11] A. G. Loeser *et.al.*, Science **273**, 325 (1996).

[12] J. M. Harris *et al*, Phys. Rev. B, **54**, R15665 (1996).

[13] O. Narikiyo and K. Miyake, submitted to Physica C

[14] H.Hotta, J. Phys. Soc. Jpn. **62**, 4126 (1994)

[15] T. Takimoto and T Moriya, J.Phys. Soc. Jpn. **66** 2459 (1997)

[16] J. schmalian, S. Grabowski and K. H. Benemann, Phys. Rev. B56 R509 (1997)

[17] Y. Ito, A. Tokiwa-Yamamoto, T. Machi and K. Tanabe, J. Phys. Soc. Jpn. **67** 2212 (1998)

[18] M.-H. Julien, P. Carretta, M. Horvatic, C. Berthier, Y. Berthier, P. Segransan, A. Carrington, and D. Colson, Phys. Rev. lett. **76**, 4238 (1996).

[19] K. Magishi, Y. Kitaoka, G.-q. Zheng, K. Asayama, K. Tokiwa, A. Iyo and H. Ihara, J. Phys. Soc. jpn. **64**, 4561 (1995).

[20] D.Tristan Jover, R.J.Wijngaarden, R.Griessen, S.M.Loureiro, J.-J. Capponi, A.Schilling and H.R.Ott, Phys. Rev. B**54** 4265 (1996)

Chapter 7

Conclusion

The normal state magnetic properties in several high-T_c compounds has been studied by means of the ^{63}Cu-NMR technique from the overdoped to the underdoped compounds.

From the scaling behavior in $1/T_1T$ and $1/T_{2G}$, it is revealed that the decrease of T_c with Ni doping is directly related to the decrease of $\chi_Q\hbar\Gamma_Q$ in Ni substituted $YBa_2Cu_3O_7$. This results provides a direct experimental evidence for the attractive force to be magnetic in origin irrespective of the theoretical model, Furthermore, the intimate relation between T_c and AF spin-fluctuation, i.e. $T_c \propto \chi_Q\hbar\Gamma_Q$ observed in common for the overdoped and the optimally doped regions, allow us to conclude that the spin-fluctuation-induced mechanism is most promising for the high-T_c superconductivity.

In underdoped region, the normal state magnetic property is characterized by the three temperature crossover at T_{mK}, T^* and T_c^* below which K, $1/T_1$ and $1/T_{2G}$ start to decrease, respectively. The decrease of K where $1/T_1T$ and $1/T_{2G}$ increase below T_{mK} is related with the development of the AF spin correlation. On the other hand, the decrease of K as well as $1/T_1T$ shows below T^* that the pseudogap opens not only in the AF spin excitation spectrum at low energy around Q=(π,π) but also in the quasiparticle density of state. The temperature dependence of the pseudogap behavior in K is well reproduced by a model which assumes that the value of the normal-state pseudogap increases linearly with d-wave symmetry. Furthermore, the temperature independent $1/T_{2G}$ where $1/T_1T$ decrease implies that the origin of the pseudogap is the spectral-weight transfer from low to high energy. The lower crossover temperature T_c^*, below which $1/T_{2G}$ as well as K and $1/T_1T$ start to decrease, indicates the formation of the preformed pairs without the long-range coherency. We propose from the relation between $1/T_1T$ and $1/T_{2G}$ that the gradual pseudogap behavior between T^* and T_c^* is ascribed to the magnetic origin, and that the sharp pseudogap behavior below T_c^* is to the precursor effect of the superconductivity.

In the multilayered compounds which has inequivalent 4- and 5-fold CuO_2 layers, we find that the outer 5-fold is given the priority to decide the doping level, and thus the inner 4-fold tend to be rather underdoped. It is suggested that T_c is determined by a plane which are nearer to the optimally doping condition, i.e. has a higher $\chi_Q\hbar\Gamma_Q$. In Hg1234, we find that the pseudogap opens up for both 4- and 5-fold Cu sites at the same temperature, $T^* \sim 190$ K,

regardless of whether the magnetic property is characterized by the z=1 or the z=2 behavior. In Cu1234, we find that a conventional d-wave superconducting state is established at the different temperature between 4- and 5-fold layers due to the large inequality of doping level. The d-wave superconducting state is established in 4-fold at T_c , but not in 5-fold for $60K < T < T_c$. This provide the evidence that the superconductivity with T_c of $117K$ is maintained only by the 4-fold layers which are near the optimum carrier condition. The conventional d-wave superconducting state is established below $60K$ in 5-fold, which is considered to be the inherent transition temperature in 5-fold due to the widely overdoped carrier content.

Published works

1. Y. Tokunaga, K. Ishida, Y. Kitaoka and K. Asayama, "Novel Relation between Spin-Fluctuation and Superconductivity in Ni substituted High-Tc Cuprate $YBa_2Cu_3O_7$ -Cu NQR Study-", Solid State Communications 103 (1997) 43

2. Y. Tokunaga, K. Ishida, Y. Kitaoka and K. Asayama, "NQR study of Ni substitution effect in High-Tc Cuprates." Physica C 282-287 (1997) 1351

3. Y. Tokunaga, K. Ishida, Y. Kitaoka and K. Asayama, "Coexistence of magnetic ordering induced by Ni spins and superconductivity in Ni-substituted $YBa_2Cu_3O_7$ -Cu NQR study-." Czechoslovak Journal of Physics, vol.46 (1996), 1139

4. K. Ishida, K. Yoshida, T. Mito, Y. Tokunaga, Y. Kitaoka, K. Asayama Y. Nakayama, J. Shimoyama and K. Kishio, "Pseudogap behavior in single-crystal $Bi_2Sr_2CaCu_2O_{8+y}$ probed by Cu NMR" Phys. Rev. **B58** (1998) 5960

5. Y. Tokunaga, K. Ishida, K. Magishi, S, Ohsugi, G.-q. Zheng, Y. Kitaoka, K. Asayama, A. Iyo, K. Tokiwa and H. Ihara, "NMR study of magnetic excitations and pseudogap in $HgBa_2Ca_3Cu_4O_y$", Physica B, to be published in 1999.

6. Y. Tokunaga, K. Ishida, K. Magishi, S. Ohsugi, G.-q. Zheng, Y. Kitaoka, K. Asayama, A. Iyo, K. Tokiwa and H. Ihara "Magnetic excitation and pseudogap in $HgBa_2Ca_3Cu_4O_{10+y}$ comprising four CuO_2 planes – Cu NMR/NQR studies–" submitted to Phys. Rev. B.

7. K. Asayama, Y. Kitaoka, G.-q. Zheng, K. Ishida, K. Magishi, T. Mito and Y. Tokunaga, "NMR of High-T_c Superconductors", Czechoslovak Journal of Physics, vol.46 (1996), 3187

8. K. Asayama, Y. Kitaoka, G.-q. Zheng, K. Ishida, K. Magishi, Y. Tokunaga and K. Yoshida, "NMR of High-T_c Superconductors", International Journal of Modern Physics B, to be published in 1999.

Acknowledgements

I am most grateful to Professor Yoshio Kitaoka for his valuable discussions, constructive comments and continuous guidance. I would like to express my sincere thanks to Professor Kunisuke Asayama for guiding me into this field and, for enlightening discussion and continuous guidance.

I would like to express my special thanks to Dr. Kenji Ishida, who taught me the method of NMR experiments and how I should study high-T_c compounds. My thanks are also due to Dr. Guo-qing Zheng, who gave me helpful advice and encouragement, to Dr's. Shigeki Ohsugi, Koichi Magishi, Shinji Matumoto and Takeshi Mito for their practical advice for the NMR experiments and providing me with their data for comparison and with valuable information, and to other colleagues in Kitaoka laboratory for their cooperation.

I am indebted to Dr.'s K.Tokiwa, A.Iyo, and Professor H.Ihara in Electrotechnical Laboratory for provision of the high-quality $HgBa_2Ca_3Cu_4O_{10+y}$ and $CuBa_2Ca_3Cu_4O_{12+y}$ samples, and to Dr.'s Y. Nakayama, J. Shimoyama, and Professor K.Kishio in University of Tokyo for provision of the high-quality $Bi_2Sr_2CaCu_2O_{8+\delta}$ single crystals. I am grateful to Professor K.Miyake and Dr O.Narikiyo for their theoretical comments and valuable suggestions.

Finally I wish to express my appreciation to my parents.